On Identification and Control of Multivariable Systems Including Multiple Delays and Their Application to Anesthesia Control(Dissertation_全文)

AUTHOR(S):

Sawaguchi, Yoshihito

On Identification and Control of Multivariable Systems Including Multiple Delays and Their Application to Anesthesia Control

Yoshihito Sawaguchi

Abstract

This thesis proposes novel methods for identification and control of multivariable systems including multiple delays and describes their application to control of general anesthesia administration. First, an identification method for multivariable systems whose input and output paths have different time delays is presented. Second, a state predictor for multivariable systems whose input and output paths have different time delays is proposed. Third, the state predictor is used for constructing a state-predictive servo control system for controlled processes whose output paths have different time delays. A robust stability analysis method of the state-predictive servo control system is also examined. Furthermore, based on results of these theoretical studies, control systems for use in general anesthesia administration are developed.

First, an identification method for multivariable systems whose input and output paths have different time delays is proposed. This method comprises two steps. In the first step, the delay lengths are estimated from the impulse response matrix identified from input and output (I/O) sequences using a subspace identification algorithm. In the second step, I/O sequences of a delay-free part are constructed from the original sequences and the delay estimates, and the system matrices of the delay-free part are identified. The proposed method is numerically stable and efficient. Moreover, it requires no complex optimization to obtain the delay estimates, nor does it require an assumption about the structure of the system matrices.

Second, a state predictor is proposed for multivariable systems whose input and output paths have different time delays. The predictor consists of a full-order observer and a prediction mechanism. The former estimates a vector consisting of past states from the output. The latter predicts the current state from the estimated vector. The prediction error converges to zero at an arbitrary rate, which can be determined using pole assignment method, etc. In the proposed predictor, the interval length of the finite interval integration fed to the observer is shorter than that of an existing delay-compensating observer. Consequently, the proposed predictor is more numerically accurate than the delay-compensating observer.

Using the proposed state predictor, a design method of a state-predictive servo controller is described for multivariable systems whose output paths have different time delays. Furthermore, a sufficient stability condition of the state-predictive servo control system against parameter mismatches is derived. Using a characteristic equation

of the perturbed closed-loop system, a stability margin can be given on a plane whose axes correspond to the magnitudes of the mismatches on system matrices and on delay lengths.

In the remainder of this thesis, development of anesthesia control systems is described to illustrate an application of the theoretical results described above. First, a hypnosis control system is presented. This system administers an intravenous hypnotic drug to regulate an electroencephalogram-derived index reflecting the patient's hypnosis. The system comprises three functions: i) a model predictive controller that can take into account effects of time delay adequately, ii) an estimation function of individual parameters, and iii) a risk-control function for preventing undesirable states such as drug over-infusion or intra-operative arousal. Results of 79 clinical trials show that the system can reduce the total amount of drug infusion and maintain hypnosis more accurately than an anesthesiologist's manual adjustment. Second, a simultaneous control system of hypnosis and muscle relaxation is described. For development of this system, a multivariable model of hypnosis and muscle relaxation is identified using the method proposed in this thesis. Then a state-predictive servo control system is designed for controlling hypnosis and muscle relaxation. Finally, the control system's performance is evaluated through simulation. The resultant simultaneous control system satisfies the performance specifications of settling time, disturbance rejection ability, and a robust stability range. Although this system is not fully developed, the procedure of constructing this control system demonstrates the effectiveness of the proposed methods: the identification method for systems whose input and output paths have different time delays and the design and stability analysis methods of the state-predictive servo control system.

Acknowledgments

The author wishes to express his genuine gratitude to President Mituhiko Araki of Matsue College of Technology. He has not only provided the author a great opportunity to study in his research group, but also always instructed and encouraged the author to complete this work. The author is greatly thankful to his adviser Professor Tetsuo Kobayashi of Department of Electrical Engineering, Kyoto University, for his support, experience and knowledge he generously offered. The author would like to appreciate Professor Tomomichi Hagiwara of Department of Electrical Engineering, Kyoto University, for his constructive and insightful comments. The author is also grateful to Associate Professor Eiko Furutani of Department of Electrical Engineering, Kyoto University, for his extremely stimulating and valuable advice and discussion. The author would like to thank Professor Kazuhiko Fukuda and Associate Professor Gotaro Shirakami of Department of Anesthesia, Kyoto University Hospital, for their helpful comments from the medical viewpoint and assistance in clinical trials of anesthesia control systems. Gratitude is also due to the past and current members of the Composite Systems Theory Laboratory, Department of Electrical Engineering, Kyoto University, and to colleagues at Kisarazu National College of Technology, for their constant assistance and encouragement.

The extreme support received from the Japan Society for the Promotion of Science (JSPS) the 21st Century COE Program (Grant No. 14213201) is greatly appreciated.

Finally yet importantly, the author likes to thank his family for their manifold support throughout the many years of education.

Contents

Chapter 1

Introduction

Many practical processes include time delays in their input and output paths: transport of materials through pipes, transmission of information on networks, detection and computation of signals in sensors, response time of actuators, and so on. In multiple-input multiple-output processes, the lengths of the delays in the input and output paths might differ because each path might have a different source of delay. Such multivariable systems can be represented as a serial cascade of delay elements and a finite dimensional state equation. Throughout this thesis, we refer to this finite dimensional state equation as a delay-free part of the process. In general, the delays prevent an immediate response of measured output to input. The delays also make the process an infinite dimensional system. Therefore, closed-loop control of such processes is more difficult than that of delay-free processes. To date, many researchers have studied the synthesis and analysis of controllers for time delay systems, as in [1, 2] and references therein.

Conventional proportional-integral-derivative (PID) controllers have been widely applied in the practice of control engineering. The Ziegler-Nichols methods [3] are the best-known methods for tuning PID parameters. In the Ziegler-Nichols reaction curve method, a controlled process is approximated by a first-order lag with a time delay. Then the PID parameters are given as a function of the time delay length and the gain and time constant of the first-order lag. Using the Ziegler-Nichols ultimate sensitivity method, we can also determine the PID parameters from the ultimate gain and the ultimate period of the controlled process. These PID parameters are adequate for single-input single-output (SISO) processes with a short time delay. However, the performance of the PID controllers for processes with a long time delay is not so high because the controller design lacks rigorous consideration of the effects of the delay.

The first approach for controlling time delay systems with rigorous consideration of the effects of the delay was the Smith predictor [4]. Using a transfer function model of the controlled process, the Smith predictor predicts the output of the controlled process. This prediction mechanism enables us to ignore the delay in synthesis of the closed-loop transfer function from the reference signal to the controlled output. Consequently, one can apply conventional design methods of closed-loop controllers for controlled process

without a delay, such as PID controller tuning methods and lead-lag compensation. A major drawback of this approach is the impossibility of controlling unstable processes.

A more powerful method for controlling time delay systems is state-predictive control [5, 6]. In this method, a controller predicts the current state of the delay-free part of the controlled process from the delayed output using a state equation model of the controlled process, and uses the predicted values for state feedback control. This state-predictive mechanism enables us to design a closed-loop controller using modern control theory for finite dimensional systems such as the pole assignment method [6], linear quadratic optimal control [7], and H_∞ control [8]. Unlike the Smith predictor, state-predictive controllers can stabilize unstable processes. In studies reported in literature, these state-predictive controllers have mainly been applied to systems with a single pure delay. Control of multivariable systems including multiple delays has been discussed in a few reports [9].

As another method for controlling time delay systems, model predictive controllers [10] have been developed and have been widely applied. These controllers predict the future behavior of the process using a process model, and select the control input that optimizes future performance. Model predictive controllers can take time delays into account, although performance analysis of closed-loop systems is not easy.

For controlling time delay systems using a prediction-type controller, a mathematical model of the controlled process fills an essential role. To obtain the mathematical model, one can use identification methods that identify the model from measured input and output sequences. To date, many identification methods have been investigated. Most have targeted delay-free systems [11]. Others have been designed to estimate the length of a pure delay [12]. However, identification of multivariable systems including multiple delays has been described in only a few reports [13, 14]. Almost all of those methods required nonlinear optimization procedures that entail enormous costs of computation. On the other hand, during the last 20 years, a new approach for system identification, subspace identification [15], has been developed. Using this method, one can obtain a state space model of the controlled process without nonlinear optimization. In fact, the subspace identification procedure consists of LQ factorization [15], singular value decomposition, and matrix operations. Moreover, the subspace identification is especially suitable for multivariable systems because no canonical form of the system model is required. For those reasons, the subspace identification is an effective means to obtain a mathematical model of a multivariable system from measured data. However, additional consideration is required if the controlled process includes long time delays because such delays increase the system order remarkably.

Once an adequate model of the process is obtained, one can predict the state of the delay-free part of the process using measurements of input and output. The predicted state is useful not only for closed-loop control but also for analysis of the process. The state prediction of a process including a pure delay has been investigated in detail [5–8], as in the state-predictive controllers. However, state prediction of processes whose input and output paths have different time delays is not so straightforward. One can use a

delay-compensating observer [9] whose prediction error theoretically converges to zero according to the location of finite poles assigned arbitrarily. However, this observer sometimes shows poor performance in numerical simulation, because the delay-compensation in this observer is based on finite interval integration, which includes numerical errors.

Using the estimated state of the delay-free part of the process, servo-tracking control of multivariable systems whose output paths have different time delays is achieved as similar to state-predictive servo control of systems with a single pure delay [7]. In the design procedure of such control systems, robust stability analysis is an important step. Because prediction-type controllers use a model to predict the system behavior, mismatches of the model drastically affect the control performance. Although robust stability analysis of time delay systems has been explained in numerous works [1, 2, 16], few have contributed to quantitative analysis of prediction-type control systems. A pioneer work [17] examines systems with the Smith predictor. Extending this approach, a graphical method was derived [18] to obtain the stability margins in the gain and the delay length. This method is applicable to both closed-loop systems with the Smith predictor and with the state-predictive controller, but the applicable controlled process is restricted to an SISO system with a single delay element.

Based on that background, the author has investigated identification and control of multivariable systems whose input and/or output paths have different time delays. First, a novel subspace identification method is proposed for multivariable systems whose input and output paths have different time delays. Second, a state predictor is developed for multivariable systems whose input and output paths have different time delays. Third, a state-predictive servo controller for multivariable systems whose output paths have different time delays is proposed. Furthermore, a robust stability analysis method for the proposed closed-loop system is investigated, assuming parameter mismatches on system matrices and delay lengths. As applications of these theoretical results, the author has developed anesthesia control systems because the time courses of drug effects during general anesthesia include considerable time delays of different lengths. The author developed an SISO control system that regulates a patient's hypnosis by administering a hypnotic drug. The system is subsequently extended to a multiple-input multiple-output control system which regulates hypnosis and muscle relaxation simultaneously by administering multiple drugs.

The contents of this thesis are as follows.

In Chapter 2, the author proposes a subspace identification method for multivariable systems whose input and output paths have different time delays. Using this method, one can obtain estimates of delay lengths and system matrices of the delay-free part of the controlled process. This method comprises two steps. Delay lengths in the respective input and output paths are estimated from an impulse response matrix that is obtained based on a subspace identification method [19]. Then a state-space realization of the delay-free part is identified using the subspace identification method. This identification procedure is numerically stable and efficient because no complicated numerical search is required. A numerical example is shown to demonstrate the superiority of the proposed

method over existing methods in terms of the accuracy of estimates of the impulse response matrix.

In Chapter 3, a novel state predictor is proposed for multivariable systems whose input and output paths have different time delays. This state predictor estimates the current state of the delay-free part of the controlled process from measurements of output and input. The state predictor consists of a full-order observer and a prediction mechanism. The former estimates a vector consisting of past states from the measured output; the latter predicts the current state from the estimated vector. The interval length of integration in the observer is shorter than that of the delay-compensating observer [9]. Therefore, the proposed predictor would show better performance than the delay-compensating observer, as in a numerical example presented in this chapter.

Chapter 4 is devoted to establishing design and analysis methods of state-predictive servo control systems for processes whose output paths have different time delays. First, a state-predictive servo controller is proposed. This controller includes the state predictor proposed in Chapter 3, an integral compensator for tracking a step reference, and a prediction mechanism that predicts the future value of the integral compensator. Using the predicted states, the current input is determined by a state feedback law with a constant gain matrix. Second, a robust stability condition is derived for this closed-loop system. Assuming mismatches of system matrices and delay lengths, a characteristic function of the closed-loop system is derived. Then a sufficient condition of robust stability is derived from the characteristic function. This stability condition gives a stability region on a plane whose vertical and horizontal axes respectively represent a norm of mismatches on system matrices and the maximum mismatch on the delay lengths. This condition is rather conservative, but it is easy to derive. For that reason, it is useful for synthesis and analysis of the state-predictive servo control system.

Chapters 5 and 6 describe application of predictive controllers to general anesthesia.

Development of a system for hypnosis control was described in Chapter 5. Initially, a model of hypnosis change to drug infusion is constructed, with reference to the relevant pharmacological literature [20–22]. Then a model predictive controller is designed considering nonlinearity of the model and the constraints of drug infusion. Based on the range of individual differences estimated from actual measurement data, the robust stability region of the control system is confirmed to cover the presumed uncertainty of the patient model. Moreover, an estimation function of individual model parameters for coping with individual differences and a risk-control function are implemented in the control system. Results of clinical trials show the potential of this system for reduction of drug amounts and accurate maintenance of hypnosis.

Development of another anesthesia control system was explained in Chapter 6. In this system, the infusion rates of a muscle relaxant and a hypnotic drug are adjusted simultaneously so that the indices of muscle relaxation and hypnosis approach and remain at their target values. The controlled process of this system is a multivariable (two-input two-output) system whose output paths have different time delays. The identification method presented in Chapter 2 is applied to 10 measured data to obtain a model of the

controlled process. Then a robust state-predictive servo controller proposed in Chapter 4 is constructed. Finally, the closed-loop performance, including tracking ability and robust stability, are analyzed using numerical examples. Results show that the control system achieves simultaneous control of hypnosis and muscle relaxation.

Finally, Chapter 7 summarizes and concludes this thesis with a discussion of future directions of research in this area.

Chapter 2

Subspace identification of multivariable systems whose input and output paths have different time delays

A mathematical model of the process is useful to analyze the behavior of a process and to design a controller for the process. We should identify the model from input and output sequences of the process when such a model is unavailable. For identification of systems including multiple delays, traditional system identification methods [11, 15] are applicable to obtain a model of a delay-free augmented system by introducing a delayed state whose number equals the sum of the delay lengths. Simultaneous identification methods of both the lengths of the delays and parameters of the system's delay-free part have been investigated [13,14]. However, these methods often present some difficulties in practice: the high-order model identified using the former methods would be inaccurate because numerical accuracy of computation tends to be lost: furthermore, the nonlinear optimizations required in the latter methods would have local sub-optimal solutions in spite of their enormous cost of computation.

On the other hand, if the lengths of the delays are known, we can identify an accurate model of the delay-free part from its input and output sequences obtained by shifting the original sequences according to the delays using conventional system identification methods [23]. The knowledge of lengths of the delays is crucial for accurate identification using this approach. To date, many investigators have studied delay lengths estimation methods. However, most have investigated only single delay cases [12]. In general, because of the interactions among their inputs and outputs. their methods are not directly applicable to multivariable systems whose input and output paths have different time delays.

In this chapter, the author proposes a novel identification method for multivariable systems whose input and output paths have different time delays. This method consists

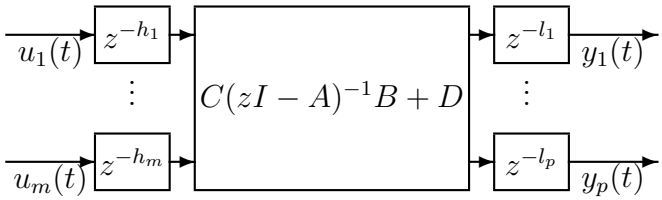

Figure 2.1: Multivariable system whose input and output paths have different time delays

of two steps. In the first step, an impulse response matrix is estimated from input and output sequences, then the lengths of the delays are estimated from the impulse response matrix. In the second step, using information of delay lengths, system matrices of the delay-free part are identified from the input and output sequences of the delay-free part. Both of these steps are based on a subspace identification method [19]. Therefore, the proposed method requires no complex nonlinear optimization procedure, nor does it require an assumption about the structure of the delay-free part.

The structure of this chapter is as follows. First, the structure of systems is described; then the problem treated in this chapter is formulated in Section 2.1. Section 2.2 presents a detailed explanation of the proposed method. In Section 2.3, a numerical example is given to evaluate the performance of the proposed method.

2.1 Problem formulation

Consider a discrete-time linear multivariable system whose input and output paths have different time delays:

$$x(t+1) = Ax(t) + B\tilde{u}(t), \tag{2.1}$$

$$\tilde{y}(t) = Cx(t) + D\tilde{u}(t), \tag{2.2}$$

$$\tilde{u}(t) = [u_1(t-h_1) \ \cdots \ u_m(t-h_m)]^{\mathrm{T}}, \quad y(t) = [\tilde{y}_1(t-l_1) \ \cdots \tilde{y}_p(t-l_p)]^{\mathrm{T}}. \tag{2.3}$$

Here, $x(t)$ is an n-dimensional state vector of the delay-free part (Eqs. (2.1) and (2.2)) of the system, where $\tilde{u}(t)$ is an m-dimensional input vector to the delay-free part, $\tilde{y}(t)$ is a p-dimensional output vector from the delay-free part, $\tilde{y}_j(t)$ for $j = 1, \cdots, p$ are the j-th scalar elements of the delay-free output $\tilde{y}(t)$, $u(t) = [u_1(t) \ \cdots \ u_m(t)]^{\mathrm{T}}$ is an m-dimensional input vector to the system, $y(t) = [y_1(t) \ \cdots \ y_p(t)]^{\mathrm{T}}$ is a p-dimensional output vector from the system, $h_i \geq 0$ for $i = 1, \cdots, m$ are time delays in the i-th input path and $l_j \geq 0$ for $j = 1, \cdots, p$ are time delays in the j-th output path. We assume that the pair (A, B) is reachable and that the pair (C, A) is observable. The structure of this system is depicted in Fig. 2.1.

For this system, consider an (N_0+1)-length output sequence $Y = [y(0)\ y(1)\ \cdots\ y(N_0)]$, as a response to an (N_0+1)-length input sequence $U = [u(0)\ u(1)\ \cdots\ u(N_0)]$. We assume that the input sequence satisfies the generic persistency of excitation (PE) condition [15], and that all rows of U are linearly independent of that of the state sequences $X_i = [x(-h_i)\ x(-h_i+1)\ \cdots\ x(-h_i+N_0)]$ for $i = 1, \cdots, m$. Moreover, data length N_0 is assumed to satisfy the following inequality:

$$N_0 \ \geq \ (n+H+L)(p+m+1)+2(p+m), \tag{2.4}$$

where $H = \sum_{i=1}^{m} h_i$ and $L = \sum_{j=1}^{p} l_j$. This condition pertains because of a matrix size limitation of block Hankel matrices which appear later in this chapter. For these input and output sequences, we consider the following identification problem.

Problem *Given the input and output sequences U and Y, estimate the input and output delays h_i for $i = 1, \cdots, m$ and l_j for $j = 1, \cdots, p$ and identify a particular realization (A, B, C, D) of the delay-free part of the system.*

Here we mention freedom of the lengths of the delays. We can displace the input and output delays h_i and l_j by $h_i' = h_i + \delta$ and $l_j' = l_j - \delta$, respectively, where δ is an integer satisfying $-\min_i(h_i) \leq \delta \leq \min_j(l_j)$. To eliminate this freedom of the delay lengths, the minimum length of the input delays is set to 0 by replacing the length of the input delay h_i' by $h_i' = h_i - \min_i(h_i)$ and the length of the output delay l_j' by $l_j' = l_j + \min_i(h_i)$, and treating them respectively as h_i and l_j.

2.2 Novel identification method

In this section, a novel identification method for solving the **Problem** is proposed. The procedure of the proposed method is as follows:

1. An impulse response matrix of the system is estimated from the input and output sequences U and Y. Then the input and output delays h_i and l_j are estimated from the impulse response matrix.

2. Input and output of the delay-free part are constructed by receding and advancing the original input and output using the estimated delays respectively, as

$$\tilde{u}(t) \ = \ [u_1(t-h_1)\ \cdots\ u_m(t-h_m)]^{\mathrm{T}}, \quad \tilde{y}(t) = [y_1(t+l_1)\ \cdots\ y_p(t+l_p)]^{\mathrm{T}}. \tag{2.5}$$

   The system matrices (A, B, C, D) are identified from the sequences of the input $\tilde{u}(t)$ and output $\tilde{y}(t)$ of the delay-free part.

In the following, we first introduce a delay-free augmented system for estimation of the impulse response matrix in Subsection 2.2.1. Then methods for estimating the impulse response matrix of the system and the lengths of the delays are given respectively in Subsections 2.2.2 and 2.2.3. An identification method of system matrices of the delay-free part is explained in Subsection 2.2.4.

2.2.1 Transformation to a delay-free augmented system

In discrete-time cases, a system whose input and output paths have different time delays can be transformed to a delay-free augmented system by introducing a new state which represents the values of past inputs and future outputs. Consequently, using an augmented state $\hat{x}(t)$, the system (2.1)–(2.3) can be represented as a delay-free augmented system:

$$\hat{x}(t+1) = \hat{A}\hat{x}(t) + \hat{B}u(t), \tag{2.6}$$
$$y(t) = \hat{C}\hat{x}(t) + \hat{D}u(t), \tag{2.7}$$

where $\hat{x}(t) = \left[\bar{y}_1^{\mathrm{T}}(t) \ \cdots \ \bar{y}_p^{\mathrm{T}}(t) \quad x^{\mathrm{T}}(t) \quad \bar{u}_1^{\mathrm{T}}(t) \ \cdots \ \bar{u}_m^{\mathrm{T}}(t)\right]^{\mathrm{T}}$,

$$\bar{y}_j(t) = [\tilde{y}_j(t-l_j) \ \cdots \ \tilde{y}_j(t-1)]^{\mathrm{T}} \quad (j = 1, \cdots, p), \tag{2.8}$$
$$\bar{u}_i(t) = [u_i(t-h_i) \ \cdots \ u_i(t-1)]^{\mathrm{T}} \quad (i = 1, \cdots, m), \tag{2.9}$$

$$\hat{A} = \left[\begin{array}{cccc|c|cccc} \hat{J}_{l_1} & 0_{l_1\times l_2} & \cdots & 0_{l_1\times l_p} & \hat{C}_1 & \hat{D}_{11} & \hat{D}_{12} & \cdots & \hat{D}_{1m} \\ 0_{l_2\times l_1} & \hat{J}_{l_2} & \cdots & 0_{l_2\times l_p} & \hat{C}_2 & \hat{D}_{21} & \hat{D}_{22} & \cdots & \hat{D}_{2m} \\ \vdots & \vdots & \ddots & \vdots & \vdots & \vdots & \vdots & \ddots & \vdots \\ 0_{l_p\times l_1} & 0_{l_p\times l_2} & \cdots & \hat{J}_{l_p} & \hat{C}_p & \hat{D}_{p1} & \hat{D}_{p2} & \cdots & \hat{D}_{pm} \\ \hline 0_{n\times l_1} & 0_{n\times l_2} & \cdots & 0_{n\times l_p} & A & \hat{B}_1 & \hat{B}_2 & \cdots & \hat{B}_m \\ \hline 0_{h_1\times l_1} & 0_{h_1\times l_2} & \cdots & 0_{h_1\times l_p} & 0_{h_1\times n} & \hat{J}_{h_1} & 0_{h_1\times h_2} & \cdots & 0_{h_1\times h_m} \\ 0_{h_2\times l_1} & 0_{h_2\times l_2} & \cdots & 0_{h_2\times l_p} & 0_{h_2\times n} & 0_{h_2\times h_1} & \hat{J}_{h_2} & \cdots & 0_{h_2\times h_m} \\ \vdots & \vdots & \ddots & \vdots & \vdots & \vdots & \vdots & \ddots & \vdots \\ 0_{h_m\times l_1} & 0_{h_m\times l_2} & \cdots & 0_{h_m\times l_p} & 0_{h_m\times n} & 0_{h_m\times h_1} & 0_{h_m\times h_2} & \cdots & \hat{J}_{h_m} \end{array}\right], \tag{2.10}$$

$$\hat{J}_k = \begin{cases} \phi & (\text{if } k = 0), \\ 0 & (\text{if } k = 1), \\ \left[\begin{array}{c|c} 0_{(k-1)\times 1} & I_{k-1} \\ \hline 0_{1\times 1} & 0_{1\times(k-1)} \end{array}\right] & (\text{otherwise}), \end{cases} \tag{2.11}$$

$$\hat{C}_j = \begin{cases} \phi & (\text{if } l_j = 0)\,, \\ C_j & (\text{if } l_j = 1)\,, \\ \left[\begin{array}{c} 0_{(l_j-1)\times n} \\ \hline C_j \end{array}\right] & (\text{otherwise})\,, \end{cases} \quad \hat{B}_i = \begin{cases} \phi & (\text{if } h_i = 0)\,, \\ B_i & (\text{if } h_i = 1)\,, \\ \left[\begin{array}{c|c} B_i & 0_{n\times(h_i-1)} \end{array}\right] & (\text{otherwise})\,, \end{cases} \tag{2.12}$$

$$\hat{D}_{ji} = \begin{cases} \phi & (\text{if } l_j = 0 \text{ or } h_i = 0)\,, \\ d_{ji} & (\text{if } l_j = 1 \text{ and } h_i = 1)\,, \\ \left[\begin{array}{c|c} d_{ji} & 0_{1\times(h_i-1)} \end{array}\right] & (\text{if } l_j = 1 \text{ and } h_i \geq 2)\,, \\ \left[\begin{array}{c} 0_{(l_j-1)\times 1} \\ \hline d_{ji} \end{array}\right] & (\text{if } l_j \geq 2 \text{ and } h_i = 1)\,, \\ \left[\begin{array}{c|c} 0_{(l_j-1)\times 1} & 0_{(l_j-1)\times(h_i-1)} \\ \hline d_{ji} & 0_{1\times(h_i-1)} \end{array}\right] & (\text{otherwise})\,, \end{cases} \tag{2.13}$$

$$\hat{B} = \left[\begin{array}{cccc} \hat{B}^0 & \hat{B}^0 & \cdots & \hat{B}^0 \\ \hline \tilde{B}_1 & \tilde{B}_2 & \cdots & \tilde{B}_m \\ \hline \hat{b}_{11} & \hat{b}_{10} & \cdots & \hat{b}_{10} \\ \hat{b}_{20} & \hat{b}_{21} & \cdots & \hat{b}_{20} \\ \vdots & \vdots & \ddots & \vdots \\ \hat{b}_{m0} & \hat{b}_{m0} & \cdots & \hat{b}_{m1} \end{array}\right], \quad \hat{B}^0 = \begin{cases} \phi & (\text{if } L = 0), \\ 0_{L\times 1} & (\text{otherwise}), \end{cases} \tag{2.14}$$

$$\tilde{B}_i = \begin{cases} B_i & (\text{if } h_i = 0)\,, \\ 0_{n\times 1} & (\text{otherwise})\,, \end{cases} \quad \hat{b}_{ik} = \begin{cases} \phi & (\text{if } h_i = 0)\,, \\ k & (\text{if } h_i = 1)\,, \\ \left[\begin{array}{c} 0_{(h_i-1)\times 1} \\ k \end{array}\right] & (\text{otherwise})\,, \end{cases} \tag{2.15}$$

$$\hat{C} = \left[\begin{array}{cccc|c|c} \hat{c}_{11} & \hat{c}_{10} & \cdots & \hat{c}_{10} & \tilde{C}_1 & \hat{C}^0 \\ \hat{c}_{20} & \hat{c}_{21} & \cdots & \hat{c}_{20} & \tilde{C}_2 & \hat{C}^0 \\ \vdots & \vdots & \ddots & \vdots & \vdots & \vdots \\ \hat{c}_{p0} & \hat{c}_{p0} & \cdots & \hat{c}_{p1} & \tilde{C}_p & \hat{C}^0 \end{array}\right], \quad \hat{c}_{jk} = \begin{cases} \phi & (\text{if } l_j = 0)\,, \\ k & (\text{if } l_j = 1)\,, \\ \left[\begin{array}{cc} k & 0_{1\times(l_j-1)} \end{array}\right] & (\text{otherwise})\,, \end{cases} \tag{2.16}$$

$$\tilde{C}_j = \begin{cases} C_j & (\text{if } l_j = 0)\,, \\ 0_{1\times n} & (\text{otherwise})\,, \end{cases} \quad \hat{C}^0 = \begin{cases} \phi & (\text{if } H = 0), \\ 0_{1\times H} & (\text{otherwise}), \end{cases} \tag{2.17}$$

$$\hat{D} = \begin{bmatrix} \tilde{d}_{11} & \tilde{d}_{12} & \cdots & \tilde{d}_{1m} \\ \tilde{d}_{21} & \tilde{d}_{22} & \cdots & \tilde{d}_{2m} \\ \vdots & \vdots & \ddots & \vdots \\ \tilde{d}_{p1} & \tilde{d}_{p2} & \cdots & \tilde{d}_{pm} \end{bmatrix}, \quad \tilde{d}_{ji} = \begin{cases} d_{ji} & (\text{if } l_j = h_i = 0)\,, \\ 0 & (\text{otherwise})\,. \end{cases} \tag{2.18}$$

In those equations, B_i for $i = 1, \cdots, m$ are the i-th column vectors of the matrix B, C_j for $j = 1, \cdots, p$ are the j-th row vectors of the matrix C and d_{ji} are the (j, i) elements of the matrix D. In addition, I_n is the n-th order identity matrix and $0_{i\times j}$ is an $i \times j$ zero matrix. In this augmented system, the input and output sequences respectively coincide with U and Y under a certain initial condition $\hat{x}(0)$. The order of the augmented system is $(L + n + H)$. Therefore, the order becomes enormous when the system includes large delays.

For this system, we can apply existing subspace identification methods [15] and identify the system matrices $(\hat{A}, \hat{B}, \hat{C}, \hat{D})$ of the augmented system. However, these methods sometimes produce an inaccurate result if the size of the system matrices is large, for

the reason that the numerical accuracy of computation decreases with increasing matrix size. We require another method to identify an accurate model of such a system.

On the other hand, we can identify an accurate model of the delay-free part using existing identification methods if the lengths of the delays are known in advance. Therefore, the author proposes a novel method that separately identifies the lengths of the delays and system matrices of the delay-free part. Using this method, we would obtain a more accurate model than that obtained using existing identification methods for augmented systems.

2.2.2 Estimation of the impulse response matrix

For estimating the impulse response matrix from input and output sequences, we can apply a standard prediction error method [24] after having prefiltered the input and output sequences so that the input sequence becomes "as white as possible" [24]. This method produces an adequate result when the data sequences are sufficiently long. However, when the data sequences are short and the system has poles close to one, this method produces an inaccurate result because an impulse response matrix that is approximated by limited sequences has a large truncation error. Furthermore, the initial state of the delay-free part perturbs the result.

To eliminate these defects, a novel method for estimation of the impulse response matrix is proposed, based on the ordinary Multivariable Output Error State sPace (MOESP) method [19]. In this method, the output sequence is decomposed into two subspaces: one spanned by the input sequence and the other orthogonal to that. This decomposition enables us to eliminate the effect of the initial state of the delay-free part. This estimation method consists of four steps: the LQ-decomposition of a matrix consisting of input and output sequences, the singular value decomposition of the decomposed matrix, computation of least-square estimates, and calculation of the impulse response matrix. In the following, details of the steps are given.

First, the LQ-decomposition of a matrix consisting of block Hankel matrices of the input and output is calculated. The block Hankel matrices of the input and output are given as

$$U_{0|k} = \begin{bmatrix} U_0^{\mathrm{T}} & U_1^{\mathrm{T}} & \cdots & U_k^{\mathrm{T}} \end{bmatrix}^{\mathrm{T}},\ Y_{0|k} = \begin{bmatrix} Y_0^{\mathrm{T}} & Y_1^{\mathrm{T}} & \cdots & Y_k^{\mathrm{T}} \end{bmatrix}^{\mathrm{T}}, \tag{2.19}$$

$$U_i = \begin{bmatrix} u(i) & u(i+1) & \cdots & u(i+N_0-k) \end{bmatrix} \quad (i = 0, \cdots, k), \tag{2.20}$$

$$Y_j = \begin{bmatrix} y(j) & y(j+1) & \cdots & y(j+N_0-k) \end{bmatrix} \quad (j = 0, \cdots, k), \tag{2.21}$$

for an integer k satisfying $(n + H + L) < k \leq (N_0 - p - m + 1)/(p + m + 1)$. The columns of these block Hankel matrices are more numerous than their rows because the inequality (2.4) holds. Moreover, the block Hankel matrix $U_{0|k}$ has a full row rank because the input sequence satisfies the PE condition. Furthermore, these block Hankel matrices satisfy

$$Y_{0|k} = \hat{\mathcal{O}}_k \hat{X}_0 + \hat{\Psi}_k U_{0|k}, \tag{2.22}$$

where $\hat{X}_0 = [\hat{x}(0)\ \hat{x}(1)\ \cdots\ \hat{x}(N_0-k)]$,

$$\hat{\mathcal{O}}_k = \begin{bmatrix} \hat{C} \\ \hat{C}\hat{A} \\ \vdots \\ \hat{C}\hat{A}^{k-1} \end{bmatrix}, \quad \hat{\Psi}_k = \begin{bmatrix} \hat{D} & 0_{m\times p} & \cdots & 0_{m\times p} \\ \hat{C}\hat{B} & \hat{D} & \ddots & \vdots \\ \vdots & \ddots & \ddots & 0_{m\times p} \\ \hat{C}\hat{A}^{k-2}\hat{B} & \cdots & \hat{C}\hat{B} & \hat{D} \end{bmatrix}. \tag{2.23}$$

Using these block Hankel matrices, the LQ-decomposition is calculated as

$$\begin{bmatrix} U_{0|k} \\ Y_{0|k} \end{bmatrix} = \begin{bmatrix} L_{11} & 0_{(k+1)m\times(k+1)p} \\ L_{21} & L_{22} \end{bmatrix} \begin{bmatrix} Q_1^{\mathrm{T}} \\ Q_2^{\mathrm{T}} \end{bmatrix}. \tag{2.24}$$

Here, L_{11} and L_{22} are $(k+1)m \times (k+1)m$ and $(k+1)p \times (k+1)p$ lower triangular matrices, respectively, and L_{21} is a $(k+1)p\times(k+1)m$ matrix, Q_1^{T} and Q_2^{T} are, respectively, $(k+1)m\times(N_0-k+1)$ and $(k+1)p\times(N_0-k+1)$ matrices. The matrix L_{11} is nonsingular because $U_{0|k}$ has full row rank. Moreover, the matrix $[Q_1\ Q_2]$ is an orthogonal matrix. Using Eq. (2.24), we have

$$Q_1^{\mathrm{T}} = L_{11}^{-1}U_{0|k}, \tag{2.25}$$

and

$$Y_{0|k} = L_{21}L_{11}^{-1}U_{0|k} + L_{22}Q_2^{\mathrm{T}}. \tag{2.26}$$

Using Eqs. (2.22), (2.25) and (2.26), we find that

$$\hat{\mathcal{O}}_k\hat{X}_0 + \hat{\Psi}_k L_{11}Q_1^{\mathrm{T}} = L_{21}Q_1^{\mathrm{T}} + L_{22}Q_2^{\mathrm{T}}. \tag{2.27}$$

Multiplying Q_2 from the right side of Eq. (2.27), we obtain $\hat{\mathcal{O}}_k\hat{X}_0Q_2 = L_{22}$.

Second, a singular value decomposition of the matrix L_{22} is calculated as

$$L_{22} = [U_1\ U_2]\begin{bmatrix} \Sigma_1 & 0 \\ 0 & \Sigma_2 \end{bmatrix}\begin{bmatrix} V_1^{\mathrm{T}} \\ V_2^{\mathrm{T}} \end{bmatrix} = U_1\Sigma_1V_1^{\mathrm{T}}, \tag{2.28}$$

where Σ_1 is a $\tilde{n}\times\tilde{n}$ diagonal matrix, Σ_2 is a $((k+1)p-\tilde{n})\times((k+1)p-\tilde{n})$ zero matrix, U_1, U_2, V_1 and V_2 are $(k+1)p\times\tilde{n}$, $(k+1)p\times((k+1)p-\tilde{n})$, $(k+1)p\times\tilde{n}$ and $(k+1)p\times((k+1)p-\tilde{n})$ matrices, respectively, and $\tilde{n}$ is the number of nonzero singular values of L_{22}. Using this singular value decomposition, we obtain an estimate $\tilde{\mathcal{O}}_k$ of matrix $\hat{\mathcal{O}}_k$ as $\tilde{\mathcal{O}}_k = U_1\Sigma_1^{1/2}$, which is similar to the ordinary MOESP method.

Third, the estimates of the matrices $\hat{B}$ and $\hat{D}$ are calculated from U_2, L_{21} and L_{11}. Multiplying U_2^{T} from the left side of Eq. (2.27), we obtain

$$U_2^{\mathrm{T}}\hat{\Psi}_k L_{11}Q_1^{\mathrm{T}} = U_2^{\mathrm{T}}L_{21}Q_1^{\mathrm{T}}, \tag{2.29}$$

because $U_2^{\mathrm{T}} L_{22} = U_2^{\mathrm{T}} U_1 \Sigma_1 V_1^{\mathrm{T}} = 0$ and $U_2^{\mathrm{T}} \hat{\mathcal{O}}_k = U_2^{\mathrm{T}} U_1 \Sigma_1^{1/2} = 0$. Multiplying $Q_1 L_{11}^{-1}$ from the right side of Eq. (2.29), we have

$$U_2^{\mathrm{T}} \begin{bmatrix} \hat{D} & 0_{m\times p} & \cdots & 0_{m\times p} \\ \hat{C}\hat{B} & \hat{D} & \ddots & \vdots \\ \vdots & \ddots & \ddots & 0_{m\times p} \\ \hat{C}\hat{A}^{k-2}\hat{B} & \cdots & \hat{C}\hat{B} & \hat{D} \end{bmatrix} = U_2^{\mathrm{T}} L_{21} L_{11}^{-1}. \tag{2.30}$$

Using the least squares method, we can estimate $\hat{B}$ and $\hat{D}$ using

$$\begin{bmatrix} \tilde{D} \\ \tilde{B} \end{bmatrix} = \begin{bmatrix} \mathcal{L}_1 & \bar{\mathcal{L}}_2 \tilde{\mathcal{O}}_k[1:kp] \\ \mathcal{L}_2 & \bar{\mathcal{L}}_3 \tilde{\mathcal{O}}_k[1:(k-1)p] \\ \vdots & \vdots \\ \mathcal{L}_k & \bar{\mathcal{L}}_{k+1} \tilde{\mathcal{O}}_k[1:p] \\ \mathcal{L}_{k+1} & 0_{(pk+p-\tilde{n})\times\tilde{n}} \end{bmatrix}^{\dagger} \begin{bmatrix} \mathcal{M}_1 \\ \mathcal{M}_2 \\ \vdots \\ \mathcal{M}_k \\ \mathcal{M}_{k+1} \end{bmatrix}. \tag{2.31}$$

Here, $\mathcal{L}_i$, $\bar{\mathcal{L}}_i$ and $\mathcal{M}_i$ for $i = 1, \cdots, k+1$ are $(pk+p-\tilde{n}) \times p$, $(pk+p-\tilde{n}) \times (pk+2p-pi)$ and $(pk+p-\tilde{n}) \times m$ matrices given, respectively, as

$$[\mathcal{L}_1 \ \cdots \mathcal{L}_{k+1}] = U_2^{\mathrm{T}}, \tag{2.32}$$

$$\bar{\mathcal{L}}_i = [\mathcal{L}_i \ \cdots \ \mathcal{L}_{k+1}], \tag{2.33}$$

$$[\mathcal{M}_1 \cdots \mathcal{M}_{k+1}] = U_2^{\mathrm{T}} L_{21} L_{11}^{-1}, \tag{2.34}$$

where $\tilde{\mathcal{O}}_k[k_1 : k_2]$ is a matrix constructed from the k_1-th to the k_2-th rows of the matrix $\tilde{\mathcal{O}}_k$. Furthermore, $X^{\dagger}$ signifies the Moore-Penrose pseudo-inverse of the matrix X.

Fourth, we obtain an estimate of the impulse response matrix using the matrices $\tilde{\mathcal{O}}_k$, $\tilde{D}$, and $\tilde{B}$, by

$$\tilde{G}(t) = \begin{cases} \tilde{D}, & t = 0, \\ \tilde{\mathcal{O}}_k[(t-1)p+1 : tp]\tilde{B}, & t = 1, \cdots, k, \end{cases} \tag{2.35}$$

because $\tilde{\mathcal{O}}_k[(t-1)p+1 : tp]$ is an estimate of $\hat{C}\hat{A}^{t-1}$ and the impulse response matrix $\hat{G}(t)$ of the augmented system $(\hat{A}, \hat{B}, \hat{C}, \hat{D})$ is given as

$$\hat{G}(t) = \begin{cases} \hat{D}, & t = 0, \\ \hat{C}\hat{A}^{t-1}\hat{B}, & t = 1, \cdots, k. \end{cases} \tag{2.36}$$

The only procedural difference between our method and the ordinary MOESP method is the forth step. In our method, the impulse response matrix $\tilde{G}(t)$ is estimated from the matrices $\tilde{\mathcal{O}}_k$, $\tilde{D}$ and $\tilde{B}$. In contrast, in the ordinary MOESP method, the matrices $\hat{A}$ and $\hat{C}$ are estimated from $\tilde{\mathcal{O}}_k$ using

$$\tilde{A} = \left\{\tilde{\mathcal{O}}_k[1:(k-1)p]\right\}^{\dagger} \tilde{\mathcal{O}}_k[p+1:kp], \quad \tilde{C} = \tilde{\mathcal{O}}_k[1:p]. \tag{2.37}$$

We can estimate the impulse response matrix by Eq. (2.36) using the system matrices $(\tilde{A}, \tilde{B}, \tilde{C}, \tilde{D})$ identified using the ordinary MOESP method. However, this impulse response matrix is inaccurate because Eq. (2.36) accumulates the estimation error of the matrix $\tilde{A}$. On the other hand, this cumulative error does not appear in Eq. (2.35). Therefore, Eq. (2.35) is more suitable for estimation of the impulse response matrix than Eq. (2.36) with matrices $(\tilde{A}, \tilde{B}, \tilde{C}, \tilde{D})$ identified using the ordinary MOESP method.

2.2.3 Estimation of input and output delays

In this subsection, a method is described for estimation of the input delays h_i for $i = 1, \cdots, m$ and the output delays l_j for $j = 1, \cdots, p$.

A delay whose length is $(h_i + l_j)$ exists between the i-th input and the j-th output. We can obtain the estimate of $(h_i + l_j)$ as the length of zero response time of the impulse response $g_{ji}(t)$ of the j-th output to the i-th input. The maximal possible value of $(h_i + l_j)$ is obtained from $g_{ji}(t)$, which is the (j, i) element of $\tilde{G}(t)$, as the integer δ_{ji} which satisfies

$$\begin{cases} g_{ji}(t) = 0, & t = 0, 1, \cdots, \delta_{ji} - 1, \\ g_{ji}(t) \neq 0, & t = \delta_{ji}, \delta_{ji} + 1, \cdots. \end{cases} \tag{2.38}$$

Next we divide the delay $(h_i + l_j)$ into the input delay h_i and the output delay l_j. Let us remind the assumption that the minimum input delay $\min_i(h_i)$ is zero. Therefore, we can obtain estimates $\tilde{l}_j$ and $\tilde{h}_i$ of the output and input delays, respectively, as $\tilde{l}_j = \min_i(\delta_{ji})$ and $\tilde{h}_i = \min_j(\delta_{ji} - \tilde{l}_j)$.

2.2.4 Identification of system matrices

In this subsection, we identify the system matrices of the delay-free part. We can estimate the input and output sequences of the delay-free part by receding and advancing the original input and output sequences, respectively, using the estimated delays. These sequences enable us to identify the system matrices (A, B, C, D) of the delay-free part.

The input and output sequences of the delay-free part are given as

$$\tilde{U} = \begin{bmatrix} u_1(\tilde{H}_1) & \cdots & u_1(\tilde{H}_1 + \tilde{N}_0) \\ \vdots & \ddots & \vdots \\ u_m(\tilde{H}_m) & \cdots & u_m(\tilde{H}_m + \tilde{N}_0) \end{bmatrix}, \; \tilde{Y} = \begin{bmatrix} y_1(\tilde{H} + \tilde{l}_1) & \cdots & y_1(\tilde{H} + \tilde{l}_1 + \tilde{N}_0) \\ \vdots & \ddots & \vdots \\ y_p(\tilde{H} + \tilde{l}_p) & \cdots & y_p(\tilde{H} + \tilde{l}_p + \tilde{N}_0) \end{bmatrix}, \tag{2.39}$$

where $\tilde{H} = \max_i(\tilde{h}_i)$, $\tilde{H}_i = \tilde{H} - \tilde{h}_i$, and $\tilde{N}_0 = (N_0 - \tilde{H} - \max_j(\tilde{l}_i))$. Using these block Hankel matrices, the system matrices (A, B, C, D) of the delay-free part are identified using the ordinary MOESP method.

Following the procedure described above, we can estimate the input and output delays h_i and l_j from the input and output sequences U and Y, and identify the system matrices

(A, B, C, D) of the delay-free part. This identification method is a solution method of the **Problem**. In the next section, a numerical example is presented to illustrate the superiority of the proposed method.

2.3 Numerical example

Consider a two-input two-output second order system whose input and output paths have different time delays

$$A = \begin{bmatrix} 0.87 & -0.10 \\ 0.04 & 1.02 \end{bmatrix}, \quad B = \begin{bmatrix} 0.9 & 0.2 \\ 0.7 & -0.9 \end{bmatrix}, \quad C = I_2, \quad D = \begin{bmatrix} 1.1 & 0.1 \\ 0.6 & -0.9 \end{bmatrix},$$
$$(h_1, h_2, l_1, l_2) = (0, 17, 31, 19). \tag{2.40}$$

The inputs to the system are mutually uncorrelated white noise with zero mean and variance 1. The initial state of the delay-free part $x(0)$ is given by mutually uncorrelated random real numbers with zero mean and variance 10. Moreover, the output sequence is perturbed by mutually uncorrelated white noise with zero mean and variance 0.3. The data length (N_0+1) is set to 360. Under these conditions, 10 data sequences of the input and output are generated using `MATLAB` random number generator *randn* with different seeds. The results are shown by impulse response matrices of the identified models to examine the delay estimation validity.

First we show in Fig. 2.2 the impulse response matrices $\tilde{G}(t)$ (Eq. (2.35)) for delay estimation in the proposed method. In the identification procedure, size k of the block Hankel matrices is set to $k = 70$, which is larger than the sum of the system order and the delay lengths. A diagonal matrix of the singular value decomposition Eq. (2.28) is divided to Σ_1 and Σ_2 to satisfy $\sigma_{\min}(\Sigma_1) > 0.004\sigma_{\max}(\Sigma_1) \geq \sigma_{\max}(\Sigma_2)$. Here, $\sigma_{\max}(X)$ and $\sigma_{\min}(X)$ respectively signify the maximum and the minimum of the diagonal elements of the matrix X. In Fig. 2.2, we can obtain accurate estimates $(\tilde{h}_1, \tilde{h}_2, \tilde{l}_1, \tilde{h}_2) = (0, 17, 19, 31)$ of the delay lengths in all 10 cases when we regard $g_{ji}(t)$ in Eq. (2.38) as 0 if $|g_{ji}(t)| < 0.15$.

Using these delay estimates, system matrices of the delay-free part are identified. Impulse response matrices of the identified models are shown in Fig. 2.3. As presented in Fig. 2.3, we can conclude that accurate models were obtained for all sets of input and output sequences.

Next, a comparison with the existing identification methods is made. Fig. 2.4 represents the impulse response matrices estimated using the standard least squares method implemented in `MATLAB`'s *impulse* function [24]. Using Fig. 2.4, we find that the lengths of the delays cannot be estimated accurately because the dominant pole of the system is close to 1 and the data sequence is short.

Fig. 2.5 shows the impulse response matrices of the augmented system estimated using the ordinary MOESP method implemented in `MATLAB`'s *n4sid* function [24]. In Fig. 2.5, we can appropriately estimate the lengths of the delays aggregating all impulse

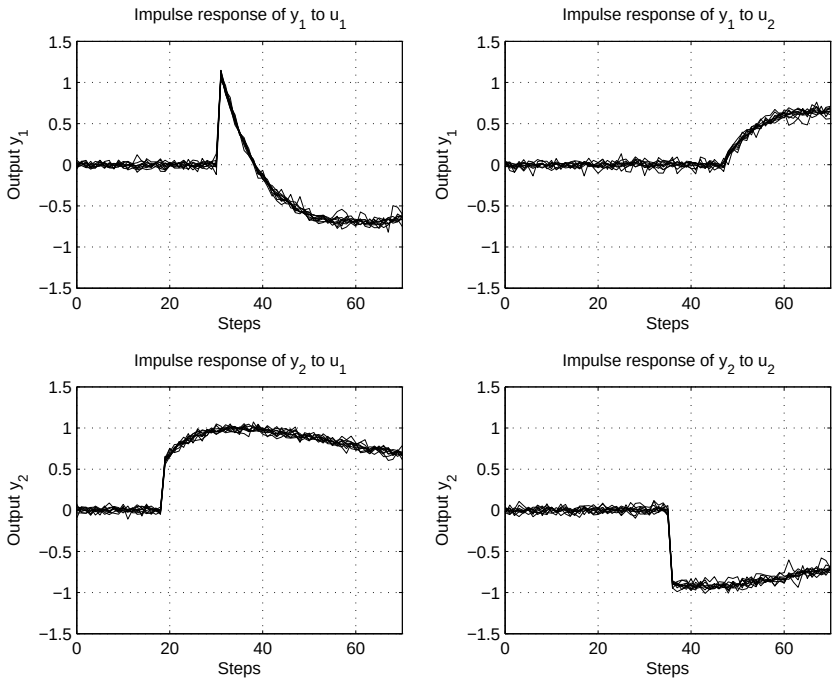

Figure 2.2: Impulse response matrices calculated from input and output sequences for delay estimation (10 cases)

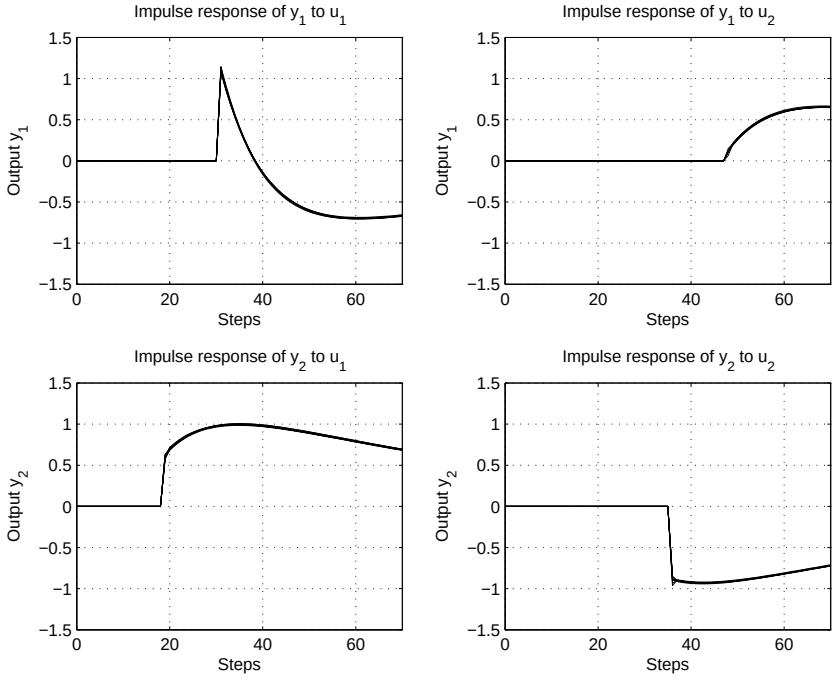

Figure 2.3: Impulse response matrices identified using the proposed method (10 cases)

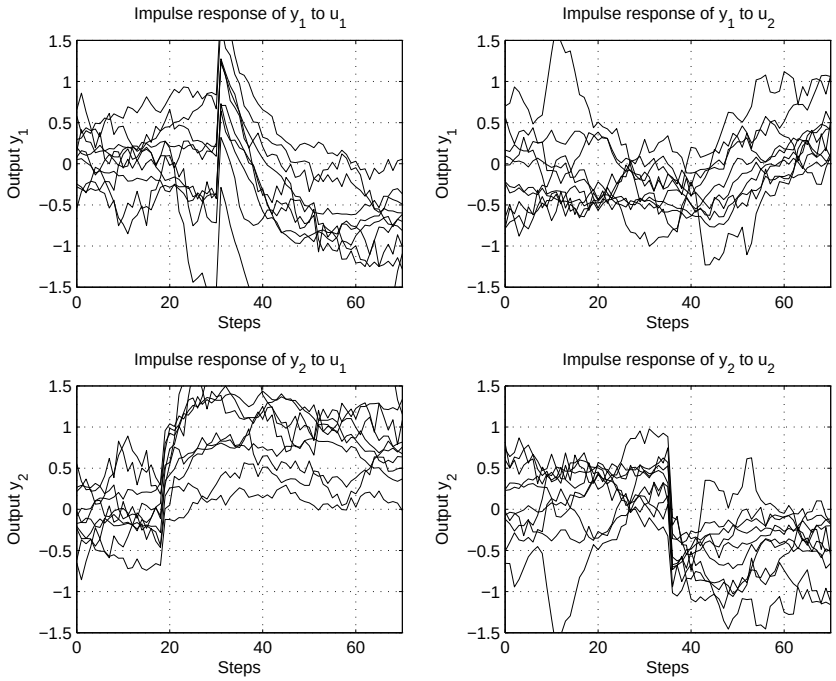

Figure 2.4: Impulse response matrices identified using the least squares method (10 cases)

response matrices. However, it is difficult to obtain an accurate result as obtained using the proposed method from one particular set of input and output sequences.

2.4 Concluding remarks

In this chapter, a subspace identification method is proposed for multivariable systems whose input and output paths have different time delays. The proposed method estimates the length of the delays from an impulse response matrix calculated from input and output sequences using a subspace method. Then the system matrices of the delay-free part are identified from the input and output sequences of the delay-free part rearranged from the original input and output sequences. The proposed method requires no complex nonlinear optimization procedure, nor does it require an assumption about the structure of the delay-free part. A numerical example demonstrates the superiority of the proposed method. The proposed method can be extended to identification of similar time delay systems whose delay-free part is a stochastic system with exogenous inputs. For identification of a closed-loop system, important modifications are required.

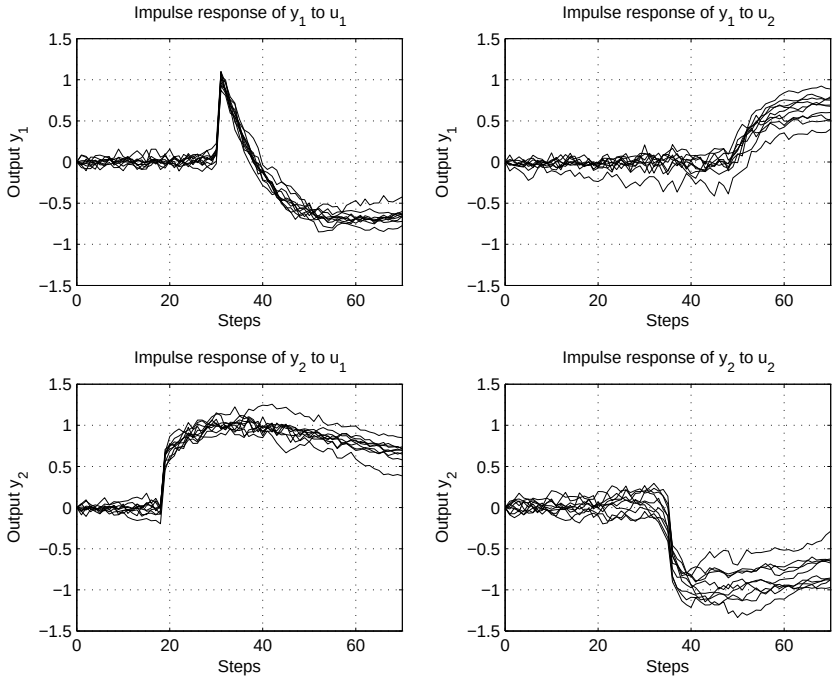

Figure 2.5: Impulse response matrices of the augmented system identified using the ordinary MOESP method (10 cases)

Chapter 3

A state predictor for multivariable systems whose input and output paths have different time delays

In this chapter, we investigate a state prediction problem for linear time-invariant multivariable systems whose input and output paths have different time delays. For controlling these systems, we may apply a traditional state feedback control designed for the delay-free part, if the information of current state of their delay-free part is available. The information of current state is also useful for analysis of these systems, such as failure detection and decision making. Therefore this state prediction problem is important.

Until now, some state predictors have been proposed for time delay systems [2, 9, 26, 27]. For systems with output delays, most of them [9, 26, 27] have utilized the duality of the state prediction and state feedback for systems with input delays, using the well-known finite spectrum assignment method [6]. One practical design method based on this approach is given in [9]. This method introduces a finite interval integration which compensates the effect of delays on the input side of a conventional observer. Hereafter we regard this observer as the delay-compensating observer. This observer can be applied not only to systems investigated in this chapter but also to a wider class of systems with input and output delays. However, this observer shows bad performance in some practical situations due to errors of the numerical integration. Therefore the author has developed a novel state predictor for systems whose input and output paths have different time delays, because such systems are frequently encountered in practice.

The key idea in developing the novel state predictor is reducing the error caused by the finite interval integration. The delay-compensating observer performs integration over an interval equal to the maximum length of the delays. The integrated value is fed to the state equation of the observer. In order to reduce the error, we shorten the interval of the integration placed in the input side of the observer by allocating part of the integration to the output equation of the predictor. A numerical example of an unstable plant is given to illustrate the properties and advantages of the proposed state

predictor.

This chapter is organized as follows. Section 3.1 gives the description of target systems and formulates a problem we investigate. In Section 3.2, the author proposes a state predictor for multivariable systems whose input and output paths have different time delays. Comparison with the delay-compensating observer [9] is also made. Finally, numerical examples are given to show the superiority of the proposed predictor in Section 3.3.

3.1 Problem formulation

We consider an m-input p-output system (Fig. 3.1) whose output paths have different time delays:

$$\frac{dx(t)}{dt} = Ax(t) + Bu(t), \tag{3.1}$$

$$y^A(t) = \begin{bmatrix} y_1^A(t) \\ \vdots \\ y_p^A(t) \end{bmatrix} = Cx(t), \tag{3.2}$$

$$y(t) = \begin{bmatrix} y_1(t) \\ \vdots \\ y_p(t) \end{bmatrix} = \begin{bmatrix} y_1^A(t - L_1) \\ \vdots \\ y_p^A(t - L_p) \end{bmatrix}, \tag{3.3}$$

where $x(t) \in R^n$ is a state vector, $u(t) \in R^m$ is an input vector, $y^A(t) \in R^p$ is an output vector of the delay-free part of the system, $y_i^A(t)$ for $i = 1, \cdots, p$ are the i-th scalar elements of $y^A(t)$, $y(t)$ is an output vector, $y_i(t)$ for $i = 1, \cdots, p$ are the i-th scalar elements of $y(t)$, $A \in R^{n \times n}$, $B \in R^{n \times m}$ and $C \in R^{p \times n}$ are constant matrices, and L_i for $i = 1, \cdots, p$ are non-negative output delays in the i-th output path, and satisfy $0 \leq L_1 \leq L_2 \leq \cdots \leq L_p$ without loss of generality. The input to the system can include delays, because we require only the past values of the input to the delay-free part for prediction of the current state $x(t)$. Therefore we refer to the input to the delay-free part as the input $u(t)$ for simplicity of notation. Measurable disturbances can also be handled by $u(t)$ in Eq. (3.1).

For this system, we assume that the following inequalities hold:

$$\text{rank}\,\{\text{obsv}(C_1, A)\} < \text{rank}\,\{\text{obsv}(C_2, A)\} < \cdots < \text{rank}\,\{\text{obsv}(C_p, A)\} = n, \tag{3.4}$$

where $\text{obsv}(C_i, A)$ for $i = 1, \cdots, p$ are the observability matrices of (C_i, A), namely $\text{obsv}(C_i, A) = \begin{bmatrix} C_i^{\mathrm{T}} & (C_iA)^{\mathrm{T}} & \cdots & (C_iA^{n-1})^{\mathrm{T}} \end{bmatrix}^{\mathrm{T}}$, and C_i for $i = 1, \cdots, p$ are $i \times n$ matrices consisting of the first i rows of C. Note that $C_p = C$ and the last equation of (3.4) means that the pair (C, A) is observable. The assumption (3.4) means that the unobservable subspace from up to the i-th output is larger than that from up to the $(i+1)$-st output for $i = 1, \cdots, p-1$.

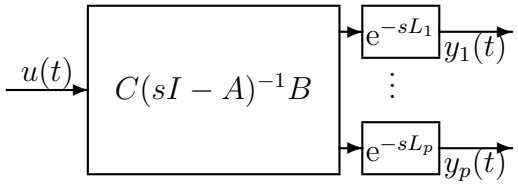

Figure 3.1: Output time delay system

Under this assumption[1], the following proposition holds.

Proposition 3.1 (Wonham [28]) The system (3.1)–(3.3) can be transformed to

$$\frac{dx_i(t)}{dt} = \sum_{j=1}^{i} A_{ij}x_j(t) + B_i u(t), \quad (i = 1, \cdots, p), \tag{3.5}$$

$$y_i(t) = C_{ii}x_i(t - L_i), \quad (i = 1, \cdots, p), \tag{3.6}$$

with a coordinate transformation

$$\left[\begin{array}{ccc} x_1(t)^{\mathrm{T}} & \cdots & x_p(t)^{\mathrm{T}} \end{array}\right]^{\mathrm{T}} = Tx(t). \tag{3.7}$$

Here, $x_i(t)$ for $i = 1, \cdots, p$ are n_i-dimensional column vectors where n_i for $i = 1, \cdots, p$ are positive integers given by

$$n_1 = \mathrm{rank}\left\{\mathrm{obsv}(C_1, A)\right\}, \tag{3.8}$$

$$n_i = \mathrm{rank}\left\{\mathrm{obsv}(C_i, A)\right\} - \sum_{j=1}^{i-1} n_j, \quad i = 2, \cdots, p. \tag{3.9}$$

The matrices $A_{ii} \in R^{n_i \times n_i}$ and $C_{ii} \in R^{1 \times n_i}$ are given by

$$A_{ii} = \left[\begin{array}{ccccc} 0 & 0 & \cdots & 0 & \alpha_1^{i,i} \\ 1 & 0 & \cdots & 0 & \alpha_2^{i,i} \\ 0 & 1 & \ddots & \vdots & \vdots \\ \vdots & \ddots & \ddots & 0 & \alpha_{n_i-1}^{i,i} \\ 0 & \cdots & 0 & 1 & \alpha_{n_i}^{i,i} \end{array}\right], \quad C_{ii} = \left[\begin{array}{cccc} 0 & \cdots & 0 & 1 \end{array}\right]. \tag{3.10}$$

The matrices A_{ij} for $i = 2, \cdots, p$ and $j = 1, \cdots, i-1$ have dimension $n_i \times n_j$. The matrix T is obtained by the following procedure.

[1]It may seem that the assumption (3.4) is rather restrictive. However, when the i-th inequality of the assumption (3.4) is not satisfied, we do not require the $(i+1)$-st output for state prediction and may omit that output, which does not shrink the unobservable subspace and includes only "past" information about the state of the delay-free part. Following this argument, the i-th inequality sign in (3.4) is relaxed to non-strict when the delay lengths of i-th and $(i+1)$-st output are the same, by treating the i-th and $(i+1)$-st outputs as a single block.

1. For $k = 1, \cdots, n_1$, let $\alpha_k^{1,1}$ to satisfy

$$c_1 A^{n_1} = a_1^{1,1} c_1 + a_2^{1,1} c_1 A + \cdots + a_{n_1}^{1,1} c_1 A^{n_1 - 1}, \tag{3.11}$$

where c_1 is the first row vector of C. Introduce vectors

$$\begin{aligned} e_{n_1} &= c_1, & (3.12)\\ e_{n_1 - k} &= e_{n_1 - k + 1} A - a_{n_1 - k + 1}^{1,1} c_1 \quad (k = 1, \cdots, n_1 - 1). & (3.13) \end{aligned}$$

Let $i = 2$.

2. Let $q = n_1 + \cdots + n_{i-1}$. For $j = 1, \cdots, i$ and $k = 1, \cdots, n_j$, let $\alpha_k^{j,i}$ to satisfy

$$\begin{aligned} c_i A^{n_i} &= a_1^{1,i} e_1 + \cdots + a_{n_1}^{1,i} e_{n_1} + \cdots + a_1^{i-1,i} e_{n_1 + \cdots + n_{i-2} + 1} + \cdots + a_{n_i - 1}^{i-1,i} e_q \\ &\quad + a_1^{i,i} c_i + a_2^{i,i} c_i A + \cdots + a_{n_i}^{i,i} c_i A^{n_i - 1}, \end{aligned} \tag{3.14}$$

where c_i is the i-th row vector of C. Introduce vectors

$$\begin{aligned} e_{q + n_i} &= c_i, & (3.15)\\ e_{q + n_i - k} &= e_{q + n_i - k + 1} A - a_{n_i - k + 1}^{i,i} c_i \quad (k = 1, \cdots, n_i - 1). & (3.16) \end{aligned}$$

Repeat this step for $i = 3, \cdots, p$.

3. The matrix T is given by $T = \begin{bmatrix} e_1^{\mathrm{T}} & \cdots & e_n^{\mathrm{T}} \end{bmatrix}^{\mathrm{T}}$.

Using this proposition, the matrices A and C are transformed into a block lower triangular matrix and a block diagonal matrix, respectively. Without loss of generality, we employ the transformed system matrices in the following sections. Namely, A, B and C in Eqs. (3.1) and (3.2) are given as follows:

$$A = \begin{bmatrix} A_{11} & & 0 \\ \vdots & \ddots & \\ A_{p1} & \cdots & A_{pp} \end{bmatrix}, \; B = \begin{bmatrix} B_1 \\ \vdots \\ B_p \end{bmatrix}, \; C = \begin{bmatrix} C_{11} & & 0 \\ & \ddots & \\ 0 & & C_{pp} \end{bmatrix}. \tag{3.17}$$

A block diagram of the transformed system with three outputs is shown in Fig. 3.2.

For this class of systems, we consider a problem for constructing a state predictor as follows:

Problem 3.1. *Given the past values of the input $u(\tau)$, $\tau < t$ and the observations of the output $y(\tau)$, $\tau \leq t$, find an asymptotic estimate $\hat{x}(t)$ of the current state $x(t)$.*

As mentioned above, the input delays do not complicate this state prediction problem. However, closed-loop control problem of systems whose input paths have different time delays is not so straightforward, because an appropriate controller requires predicted values of the future state determined by future input. In this chapter, we only argues the state prediction problem. The result cannot be applied directly to the closed-loop control problem of systems whose input paths have different delays.

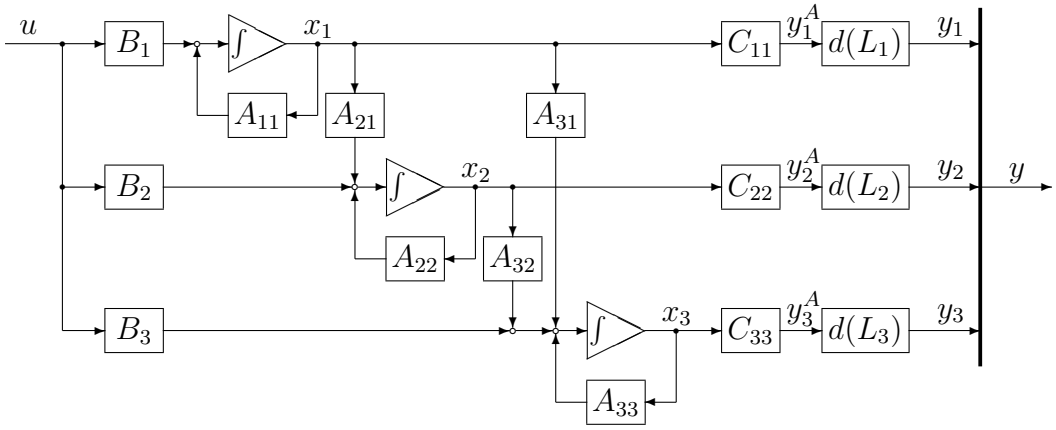

The block $d(L_i)$ means a delay whose length is L_i.

Figure 3.2: Block diagram of transformed system ($p = 3$).

3.2 A novel state predictor

In this section, the author proposes a novel state predictor. The proposed predictor consists of a full-order observer and a prediction mechanism. Figure 3.3 is a schematic diagram of action of the predictor for a system with three outputs. Because the output $y_i(t)$ includes information of a past state $x(t-L_i)$, the observer estimates the partial state x_i at the past time point $(t-L_i)$ as $\tilde{x}_i(t)$. Second, the prediction mechanism predicts the partial state x_i at the current time point as $\hat{x}_i(t)$, from the estimated partial state $\tilde{x}_i$ and the input u using a state transition equation. In Fig. 3.3, the term E_{ij} is a submatrix of a state transition matrix. The formula of E_{ij} is given in the following subsection. Both the observer and the prediction mechanism utilize block lower triangularity of the matrix A.

In the following, first we introduce a prediction mechanism to compute the current state under the assumption that the partial states at particular time points are directly obtained. Next, we give a full-order observer estimating the delayed partial states and construct a state predictor by combining the full-order observer and the prediction mechanism. Then we show that the prediction error of the predictor converges to zero at the rate according to arbitrarily assigned observer poles. Furthermore, we compare the proposed predictor with the delay-compensating observer [9] from the viewpoint integration intervals.

3.2.1 Computation of current state from past partial states

In this subsection, we give the computation algorithm that calculates the state $x(t)$ from the partial states $x_i(t-L_i)$ for $i = 1, \cdots, p$ and the input $u(t+\tau)$ for $\tau \in [-L_p, 0)$ using the state transition equation. First we introduce a lemma about the partial state x_i at the time $(t+\tau)$ for $\tau \leq 0$.

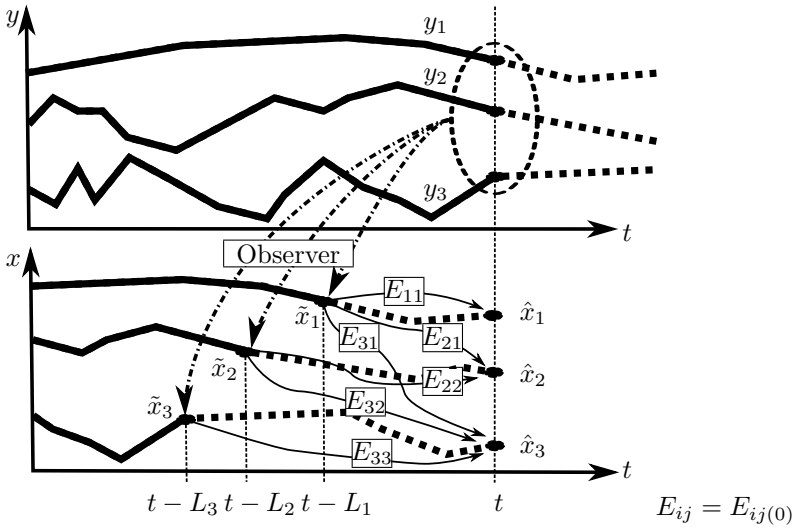

Figure 3.3: Schematic diagram of action of proposed predictor (p=3)

Lemma 3.1 Given the partial state $x_j(t-L_j)$ for $j=1,\cdots,i$ and the input $u(t+\xi)$ for $\xi \in [\min(\tau,-L_i), \max(-L_1,\tau))$, the partial state x_i for $i=1,\cdots,p$ at the time $(t+\tau)$ for $\tau \le 0$ are given by

$$x_i(t+\tau) = \sum_{j=1}^{i} E_{ij}(\tau)\left\{x_j(t-L_j) + \int_{-L_j}^{\tau} S_j(\xi)u(t+\xi)d\xi\right\}, \quad i=1,\cdots,p, \tag{3.18}$$

where $E_{ij}(\tau)$ and $S_j(\xi)$ are $n_i \times n_j$ and $n_j \times m$ matrices defined by

$$E_{ij}(\tau) = \begin{cases} \mathrm{e}^{A_{ii}(\tau+L_i)}, & i=1,\cdots,p;\ j=i, \\ \displaystyle\sum_{k=j}^{i-1}\int_{-L_i}^{\tau} \mathrm{e}^{A_{ii}(\tau-\lambda)}A_{ik}E_{kj}(\lambda)d\lambda, & i=2,\cdots,p;\ j=1,\cdots,i-1, \end{cases} \tag{3.19}$$

$$S_j(\xi) = \mathrm{e}^{-A_{jj}(L_j+\xi)}\left\{B_j - \sum_{k=1}^{j-1} E_{jk}(\xi)S_k(\xi)\right\}, \quad j=1,\cdots,p. \tag{3.20}$$

Proof. See Subsection 3.5.1.

The matrix $E_{ij}(\tau)$ is a submatrix of $\mathrm{e}^{A(\tau+L_j)}$. Namely, $E_{ij}(\tau)$ can be given by

$$E_{ij}(\tau) = \left[\begin{array}{ccc} 0_{n_i\times\hat{n}_i} & I_{n_i} & 0_{n_i\times(n-\hat{n}_{(i+1)})} \end{array}\right] \mathrm{e}^{A(\tau+L_j)} \left[\begin{array}{c} 0_{\hat{n}_j\times n_j} \\ I_{n_j} \\ 0_{(n-\hat{n}_{(j+1)}\times n_j)} \end{array}\right], \tag{3.21}$$

where $\hat{n}_i = \sum_{k=1}^{i-1} n_k$. The matrix $S_j(\xi)$ gives the state transition of $x_j(t-L_j)$ caused by $u(t+\xi)$. In another form, $S_j(\xi)$ can be given by

$$S_j(\xi) = \left[\begin{array}{ccc} 0_{n_j\times\hat{n}_j} & I_{n_j} & 0_{n_j\times(n-\hat{n}_{(j+1)})} \end{array}\right] \mathrm{e}^{-A(L_j+\xi)}B. \tag{3.22}$$

Substituting $\tau = 0$ into Eq. (3.18), we obtain partial states $x_i(t)$ for $i = 1, \cdots, p$ as

$$x_i(t) = \sum_{j=1}^{i} E_{ij}(0) \left\{ x_j(t - L_j) + \int_{-L_j}^{0} S_j(\xi) u(t + \xi) d\xi \right\}, \quad i = 1, \cdots, p. \tag{3.23}$$

We can rewrite the above equation using matrix representation as

$$x(t) = E \left\{ x^P(t) + S(u, t) \right\}. \tag{3.24}$$

Here, $x^P(t) = \left[\begin{array}{ccc} x_1^{\mathrm{T}}(t - L_1) & \cdots & x_p^{\mathrm{T}}(t - L_p) \end{array} \right]^{\mathrm{T}}$ is a vector consisting of past states, $E \in R^{n \times n}$ and $S(u, t) \in R^n$ are a constant matrix and a vector, respectively, defined by

$$E = \left[\begin{array}{ccc} E_{11}(0) & & 0 \\ \vdots & \ddots & \\ E_{p1}(0) & \cdots & E_{pp}(0) \end{array} \right], \; S(u, t) = \left[\begin{array}{c} \int_{-L_1}^{0} S_1(\xi) u(t + \xi) d\xi \\ \vdots \\ \int_{-L_p}^{0} S_p(\xi) u(t + \xi) d\xi \end{array} \right]. \tag{3.25}$$

The matrix E gives the state transition matrix that maps $x^P(t)$ to $x(t)$. Because A is block lower triangular, E is also block lower triangular. The vector $S(u, t)$ gives the effect of input on the state transition.

Using Eq.(3.24), we can compute the present state $x(t)$ from the vector $x^P(t)$ consisting of partial past states $x_i(t - L_i)$ and the input $u(t + \tau)$ for $\tau \in [-L_p, 0)$.

3.2.2 Estimation of past state from current output

Here we introduce a full-order observer to estimate the vector $x^P(t)$ from the output $y(t)$ and the input $u(t + \tau)$ for $\tau \in [-L_p, -L_1)$. The observer is given by

$$\frac{d\tilde{x}(t)}{dt} = (A^* - KC)\tilde{x}(t) + Ky(t) + B^*(u, t), \tag{3.26}$$

where $\tilde{x}(t)$ is an estimate of $x^P(t)$,

$$A^* = \left[\begin{array}{ccc} A_{11}^* & & 0 \\ \vdots & \ddots & \\ A_{p1}^* & \cdots & A_{pp}^* \end{array} \right], \tag{3.27}$$

$$A_{ij}^* = \sum_{k=j}^{i} A_{ik} E_{kj}(-L_i), \quad i = 1, \cdots, p; \; j = 1, \cdots, i, \tag{3.28}$$

$K \in R^{n \times p}$ is a gain matrix which assigns the eigenvalues of the matrix $(A^* - KC)$ into the left half plane and $B^*(u, t) \in R^n$ is a vector defined by

$$B^*(u, t) = \left[\begin{array}{c} B_1 u(t - L_1) \\ B_2 u(t - L_2) - A_{21}^* \int_{-L_2}^{-L_1} S_1(\xi) u(t + \xi) d\xi \\ \vdots \\ B_p u(t - L_p) - \sum_{j=1}^{p-1} A_{pj}^* \int_{-L_p}^{-L_j} S_j(\xi) u(t + \xi) d\xi \end{array} \right]. \tag{3.29}$$

The matrix A^*_{ij} gives the state transition of $x_i(t-L_i)$ caused by $x_j(t-L_j)$. Because A is block lower triangular, A^* is also block lower triangular. The vector $B^*(u,t)$ gives the effect of input on the state transition of $x^P(t)$. Equation (3.26) consists of partial observers which estimate the partial states $x_i(t-L_i)$ for $i=1,\cdots,p$. The partial observers are given by

$$\begin{aligned}\frac{d\tilde{x}_i(t)}{dt} &= \sum_{j=1}^{p}(A^*_{ij}-K_{ij}C_{jj})\tilde{x}_j(t)+\sum_{j=1}^{p}K_{ij}y_j(t)+B_iu(t-L_i)\\ &\quad -\sum_{j=1}^{i-1}A^*_{ij}\int_{-L_i}^{-L_j}S_j(\xi)u(t+\xi)d\xi, \quad i=1,\cdots,p. \end{aligned} \tag{3.30}$$

Here, $\tilde{x}_i(t)\in R^{n_i}$ are estimates of $x_i(t-L_i)$, A^*_{ij} for $j>i$ are zero matrices and K_{ij} for $i=1,\cdots,p$ and $j=1,\cdots,p$ are the (i,j) block of the observer gain K. We can easily confirm that the estimate $\tilde{x}(t)$ is formed by the vectors $\tilde{x}_i(t)$, as $\tilde{x}(t)=\left[\tilde{x}_1^{\mathrm{T}}(t)\cdots\tilde{x}_p^{\mathrm{T}}(t)\right]^{\mathrm{T}}$.

To confirm that Eq. (3.26) acts appropriately as an observer which estimates the vector $x^P(t)$, we analyze the behavior of the estimation error $e(t)=\tilde{x}(t)-x^P(t)$. For this estimation error, the following lemma holds.

Lemma 3.2 The state estimation error $e(t)$ of the observer Eq. (3.26) satisfies the following equation:

$$\frac{de(t)}{dt} = (A^*-KC)e(t). \tag{3.31}$$

Proof. See Subsection 3.5.2.

This lemma means that the error converges to zero at the rate according to the eigenvalues of (A^*-KC). Note that the matrices C and A^* are block diagonal and block lower triangular, respectively, and the pairs (C_{ii},A_{ii}) of their i-th diagonal blocks are observable. Thus the pair (C,A^*) is also observable and we can assign the eigenvalues of (A^*-KC) into the left half plane arbitrarily by tuning the observer gain K. Consequently, Eq. (3.26) gives the observer estimating the past state $x^P(t)$ from the output $y(t)$ and the input $u(t)$.

3.2.3 Proposed predictor

Now, we give the equation of the proposed predictor by combining the prediction mechanism Eq. (3.24) with the observer Eq. (3.26). Replacing the vector $x^P(t)$ in Eq. (3.24) with the estimate $\tilde{x}(t)$ by the observer (3.26), we obtain

$$\hat{x}(t) = E\left\{\tilde{x}(t)+S(u,t)\right\}, \tag{3.32}$$

where $\hat{x}(t)$ is an estimate of the current state $x(t)$. Equations (3.26) and (3.32) give the predictor that estimates the current state $x(t)$ from the input $u(\tau),\ \tau<t$, and the output $y(\tau),\ \tau\le t$.

For this predictor, the following theorem holds for the prediction error $\hat{e}(t)=\hat{x}(t)-x(t)$.

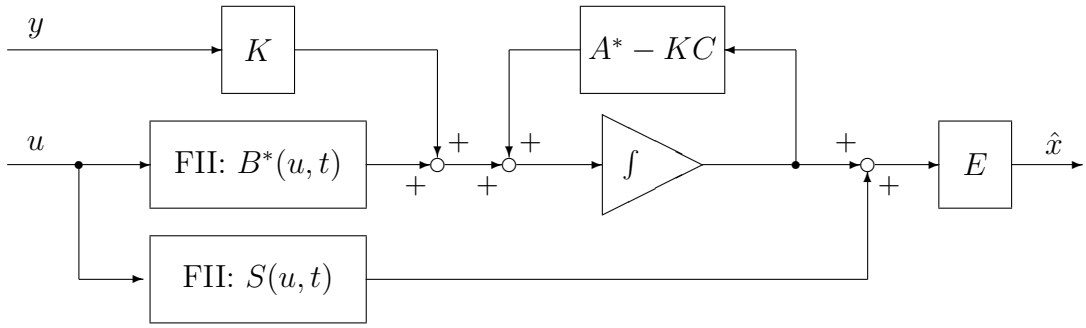

Figure 3.4: Block diagram of the proposed predictor (FII: Finite interval integration)

Theorem 3.1 The state prediction error of the predictor (3.26) converges to zero at the rate according to the eigenvalues of $(A^* - KC)$.

Proof. Subtracting Eq. (3.24) from Eq. (3.32), we find that

$$\hat{e}(t) \;=\; Ee(t). \tag{3.33}$$

Since E is the block lower triangular matrix defined by Eq. (3.25) and its diagonal blocks are matrix exponentials of $(A_{ii}L_i)$ for $i = 1, \cdots, p$, E is always nonsingular.

Differentiating the state prediction error $\hat{e}(t)$, we obtain

$$\frac{d\hat{e}(t)}{dt} \;=\; E\frac{de(t)}{dt} = E(A^* - KC)e(t). \tag{3.34}$$

Since E is nonsingular, the above equation becomes

$$\frac{d\hat{e}(t)}{dt} \;=\; E(A^* - KC)E^{-1}\hat{e}(t). \tag{3.35}$$

Consequently, the dynamic characteristics of the state prediction error $\hat{e}(t)$ converges to zero at the rate according to the eigenvalues of $(A^* - KC)$. This completes the proof of the theorem. Q.E.D.

Using Eqs. (3.26) and (3.32), we can estimate the present state $x(t)$ from the output $y(t)$ and the input $u(t)$. The prediction error of this predictor converges to zero asymptotically. Thus, the state predictor given by Eqs. (3.26) and (3.32) gives a solution of the **Problem 3.1**. Namely, an asymptotic estimate of the current state can be obtained using this state predictor. Figure 3.4 shows a block diagram of the proposed predictor.

3.2.4 Comparison with delay-compensating observer

Here, the proposed method is compared with the existing method. For linear multivariable systems with multiple delays in inputs and outputs, Watanabe and Ito [9] proposed a delay-compensating observer, which estimates the state of the system for feedback control. The estimation error of this delay-compensating observer theoretically converges to zero at the rate according to the finite poles assigned arbitrarily.

For the system (3.5), (3.6), the full-order version of the delay-compensating observer is represented by

$$\frac{d\hat{x}(t)}{dt} = (A - \hat{K}\hat{C})\hat{x}(t) + Bu(t) + \hat{K}y(t) + \hat{K}\sum_{j=1}^{p}\int_{-L_j}^{0}\hat{C}_j \mathrm{e}^{-A(L_j+\tau)}Bu(t+\tau)d\tau, \tag{3.36}$$

where $\hat{x}(t) \in R^n$ is an estimate of $x(t)$, $\hat{K} \in R^{n\times p}$ is an observer gain which assigns the eigenvalues of $(A - \hat{K}\hat{C})$ into the left half plane. $\hat{C} \in R^{p\times n}$ and $\hat{C}_j \in R^{p\times n}$ for $j = 1, \cdots, p$ are constant matrices given by

$$\hat{C} = \sum_{j=1}^{p}\hat{C}_j \mathrm{e}^{-AL_j}, \tag{3.37}$$

$$\hat{C}_j = \begin{bmatrix} 0_{(j-1)\times\hat{n}_j} & 0_{(j-1)\times n_j} & 0_{(j-1)\times(n-\hat{n}_{(j+1)})} \\ 0_{1\times\hat{n}_j} & C_{jj} & 0_{1\times(n-\hat{n}_{(j+1)})} \\ 0_{(p-j)\times\hat{n}_j} & 0_{(p-j)\times n_j} & 0_{(p-j)\times(n-\hat{n}_{(j+1)})} \end{bmatrix},\ j = 1, \cdots, p. \tag{3.38}$$

Applying a coordinate transformation to the predicted state $\omega(t) = E^{-1}\hat{x}(t)$ and the observer gain $K = E^{-1}\hat{K}$, the delay-compensating observer is expressed by the following equations:

$$\frac{d\omega(t)}{dt} = (A^* - KC)\omega(t) + E^{-1}Bu(t) + Ky(t) + KCS(u,t), \tag{3.39}$$

$$\hat{x}(t) = E\omega(t). \tag{3.40}$$

Figure 3.5 shows a block diagram of the delay-compensating observer.

Now, we compare the proposed predictor and the delay-compensating observer from the viewpoint of the length of the finite interval integration. In the proposed predictor, the term $B^*(u,t)$ in Eq. (3.26) includes finite interval integration whose interval length is up to $(L_p - L_1)$. On the other hand, the length of integration interval of the term $KCS(u,t)$ in Eq. (3.39) of the delay-compensating observer is up to L_p. In general, the cumulative error of numerical integration increases as the interval length of the integration increases. Thus the effect of the cumulative error on estimation by observer would be stronger in the delay-compensating observer than in the proposed predictor, especially for a large observer gain K.

Note that the integral interval length of the term $S(u,t)$ in the proposed predictor is up to L_p. However, the term is in the output equation (3.32) of the predictor, and does not affect state transition in the observer equation. Therefore the effect of integral errors in the term $S(u,t)$ remains small even if the observer gain K is large.

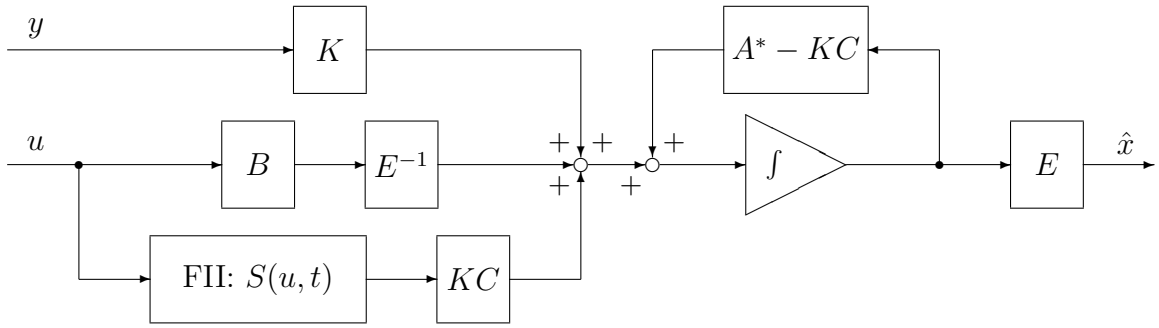

Figure 3.5: Block diagram of the delay-compensating observer (FII: Finite interval integration)

3.3 Numerical examples

Consider a fourth-order single-input two-output unstable system

$$\frac{dx(t)}{dt} = \left[\begin{array}{cc|cc} 0 & -0.01 & 0 & 0 \\ 1 & -0.3 & 0 & 0 \\ \hline -0.1 & 0 & 0 & 0.01 \\ 0 & 0 & 1 & -0.4 \end{array}\right] x(t) + \left[\begin{array}{c} 0.1 \\ 0 \\ \hline 0 \\ 0 \end{array}\right] u(t), \tag{3.41}$$

$$y^A(t) = \left[\begin{array}{cc|cc} 0 & 1 & 0 & 0 \\ \hline 0 & 0 & 0 & 1 \end{array}\right] x(t), \tag{3.42}$$

$$y(t) = \left[\begin{array}{c} y_1^A(t-9) \\ y_2^A(t-17) \end{array}\right]. \tag{3.43}$$

The lengths of the delays L_1 and L_2 are $L_1 = 9$ and $L_2 = 17$, respectively. The eigenvalues of A_{11} and A_{22} are $\{-0.038, -0.26\}$ and $\{0.024, -0.42\}$, respectively. For this system, the proposed predictor is constructed. The observer gain K is set to

$$K = \left[\begin{array}{cc|cc} 0.7692 & 1.5606 & 0.0306 & -0.0599 \\ \hline 0.2092 & 0.0708 & 1.0360 & 1.7394 \end{array}\right]^{\mathrm{T}}, \tag{3.44}$$

in order to assign the eigenvalues of $(A^* - KC)$ to $\{-0.5, -1 \pm 0.2i, -1.5\}$ using `MATLAB` standard function *place*.

First the convergence characteristics of the proposed predictor is examined. All finite interval integrals are calculated using the backwards rectangular rule [29] with sampling interval $T_s = 0.05$. The initial state of the system is given by

$$x(\tau) = 0, \ (-L_2 \le \tau < 0), \quad x(0) = [\ \ 2 \quad 0 \quad -1 \quad 0\ \ ]^{\mathrm{T}}, \tag{3.45}$$

and the initial state of the predictor is set to 0. The simulation result with a step input $u(t) = 1$, $t \ge 0$, is shown in Fig. 3.6. Figures 3.6(a), (b) and (c) represent the responses of the output $y(t)$, the state $x(t)$ and the prediction error $\hat{e}(t)$, respectively. Until the

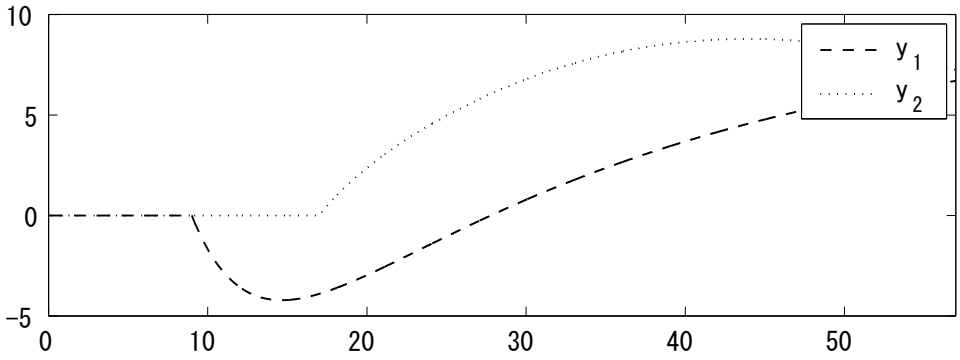

(a) Output

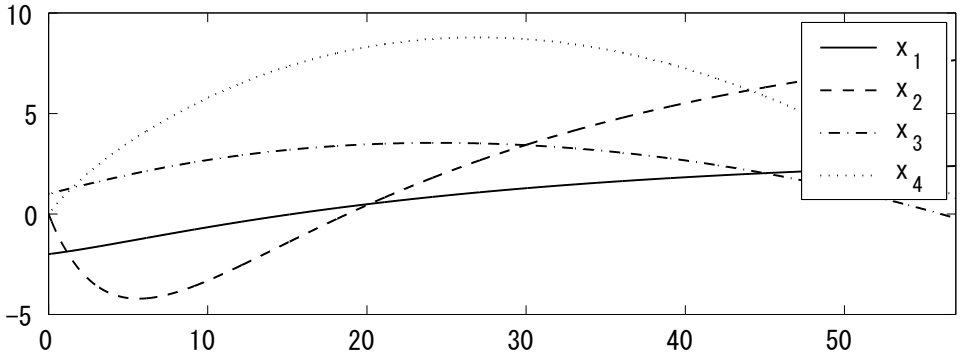

(b) Plant state

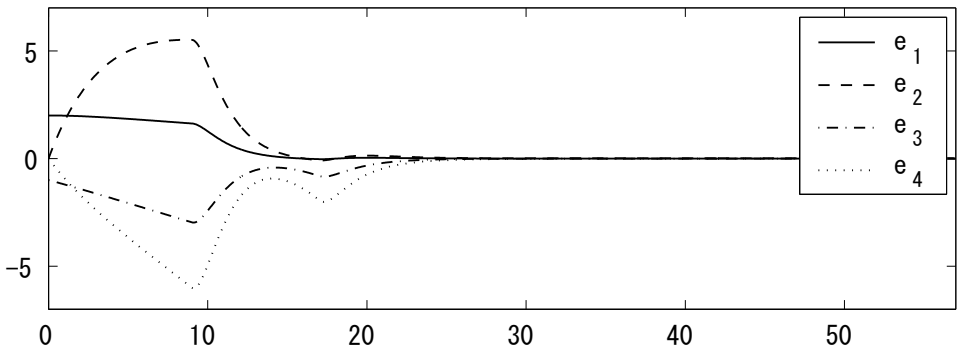

(c) Estimation error of the proposed predictor ($T_s = 0.05$)

Figure 3.6: Responses to initial perturbation: Proposed predictor

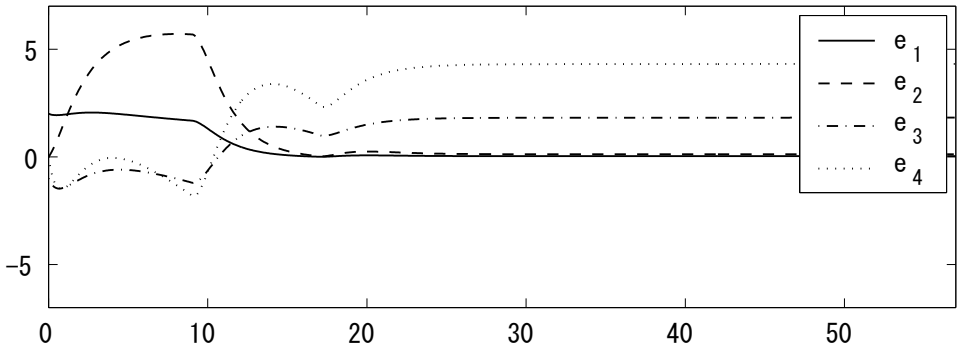

(a) Estimation error of the delay-compensating observer ($T_s = 0.05$)

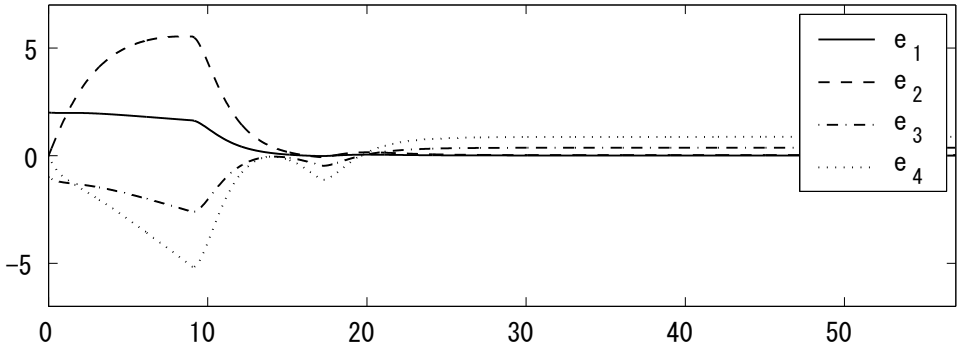

(b) Estimation error of the delay-compensating observer ($T_s = 0.01$)

Figure 3.7: Responses to initial perturbation: the delay-compensating observer

shortest delay time L_1 elapses, the prediction error increases, but after the delay time the error converges to zero at an appropriate rate.

Next a comparison is made with the delay-compensating observer [9] whose observer gain is set to the same to the proposed predictor. Figure 3.7(a) shows the estimation error of the delay-compensating observer with the same input and the same initial conditions. We can see that the estimation error of the observer does not converge, and has a steady state error. This estimation error decreases when the sampling period is made shorter ($T_s = 0.01$) as in Fig. 3.7(b). Because the input is a unit step function, the cumulative error by the rectangular rule calculation is constant. Furthermore, the cumulative error decreases when the sampling period is made shorter. Although this cumulative error exists on the proposed predictor, the effect of the error would be small because the interval length of finite interval integration is short. Therefore we conclude that the estimation error is due to the cumulative numerical error, and the proposed predictor is favorable for state prediction of systems whose output paths have large delays.

3.4 Concluding remarks

In this chapter, the author proposes a state predictor that predicts the current state of a multivariable system whose input and output paths have different time delays. The error of the predicted state converges to zero at the rate according to the observer poles, which can be adjusted arbitrarily by the observer gain. The interval length of the finite interval integration for estimating calculation of the observer is shorter than that of the delay-compensating observer. This means that the cumulative error of integration of the proposed predictor would be smaller than that of the delay-compensating observer. Numerical examples show that the proposed predictor provides better performance than the delay-compensating observer.

Recently a problem associated with the finite interval integration in closed-loop systems was found [29]. When a closed-loop system includes integrals of the input, and the integrals are approximated by using some quadrature rules, the system sometimes becomes unstable regardless of accuracy of the approximation [30]. The proposed predictor itself is not associated with this problem when used alone. However, this problem may appear if the proposed state predictor is utilized for closed-loop control. Some remedies are proposed in literature [31,32]. Further investigation is required for the stability problem [29–32] caused by the approximation of the finite interval integration in a closed-loop system with the proposed predictor.

3.5 Proofs

3.5.1 Proof of Lemma 3.1

From Eq. (3.5), we obtain

$$x_i(t+\tau) = \mathrm{e}^{A_{ii}(\tau+L_i)}x_i(t-L_i) + \int_{-L_i}^{\tau} \mathrm{e}^{A_{ii}(\tau-\xi)} \left\{ B_i u(t+\xi) + \sum_{j=1}^{i-1} A_{ij}x_j(t+\xi) \right\} d\xi, \tag{3.46}$$

for $i = 1, \cdots, p$. Using the above equation, we prove the lemma by mathematical induction.

First the case $i = 1$ is considered. Equation (3.46) becomes

$$x_1(t+\tau) = E_{11}(\tau)x_1(t-L_1) + E_{11}(\tau)\int_{-L_1}^{\tau} S_1(\xi)u(t+\xi)d\xi. \tag{3.47}$$

Thus Eq. (3.18) holds.

Next the case $i = l$ is considered under the assumption that Eq. (3.18) holds for $i = 1, \cdots, l-1$. The term $x_l(t+\tau)$ in Eq. (3.46) becomes

$$x_l(t+\tau) = \mathrm{e}^{A_{ll}(\tau+L_l)}x_l(t-L_l) + \int_{-L_l}^{\tau} \mathrm{e}^{A_{ll}(\tau-\xi)}B_l u(t+\xi)d\xi$$

$$
\begin{aligned}
&+\int_{-L_l}^{\tau} \mathrm{e}^{A_{ll}(\tau-\xi)} \sum_{j=1}^{l-1} A_{lj} \sum_{k=1}^{j} E_{jk}(\xi) \left\{ x_k(t-L_k) + \int_{-L_k}^{\xi} S_k(\lambda) u(t+\lambda) d\lambda \right\} d\xi \\
&= E_{ll}(\tau) x_l(t-L_l) + \int_{-L_l}^{\tau} \mathrm{e}^{A_{ll}(\tau-\xi)} B_l u(t+\xi) d\xi + \sum_{k=1}^{l-1} E_{lk}(\tau) x_k(t-L_k) \\
&\quad + \sum_{k=1}^{l-1} \int_{-L_k}^{\tau} \left\{ \sum_{j=k}^{l-1} \int_{-L_l}^{\tau} \mathrm{e}^{A_{ll}(\tau-\xi)} A_{lj} E_{jk}(\xi) d\xi \right\} S_k(\lambda) u(t+\lambda) d\lambda \\
&\quad - \sum_{k=1}^{l-1} \int_{-L_l}^{\tau} \mathrm{e}^{A_{ll}(\tau-\lambda)} \left\{ \sum_{j=k}^{l-1} \int_{-L_l}^{\lambda} \mathrm{e}^{A_{ll}(\lambda-\xi)} A_{lj} E_{jk}(\xi) d\xi \right\} S_k(\lambda) u(t+\lambda) d\lambda \\
&= \sum_{k=1}^{l} E_{lk}(\tau) x_k(t-L_k) + \sum_{k=1}^{l-1} \int_{-L_k}^{\tau} E_{lk}(\tau) S_k(\lambda) u(t+\lambda) d\lambda \\
&\quad + \int_{-L_l}^{\tau} \mathrm{e}^{A_{ll}(\tau-\xi)} B_l u(t+\xi) d\xi - \sum_{k=1}^{l-1} \int_{-L_l}^{\tau} \mathrm{e}^{A_{ll}(\tau-\xi)} E_{lk}(\xi) S_k(\xi) u(t+\xi) d\xi \\
&= \sum_{k=1}^{l} E_{lk}(\tau) x_k(t-L_k) + \sum_{k=1}^{l} \int_{-L_k}^{\tau} E_{lk}(\tau) S_k(\lambda) u(t+\lambda) d\lambda. \qquad (3.48)
\end{aligned}
$$

Thus Eq. (3.18) holds. Therefore Eq. (3.18) holds for all $i = 1, \cdots, p$. This completes the proof of Lemma 3.1.

3.5.2 Proof of Lemma 3.2

First we introduce estimation errors $e_i(t) = \tilde{x}_i(t) - x_i(t - L_i)$ for $i = 1, \cdots, p$, for partial states estimated by the observers (3.30), and examine the dynamic characteristics of the state estimation error $e_i(t)$. From Eq. (3.5), we have

$$
\frac{dx_i(t-L_i)}{dt} = \sum_{j=1}^{i} A_{ij} x_j(t-L_i) + B_i u(t-L_i). \qquad (3.49)
$$

Lemma 3.1 shows that the terms $x_j(t - L_i)$ for $j = 1, 2, \cdots, i$ are given as

$$
x_j(t-L_i) = \sum_{k=1}^{j} E_{jk}(-L_i) \left\{ x_k(t-L_k) + \int_{-L_k}^{-L_i} F_k(\xi) u(t+\xi) d\xi \right\}, \qquad (3.50)
$$

Substituting the above equation into Eq. (3.49) yields

$$
\frac{dx_i(t-L_i)}{dt} = \sum_{k=1}^{i} A^*_{ik} x_k(t-L_k) - \sum_{k=1}^{i} A^*_{ik} \int_{-L_i}^{-L_k} F_k(\xi) u(t+\xi) d\xi + B_i u(t-L_i). \qquad (3.51)
$$

Subtracting the above equation from Eq. (3.30), we can conclude

$$
\frac{de_i(t)}{dt} = \sum_{j=1}^{p} \left(A^*_{ij} - K_{ij} C_{jj} \right) e_j(t), \ (i = 1, \cdots, p). \qquad (3.52)
$$

From the definitions of $\tilde{x}(t)$, $x^P(t)$ and $e_i(t)$ for $i = 1, \cdots, p$, we can denote $e(t)$ by $e(t) = \left[\begin{array}{ccc} e_1^{\mathrm{T}}(t) & \cdots & e_p^{\mathrm{T}}(t) \end{array} \right]^{\mathrm{T}}$. Thus we can rewrite Eq. (3.52) as $\frac{de(t)}{dt} = (A^* - KC)e(t)$, and this completes the proof of Lemma 3.2.

Chapter 4

Synthesis and analysis of state-predictive servo controller for systems whose output paths have different time delays

In this chapter, a servo problem for multivariable systems whose output paths have different time delays is studied. Until now, servo controllers for systems with a cascaded pure delay have been proposed by many investigators, such as the Smith controller [4], a state-predictive servo controller [7], and so on. On the other hand, servo controllers for systems with multiple delays have been discussed in a few literature. One of such controllers is a modified Smith predictor [33]. We may apply this controller for multivariable systems with delays and unmeasurable step disturbances. However, this controller cannot stabilize unstable systems. To the author's best knowledge, a state-predictive servo controller for systems including multiple delays has not been proposed, and this is the first appearance of such a controller.

Furthermore, a robust stability analysis method for the state-predictive servo control system is proposed in this chapter. On robust stability analysis of time delay systems, many remarkable results have appeared [1, 16]. However, these results cannot be applied directly to state-predictive control systems based on the finite spectrum assignment method [6], because such control systems contain finite interval integration of manipulated input. The original article of the finite spectrum assignment method [6] discussed the robustness of the closed-loop system qualitatively, and showed that the closed-loop system remains stable for sufficiently small perturbations. On the other hand, quantitative analysis of closed-loop robust stability was seldom considered in literature. Only few articles [18, 34] studied robust stability margins against parameter mismatches of state-predictive control systems. Stability analysis methods in these articles are for single-input single-output systems with a pure delay. One of them [18] gives the exact stability margin of gain and time-delay mismatches. However, these methods cannot

be applied directly to state-predictive control systems for multivariable systems with multiple delays. Thus we propose a novel stability analysis method for the proposed state-predictive control systems. This method is based on the closed-loop characteristic equation and the small gain theorem [35], and derives a sufficient condition of robust stability against parameter mismatches on system matrices and delay lengths. Using this condition, a stability region can be drawn on a plane whose axes represent the magnitude of mismatches on system matrices and the maximum mismatch on delay lengths.

In Section 4.1, a state-predictive servo controller for systems whose output paths have different time delays is shown. Considering parameter mismatches between the model and the actual controlled process, a sufficient condition for the closed-loop stability against the mismatches is derived in Section 4.2. In Section 4.3, some numerical examples are given to show the design and analysis procedure of the state-predictive servo control system.

4.1 Robust servo controller for systems with output delays

In this section, we design a robust servo controller, which has a tracking ability to a step reference, for a multivariable system whose output paths have different time delays. The system may include equi-length delays in every input path, because we can transform it to a system formulated here by removing the delay to the output side. However, systems whose input paths have different time delays are not considered in this chapter.

Consider a p-input p-output n-th order system whose output paths have different time delays:

$$\frac{dx(t)}{dt} = Ax(t) + Bu(t), \tag{4.1}$$

$$y^A(t) = Cx(t), \tag{4.2}$$

$$y(t) = \left[\begin{array}{ccc} y_1^A(t-L_1) & \cdots & y_p^A(t-L_p) \end{array} \right]^{\mathrm{T}}. \tag{4.3}$$

Here, $x(t)$ is a state vector, $u(t) \in R^p$ is an input vector, $y^A(t) \in R^p$ is an output vector of a delay-free part, $y_i^A(t)$ for $i = 1, \cdots, p$ are the i-th scalar elements of the delay-free output and $y(t) \in R^p$ is an output vector of the system. $A \in R^{n \times n}$, $B \in R^{n \times p}$ and $C \in R^{p \times n}$ are constant matrices. L_i for $i = 1, \cdots, p$ are non-negative output delays in the i-th output path, and satisfy $0 \leq L_1 \leq L_2 \leq \cdots \leq L_p$, without loss of generality. We assume that the pair (A, B) is stabilizable, and that

$$\mathrm{rank}\left\{\mathrm{obsv}(C_1, A)\right\} < \mathrm{rank}\left\{\mathrm{obsv}(C_2, A)\right\} < \cdots < \mathrm{rank}\left\{\mathrm{obsv}(C_p, A)\right\} = n, \tag{4.4}$$

where $\mathrm{obsv}(C_i, A) = \left[\begin{array}{cccc} C_i^{\mathrm{T}} & (C_iA)^{\mathrm{T}} & \cdots & (C_iA^{n-1})^{\mathrm{T}} \end{array} \right]^{\mathrm{T}}$ is the observability matrix of (C_i, A), C_i for $i = 1, \cdots, p$ are $(i \times n)$ matrices consisting of the first i rows of C, as

in the preceding chapter. We also assume that the matrices $A \in R^{n\times n}$, $B \in R^{n\times p}$ and $C \in R^{p\times n}$ are given by

$$A = \begin{bmatrix} A_{11} & & 0 \\ \vdots & \ddots & \\ A_{p1} & \cdots & A_{pp} \end{bmatrix}, \; B = \begin{bmatrix} B_1 \\ \vdots \\ B_p \end{bmatrix}, \; C = \begin{bmatrix} C_{11} & & 0 \\ & \ddots & \\ 0 & & C_{pp} \end{bmatrix}. \tag{4.5}$$

Here, $A_{ij} \in R^{n_i\times n_j}$, $B_i \in R^{n_i\times p}$ and $C_{ii} \in R^{1\times n_i}$ are constant matrices where n_i for $i = 1, \cdots, p$ are positive integers defined by

$$n_1 = \mathrm{rank}\,\{\mathrm{obsv}(C_1, A)\}, \tag{4.6}$$

$$n_i = \mathrm{rank}\,\{\mathrm{obsv}(C_i, A)\} - \sum_{j=1}^{i-1} n_j, \quad i = 2, \cdots, p. \tag{4.7}$$

Obviously, the system (4.1)–(4.3) belongs to the class of systems treated in the preceding chapter.

Note that the system (4.1)–(4.3) can be represented as follows.

$$\frac{dx_i(t)}{dt} = \sum_{j=1}^{i} A_{ij}x_j(t) + B_i u(t), \quad i = 1, \cdots, p, \tag{4.8}$$

$$y_i(t) = C_{ii}x_i(t - L_i), \quad i = 1, \cdots, p, \tag{4.9}$$

where $x_i(t)$ for $i = 1, \cdots, p$ is an n_i-dimensional column vector.

In this section, we consider a problem of designing a robust servo control system whose output $y(t)$ converges to the step reference $r(t) = r$ in $t \geq 0$. For solvability of this problem, we assume

$$\det \begin{bmatrix} A & B \\ C & 0_{p\times p} \end{bmatrix} \neq 0. \tag{4.10}$$

Furthermore, we assume that the state $x(t)$ is not accessible and only the output $y(t)$ is available.

The original problem in this section is as above; however, first we review a simpler situation to explain the idea of the internal model principle [36], and then we extend this idea to the original problem. As the simpler situation, we consider a "delay-free" controlled process whose state is accessible. Namely, we can obtain the delay-free output $\bar{y}(t)$ as

$$\bar{y}(t) = Cx(t), \tag{4.11}$$

and assume that the current state $x(t)$ is accessible. To realize a robust servo control system, let us introduce an integral compensator according to the internal model principle [36], as

$$\bar{w}(t) = \int_0^t (r(\tau) - \bar{y}(\tau))\, d\tau + \bar{w}_0, \tag{4.12}$$

where $\bar{w}(t)$ is the integral of the tracking error between the reference and the delay-free output, $\bar{w}_0$ is an initial value of the integral compensator. Then we construct an augmented system as

$$\frac{d\bar{x}(t)}{dt} = \bar{A}\bar{x}(t) + \bar{B}u(t) + \bar{B}_r r(t), \quad \bar{x}(0) = \bar{x}_0, \tag{4.13}$$

where

$$\bar{x} = \begin{bmatrix} \bar{w}(t) \\ x(t) \end{bmatrix}, \quad \bar{x}_0 = \begin{bmatrix} \bar{w}_0 \\ x_0 \end{bmatrix}, \quad \bar{A} = \begin{bmatrix} 0_{p\times p} & -C \\ 0_{n\times p} & A \end{bmatrix}, \quad \bar{B} = \begin{bmatrix} 0_{p\times p} \\ B \end{bmatrix}, \tag{4.14}$$

$$\bar{B}_r = \begin{bmatrix} I_p \\ 0_{n\times p} \end{bmatrix}, \tag{4.15}$$

I_p is a $p \times p$ identity matrix and x_0 is an initial state of the controlled process. We can apply a state feedback control law to the augmented system as

$$u(t) = -\bar{F}\bar{x}(t), \tag{4.16}$$

where $\bar{F} \in R^{p\times(n+p)}$ is a feedback gain matrix which assigns the eigenvalues of the matrix $\left(\bar{A} - \bar{B}\bar{F}\right)$ into the left half plane. In this case, the state equation of the closed-loop system is

$$\frac{d\bar{x}(t)}{dt} = \left(\bar{A} - \bar{B}\bar{F}\right)\bar{x}(t) + \bar{B}_r r(t), \tag{4.17}$$

and the closed-loop poles are given by the eigenvalues of the matrix $(\bar{A} - \bar{B}\bar{F})$. Because all the eigenvalues of the matrix $(\bar{A} - \bar{B}\bar{F})$ are on the left half plane, $\bar{x}(t)$ converges to zero. Consequently, the output asymptotically converges to the reference. This is a brief overview of the robust servo controller for the "delay-free" case. A block diagram of this control system is shown in Fig. 4.1.

Let us return to the original problem. To apply the above idea to the system whose output paths have different time delays, we must predict the current state $\bar{x}(t)$ of the augmented system (4.13) — not only the current state $x(t)$ of the delay-free part (4.1) but also the state $\bar{w}(t)$ of the integral compensator (4.12) — from only the output $y(t)$, the input $u(t)$ and the reference signal $r(t)$. Thus we introduce an observer, an integral compensator and a prediction mechanism. The observer estimates a vector consisting of past states of the delay-free part from measured output. The integral compensator integrates the difference between the reference and the output, which contains the information of the past state. The prediction mechanism predicts the current state of the augmented system from the outputs of the observer and the integral compensator. Hereafter these three elements are explained in detail.

First the observer estimating the vector consisting of past states is given. As in the preceding chapter, we can estimate the partial states $x_i(t - L_i)$ for $i = 1, \cdots, p$ using the following observer:

$$\frac{d\tilde{x}(t)}{dt} = (A^* - KC)\tilde{x}(t) + Ky(t) + B^*(u, t), \quad \tilde{x}(0) = \tilde{x}^0, \tag{4.18}$$

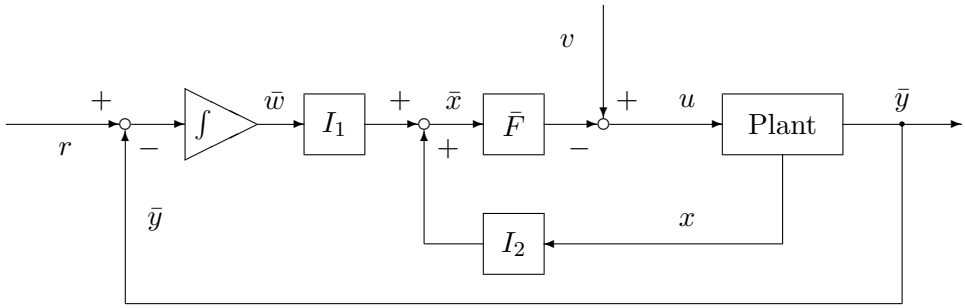

$$I_1 = \begin{bmatrix} I_p \\ 0_{n\times p} \end{bmatrix}, I_2 = \begin{bmatrix} 0_{p\times n} \\ I_n \end{bmatrix}.$$

Figure 4.1: Robust servo control system for "delay-free" case

where

$$\tilde{x}(t) = \begin{bmatrix} \tilde{x}_1^{\mathrm{T}}(t) & \cdots & \tilde{x}_p^{\mathrm{T}}(t) \end{bmatrix}^{\mathrm{T}}, \quad \tilde{x}_i(t) \in R^{n_i}, \tag{4.19}$$

$$A^* = \begin{bmatrix} A_{11}^* & & 0 \\ \vdots & \ddots & \\ A_{p1}^* & \cdots & A_{pp}^* \end{bmatrix}, \tag{4.20}$$

$$A_{ij}^* = \sum_{k=j}^{i} A_{ik} E_{kj}(-L_i), i = 1, \cdots, p;\ j = 1, \cdots, i, \tag{4.21}$$

$$E_{kj}(\tau) = \begin{cases} \mathrm{e}^{A_{kk}(\tau+L_k)}, & k = 1, \cdots, p;\ j = i, \\ \displaystyle\sum_{i=j}^{k-1} \int_{-L_k}^{\tau} \mathrm{e}^{A_{kk}(\tau-\lambda)} A_{ki} E_{ij}(\lambda) d\lambda, & k = 2, \cdots, p;\ j = 1, \cdots, i-1, \end{cases} \tag{4.22}$$

$$B^*(u,t) = \begin{bmatrix} B_1 u(t-L_1) \\ B_2 u(t-L_2) - A_{21}^* \displaystyle\int_{-L_2}^{-L_1} S_1(\xi) u(t+\xi) d\xi \\ \vdots \\ B_p u(t-L_p) - \displaystyle\sum_{j=1}^{p} A_{pj}^* \int_{-L_p}^{-L_j} S_j(\xi) u(t+\xi) d\xi \end{bmatrix}, \tag{4.23}$$

$$S_j(\xi) = \mathrm{e}^{-A_{jj}(L_j+\xi)} \left\{ B_j - \sum_{k=1}^{j-1} E_{jk}(\xi) S_k(\xi) \right\}, \quad i = 1, \cdots, p, \tag{4.24}$$

and K is an observer gain that assigns the eigenvalues of the matrix $(A^* - KC)$ into the left half plane. The vectors $\tilde{x}_i(t)$ for $i = 1, \cdots, p$ are the estimates of the partial states $x_i(t - L_i)$ for $i = 1, \cdots, p$.

Second an integral compensator is introduced. This integral compensator is given by

$$w(t) = \int_0^t \{r(\tau) - y(\tau)\} d\tau + w^0, \tag{4.25}$$

where w^0 is the initial value of $w(t)$. In the above equation, the i-th element w_i of the vector w includes only the information up to time $(t - L_i)$ about the delay-free output $y_i^A = C_{ii}x_i$, while the value w_i includes the information up to time t about the i-th element r_i of the reference r. Thus we should add the integrated values of $C_{ii}x_i$ over $t \in (t - L_i, t]$ for $i = 1, \cdots, p$, to $w(t)$.

To obtain the predicted state of the delay-free part and the integral compensator, we introduce an augmented equation whose state consists of the delayed state $x_i(t - L_i)$ for $i = 1, \cdots, p$ and the state $w(t)$ of the integral compensator, and construct a prediction mechanism which calculates the current state $x(t)$ and the integrated values of $C_{ii}x_i$ over $t \in (-L_i, 0]$ for $i = 1, \cdots, p$. The prediction mechanism for the augmented system is given by

$$\begin{bmatrix} \hat{w}(t) \\ \hat{x}(t) \end{bmatrix} = \begin{bmatrix} I_p & -\tilde{C} \\ 0_{n\times p} & E \end{bmatrix} \begin{bmatrix} w(t) + S_w(u,t) \\ \tilde{x}(t) + S_x(u,t) \end{bmatrix}, \tag{4.26}$$

where $\hat{w}(t)$ is the predicted value of the state $\bar{w}(t)$ of the delay-free integral compensator, $\hat{x}(t)$ is the predicted value of the current state, and

$$\tilde{C} = \begin{bmatrix} \tilde{C}_{11}(0) & & 0 \\ \vdots & \ddots & \\ \tilde{C}_{p1}(0) & \cdots & \tilde{C}_{pp}(0) \end{bmatrix}, \tag{4.27}$$

$$\tilde{C}_{ij}(\tau) = C_{ii} \int_{-L_i}^{\tau} E_{ij}(\lambda) d\lambda, \quad i = 1, \cdots, p;\ j = 1, \cdots, i-1, \tag{4.28}$$

$$E = \begin{bmatrix} E_{11}(0) & & 0 \\ \vdots & \ddots & \\ E_{p1}(0) & \cdots & E_{pp}(0) \end{bmatrix}, \tag{4.29}$$

$$S_w(u,t) = \begin{bmatrix} \int_{-L_1}^{0} \sum_{j=1}^{1} \tilde{C}_{1j}(\xi) S_j(\xi) u(t+\xi) d\xi \\ \vdots \\ \int_{-L_p}^{0} \sum_{j=1}^{p} \tilde{C}_{pj}(\xi) S_j(\xi) u(t+\xi) d\xi \end{bmatrix}, \tag{4.30}$$

$$S_x(u,t) = \begin{bmatrix} \int_{-L_1}^{0} S_1(\xi) u(t+\xi) d\xi \\ \vdots \\ \int_{-L_p}^{0} S_p(\xi) u(t+\xi) d\xi \end{bmatrix}. \tag{4.31}$$

The matrix $\tilde{C}$ maps the state $x_i(t - L_i)$ for $i = 1, \cdots, p$ to the integrated value $w(t)$. The vectors $S_w(u,t)$ and $S_x(u,t)$ mean the effects of past input on the integrated value $w(t)$ and on the predicted state $\hat{x}(t)$, respectively.

Since the vector $[\hat{w}^{\mathrm{T}}(t)\ \hat{x}^{\mathrm{T}}(t)]^{\mathrm{T}}$ is an estimate of the state $\bar{x}$ of the "delay-free" augmented system (4.13), we may apply a state feedback

$$u(t) = -\bar{F} \begin{bmatrix} \hat{w}(t) \\ \hat{x}(t) \end{bmatrix}, \tag{4.32}$$

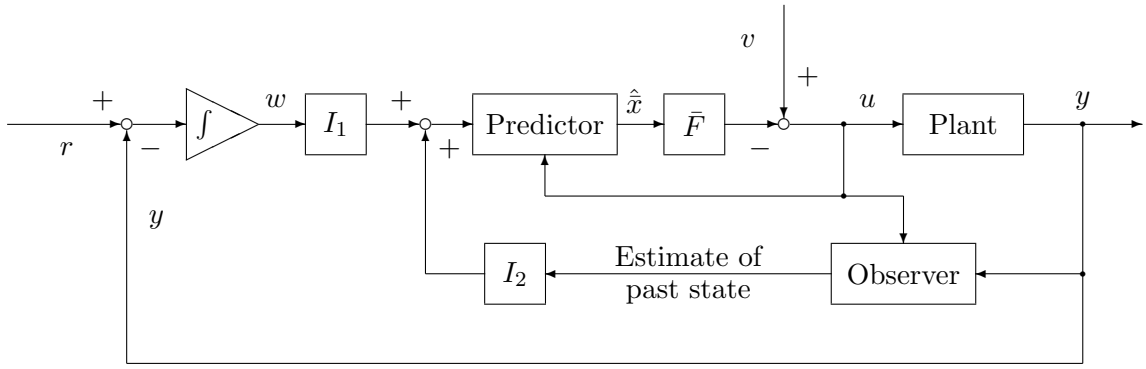

$$I_1 = \begin{bmatrix} I_p \\ 0_{n\times p} \end{bmatrix}, \quad I_2 = \begin{bmatrix} 0_{p\times n} \\ I_n \end{bmatrix}, \quad \hat{\bar{x}} = \begin{bmatrix} \hat{w}(t) \\ \hat{x}(t) \end{bmatrix}.$$

Figure 4.2: Robust servo control system for multiple delay system

to obtain a servo control system, as in Eq. (4.16). In the following, the matrix $\bar{F}$ is given by $\bar{F} = [F_w \ F_x]$, where $F_w \in R^{p\times p}$ and $F_x \in R^{p\times n}$ are constant matrices. Using F_w and F_x, the control law (4.32) is expressed by

$$u(t) \ = \ -\begin{bmatrix} F_w & F_p \end{bmatrix} \begin{bmatrix} w(t) + S_w(u,t) \\ \tilde{x}(t) + S_x(u,t) \end{bmatrix}, \tag{4.33}$$

where

$$F_p = F_x E - F_w \tilde{C}. \tag{4.34}$$

Here we obtain the state-predictive servo control system proposed in this chapter as Eqs. (4.18), (4.25) and (4.33). A block diagram of this servo control system is shown in Fig. 4.2. In the nominal case, this closed-loop system has only finite poles consisting of the eigenvalues of the matrices $(\bar{A} - \bar{B}\bar{F})$ and $(A^* - KC)$. Because all of these poles are assigned into the left half plane, the closed-loop system is stable. The discussion on the pole location is made in the following section in more general form.

4.2 Robust stability analysis of state-predictive servo control system

In this section, a sufficient condition of robust stability of the state-predictive servo system is derived based on the small gain theorem [35]. Considering parameter mismatches between the model and the actual controlled process, the characteristic function of the state-predictive servo control system is calculated in Subsection 4.2.1. Subsection 4.2.2 is devoted to derive a sufficient condition for the closed-loop stability against the mismatches.

4.2.1 Characteristic function of closed-loop system with mismatches

In this subsection, the characteristic function of the proposed state-predictive servo control system is derived under the existence of model uncertainties. First we introduce a class of model uncertainties. In the following, we only consider the parameter mismatches on system matrices and the lengths of the delays. Namely, we assume that the actual controlled process is described as

$$\frac{dx^r(t)}{dt} = A^r x^r(t) + B^r u(t),\ x^r(0) = x_0^r, \tag{4.35}$$

$$y^A(t) = \begin{cases} y^0(t), & -L \le t < 0, \\ C^r x^r(t), & t \ge 0, \end{cases} \tag{4.36}$$

$$y(t) = \begin{bmatrix} y_1^A(t - L_1^r) \\ \vdots \\ y_p^A(t - L_p^r) \end{bmatrix}, \tag{4.37}$$

$$u(t) = u^0(t), \quad -L \le t < 0, \tag{4.38}$$

where $x^r(t) \in R^n$ is a state vector, $A^r \in R^{n\times n}$, $B^r \in R^{n\times p}$ and $C^r \in R^{p\times n}$ are constant matrices, which may differ from the nominal matrices A, B and C, respectively, L_i^r for $i = 1 \cdots p$ are nonnegative real numbers and L is the maximum value of L_i^r. The vectors x_0^r, $u^0(\tau)$ and $y^0(\tau)$ for $\tau \in [-L, 0)$ mean the initial values of state, input and output, respectively. The superscript r means that the values are of the actual controlled process. Additionally, we assume that Eq. (4.10) also holds for the perturbed system. Namely,

$$\det \begin{bmatrix} A^r & B^r \\ C^r & 0_{p\times p} \end{bmatrix} \neq 0. \tag{4.39}$$

Under the above conditions, we can always find a nonsingular matrix T_B such that $B = T_B B^r$. Using this nonsingular matrix, we can apply a coordinate transformation $x^\Delta(t) = T_B x^r(t)$ and obtain a transformed system

$$\frac{dx^\Delta(t)}{dt} = (A + \Delta_A)x^\Delta(t) + Bu(t),\ x(0) = x_0^\Delta, \tag{4.40}$$

$$y^A(t) = \begin{cases} y^0(t), & -L \le t < 0, \\ (C + \Delta_C)x^\Delta(t), & t \ge 0, \end{cases} \tag{4.41}$$

$$y(t) = \begin{bmatrix} y_1^A(t - L_1 - \Delta_{L_1}) \\ \vdots \\ y_p^A(t - L_p - \Delta_{L_p}) \end{bmatrix}, \tag{4.42}$$

where

$$\Delta_A = T_B^{-1} A^r T_B - A, \quad \Delta_C = C^r T_B^{-1} - C, \tag{4.43}$$

$x_0^\Delta = T_B x^r(0)$ and $\Delta_{L_i} = L_i^r - L_i$ for $i = 1 \cdots, p$.

In the following, we derive the characteristic equation of the state-predictive servo control system consisting of the actual controlled process (4.40)–(4.42), the delayed-state observer (4.18), the integral compensator (4.25) and the predictive controller (4.33).

First we apply Laplace transformation to Eqs. (4.40)–(4.42), and obtain

$$(sI_n - A - \Delta_A)\, X^\Delta(s) - BU(s) = x_0^\Delta, \tag{4.44}$$

$$Y(s) = \bar{C}^r(s) X^\Delta(s) + y^0(s), \tag{4.45}$$

where $X^\Delta(s)$, $U(s)$ and $Y(s)$ are Laplace transforms of $x^\Delta(t)$, $u(t)$ and $y(t)$, respectively,

$$\bar{C}^r(s) = L(s)\left\{C + CL_\Delta(s) + C_\Delta(s)\right\}, \tag{4.46}$$

$$L(s) = \begin{bmatrix} \mathrm{e}^{-sL_1} & & 0 \\ & \ddots & \\ 0 & & \mathrm{e}^{-sL_p} \end{bmatrix}, \tag{4.47}$$

$$L_\Delta(s) = \begin{bmatrix} \mathrm{e}^{-s\Delta_{L_1}} I_{n_1} & & 0 \\ & \ddots & \\ 0 & & \mathrm{e}^{-s\Delta_{L_p}} I_{n_p} \end{bmatrix} - I_n, \tag{4.48}$$

$$C_\Delta(s) = \begin{bmatrix} \mathrm{e}^{-s\Delta_{L_1}} & & 0 \\ & \ddots & \\ 0 & & \mathrm{e}^{-s\Delta_{L_p}} \end{bmatrix} \Delta_C, \tag{4.49}$$

$$y^0(s) = \begin{bmatrix} \int_0^{L_1^r} \mathrm{e}^{-s\tau} y_1^0(L_1^r - \tau) d\tau \\ \vdots \\ \int_0^{L_p^r} \mathrm{e}^{-s\tau} y_p^0(L_p^r - \tau) d\tau \end{bmatrix}, \tag{4.50}$$

and $y_i^0(\tau)$ for $i = 1 \cdots, p$, $\tau \in [-L_i^r, 0)$ are the i-th elements of the initial condition $y^0(\tau)$ of the output $y_i^A(\tau)$.

Second we derive Laplace transforms of Eqs. (4.18) and (4.25). We have

$$(sI_n - A_o)\tilde{X}(s) - K\bar{C}^r(s) X^\Delta(s) - \tilde{B}(s)U(s) = \tilde{X}^0(s), \tag{4.51}$$

$$sW(s) + \bar{C}^r(s) X^\Delta(s) = W^0(s) + R(s), \tag{4.52}$$

where $\tilde{X}(s)$, $W(s)$ and $R(s)$ are Laplace transforms of $\tilde{x}(t)$, $w(t)$ and $r(t)$, respectively,

$$A_o = A^* - KC, \tag{4.53}$$

$$\tilde{B}(s) = (sI_n - A^*)\tilde{L}(s)(sI_n - A)^{-1}B, \tag{4.54}$$

$$\tilde{L}(s) = \begin{bmatrix} \mathrm{e}^{-sL_1} I_{n_1} & & 0 \\ & \ddots & \\ 0 & & \mathrm{e}^{-sL_p} I_{n_p} \end{bmatrix}, \tag{4.55}$$

$$\tilde{X}^0(s) = \tilde{x}^0 + Ky^0(s), \tag{4.56}$$

$$W^0(s) = w^0 - y^0(s). \tag{4.57}$$

For the details of the derivation of Eq. (4.51), see Subsection 4.5.2.

Third we perform Laplace transformation to Eq. (4.33), and obtain

$$\{I_p + f_u(s)\}\, U(s) + F_w W(s) + F_p \tilde{X}(s) \;=\; U^0(s), \tag{4.58}$$

where

$$\begin{aligned} f_u(s) &= F_w \left\{ \tilde{C}E^{-1} - s^{-1}C + s^{-1}L(s)C \right\} (sI_n - A)^{-1}B \\ &\quad + F_p \left\{ E^{-1} - \tilde{L}(s) \right\} (sI_n - A)^{-1}B, \end{aligned} \tag{4.59}$$

$$\begin{aligned} U^0(s) &= F_w \begin{bmatrix} \sum_{j=1}^{1} \int_{-L_1}^{0} \mathrm{e}^{s\xi} \tilde{C}_{1j}(\xi) S_j(\xi) \int_0^\xi \mathrm{e}^{-s\lambda} u(\lambda) d\lambda d\xi \\ \vdots \\ \sum_{j=1}^{p} \int_{-L_p}^{0} \mathrm{e}^{s\xi} \tilde{C}_{pj}(\xi) S_j(\xi) \int_0^\xi \mathrm{e}^{-s\lambda} u(\lambda) d\lambda d\xi \end{bmatrix} \\ &\quad + F_p \begin{bmatrix} \int_{-L_1}^{0} \mathrm{e}^{s\xi} S_1(\xi) \int_0^\xi \mathrm{e}^{-s\lambda} u(\lambda) d\lambda d\xi \\ \vdots \\ \int_{-L_p}^{0} \mathrm{e}^{s\xi} S_p(\xi) \int_0^\xi \mathrm{e}^{-s\lambda} u(\lambda) d\lambda d\xi \end{bmatrix}. \end{aligned} \tag{4.60}$$

The details of the derivation of Eq. (4.58) are shown in Subsection 4.5.3.

From Eqs. (4.44), (4.51), (4.52) and (4.58), we have

$$\begin{bmatrix} sI_p & \bar{C}^r(s) & 0_{p\times n} & 0_{p\times p} \\ 0_{n\times p} & sI_n - A - \Delta_A & 0_{n\times n} & -B \\ 0_{n\times p} & -K\bar{C}^r(s) & sI_n - A_o & -\tilde{B}(s) \\ F_w & 0_{p\times n} & F_p & I_p + f_u(s) \end{bmatrix} \begin{bmatrix} W(s) \\ X^\Delta(s) \\ \tilde{X}(s) \\ U(s) \end{bmatrix} = \Omega(s), \tag{4.61}$$

where

$$\Omega(s) \;=\; \begin{bmatrix} W^0(s) + R(s) \\ x_0^\Delta \\ \tilde{X}^0(s) \\ U^0(s) \end{bmatrix}. \tag{4.62}$$

For the state-predictive servo control system, its internal stability is not affected by external inputs. Thus we ignore the term $R(s)$. Then the right hand side of Eq. (4.61), $\Omega(s)$, is a regular function of s determined only by the initial values $x_0^\Delta, \tilde{x}^0, w^0, u(\tau)$ and $y^0(\tau)$ for $\tau \in [-L, 0)$ of the closed-loop system. Consequently, the characteristic function of the closed-loop system is given by

$$f(s) = \det \begin{bmatrix} sI_p & \bar{C}^r(s) & 0_{p\times n} & 0_{p\times p} \\ 0_{n\times p} & sI_n - A - \Delta_A & 0_{n\times n} & -B \\ 0_{n\times p} & -K\bar{C}^r(s) & sI_n - A_o & -\tilde{B}(s) \\ F_w & 0_{p\times n} & F_p & I_p + f_u(s) \end{bmatrix}. \tag{4.63}$$

We may transform the above characteristic function to a more concise form:

$$f(s) \;=\; \det \left\{ sI_{n+p} - \bar{A} + \bar{B}\bar{F} \right\} \det \{sI_n - A_o\} \det \{I_n - G_A(s)\Delta_A - G_\Delta(s)\Delta(s)\}, \tag{4.64}$$

where

$$\Delta(s) = \{CL_\Delta(s) + C_\Delta(s)\}, \tag{4.65}$$
$$G_A(s) = \{I_n + G_\Delta(s)C\}(sI_n - A)^{-1}, \tag{4.66}$$
$$G_\Delta(s) = \left\{sI_n - \hat{A}_F(s)\right\}^{-1} B\left\{s^{-1}F_w - F_p(sI_n - A_o)^{-1}K\right\} L(s), \tag{4.67}$$
$$\hat{A}_F(s) = A - BF_x + s^{-1}BF_wC. \tag{4.68}$$

For more detail, see Subsection 4.5.4.

4.2.2 Stability condition against mismatches

In this subsection, we derive a sufficient condition of robust stability of the closed-loop system against the parameter mismatches on the system matrices and the lengths of the delays.

In the nominal case, all the mismatches Δ_A, Δ_C, Δ_{L_i} for all $i = 1, \cdots, p$ and therefore $\Delta(s)$ are zero. Thus the last factor of Eq. (4.64) becomes one, and the closed-loop poles are given by the eigenvalues of the matrices $(\bar{A} - \bar{B}\bar{F})$ and $(A^* - KC)$, which are designed to be stable. Therefore the closed-loop system is stable in the nominal case.

On the other hand, the mismatches on the parameters yield additional poles to the closed-loop equation, and affect the stability of the closed-loop system. From Eq. (4.64), the following theorem is derived.

Theorem 4.1 The state-predictive servo control system is robustly stable against the parameter mismatches Δ_A, Δ_C and Δ_{L_i} for $i = 1, \cdots, p$, if the following conditions hold.

$$\text{(i)} \quad A \text{ is stable, or } \Delta_A = 0. \tag{4.69}$$
$$\text{(ii)} \quad \Gamma(\Delta_L) + \gamma_C||\Delta_C|| + \gamma_A||\Delta_A|| < 1. \tag{4.70}$$

Here, $\Delta_L = \max_i\{|\Delta_{L_i}|\}$, $\gamma_C = ||G_\Delta(s)||_\infty$, $\gamma_A = ||G_A(s)||_\infty$,

$$\Gamma(\Delta_L) = 2\sup_{\omega \in R}\left[\sigma_{\max}\{G_\Delta(j\omega)C\} W_L(\omega\Delta_L)\right], \tag{4.71}$$
$$W_L(\omega\Delta_L) = \begin{cases} \left|\sin(\omega\Delta_L/2)\right|, & |\omega\Delta_L| \le \pi, \\ 1, & |\omega\Delta_L| > \pi. \end{cases} \tag{4.72}$$

To prove the above theorem, we introduce a simple closed-loop system whose poles coincide with the additional poles of the perturbed state-predictive servo control system. Then we derive a sufficient condition for the stability of the simple closed-loop system.

First we investigate the location of roots of the characteristic equation of Eq. (4.64). The first two factors of the characteristic function (4.64) coincide with the characteristic functions of the augmented delay-free state feedback system consisting of Eqs. (4.13) and (4.17), and the observer (4.18), respectively, which are designed to be stable. Therefore the stability of the state-predictive servo control system under the existence of

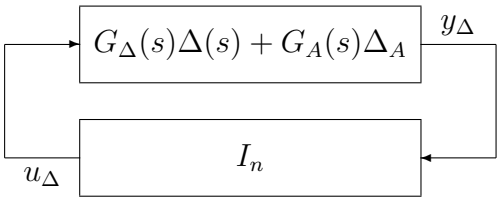

Figure 4.3: A closed-loop system of I_n and $(G_\Delta(s)\Delta(s) + G_A(s)\Delta_A)$

the parameter mismatches is determined by the third factor of the characteristic function (4.64):

$$f_\Delta(s) = \det\{I_n - G_\Delta(s)\Delta(s) - G_A(s)\Delta_A\}. \tag{4.73}$$

Namely, the closed-loop system with the parameter mismatches Δ_A, Δ_C and Δ_{L_i} for $i = 1, \cdots, p$ is stable, if and only if all roots of

$$f_\Delta(s) = 0, \tag{4.74}$$

are on the left half plane.

Next we focus on the position of roots of Eq. (4.74). We introduce a closed-loop system

$$y_\Delta(s) = (G_\Delta(s)\Delta(s) + G_A(s)\Delta_A)u_\Delta(s), \tag{4.75}$$
$$u_\Delta(s) = y_\Delta(s). \tag{4.76}$$

A block diagram of this closed-loop system is shown in Fig. 4.3. Obviously, the roots of Eq. (4.74) coincide with the poles of the closed-loop system (4.75), (4.76). Thus a stability condition for the closed-loop system (4.75), (4.76) is equivalent to that of the perturbed state-predictive control system.

Now, we derive a stability condition for the closed-loop system (4.75), (4.76). First, we analyze the stability of the term $G_\Delta(s)\Delta(s) + G_A(s)\Delta_A$. The term $\Delta(s)$ is stable due to its definition (Eq. (4.65)). The term $G_\Delta(s)$ becomes

$$G_\Delta(s) = \begin{bmatrix} I_n & 0_{n\times p} & 0_{n\times n} \end{bmatrix} \begin{bmatrix} sI_n - \hat{A}_F(s) & -BF_w & BF_p \\ 0_{p\times n} & sI_p & 0_{p\times n} \\ 0_{n\times n} & 0_{n\times p} & sI_n - A_0 \end{bmatrix}^{-1} \begin{bmatrix} 0_{n\times p} \\ L(s) \\ KL(s) \end{bmatrix}. \tag{4.77}$$

Therefore $G_\Delta(s)$ is stable because its poles coincide with the nominal closed-loop poles. The term $G_A(s)$ becomes

$$G_A(s) = \begin{bmatrix} I_n & 0_{n\times p} & 0_{n\times n} & I_n \end{bmatrix} \begin{bmatrix} sI_n - \hat{A}_F(s) & -BF_w & BF_p & 0_{n\times n} \\ 0_{p\times n} & sI_p & 0_{p\times n} & -L(s)C \\ 0_{n\times n} & 0_{n\times p} & sI_n - A_0 & -KL(s)C \\ 0_{n\times n} & 0_{n\times p} & 0_{n\times n} & sI_n - A \end{bmatrix}^{-1}$$

$$\times \begin{bmatrix} 0_{n\times n} \\ 0_{p\times n} \\ 0_{n\times n} \\ I_n \end{bmatrix}. \tag{4.78}$$

Therefore $G_A(s)$ is stable if A is stable, because the nominal closed-loop poles and the eigenvalues of A comprise the poles of $G_A(s)$. Consequently, $G_\Delta(s)\Delta(s) + G_A(s)\Delta_A$ is stable if the condition (4.69) holds. Hereafter we assume that condition (4.69) holds.

Using the small gain theorem [35], it is proved that the closed-loop system (4.75), (4.76) is stable if the following inequality holds:

$$||G_\Delta(s)\Delta(s) + G_A(s)\Delta_A||_\infty < 1. \tag{4.79}$$

From the well-known properties of the H_∞ gain, we have the following inequalities.

$$\begin{aligned} ||G_\Delta(s)\Delta(s) + G_A(s)\Delta_A||_\infty &\le ||G_\Delta(s)\Delta(s)||_\infty + ||G_A(s)\Delta_A||_\infty \\ &\le ||G_\Delta(s)CL_\Delta(s)||_\infty + \gamma_C||\Delta_C|| + \gamma_A||\Delta_A||. \end{aligned} \tag{4.80}$$

Consequently, the stability of the state-predictive servo control system is guaranteed if the following inequality holds.

$$||G_\Delta(s)CL_\Delta(s)||_\infty + \gamma_C||\Delta_C|| + \gamma_A||\Delta_A|| < 1. \tag{4.81}$$

Next we derive an upper bound of the term $||G_\Delta(s)CL\Delta(s)||_\infty$. From the definition of H_∞ norm, we have

$$\begin{aligned} ||G_\Delta(s)CL_\Delta(s)||_\infty &= \sup_{\omega\in R}\left[\sigma_{\max}\left\{G_\Delta(j\omega)CL_\Delta(j\omega)\right\}\right] \\ &\le \sup_{\omega\in R}\left[\sigma_{\max}\left\{G_\Delta(j\omega)C\right\}\sigma_{\max}\left\{L_\Delta(j\omega)\right\}\right], \end{aligned} \tag{4.82}$$

where $\sigma_{\max}(X)$ means the maximum singular value of matrix X. From the definitions of $L_\Delta(j\omega)$ and $W_L(\omega\Delta_L)$, we find that

$$\begin{aligned} \sigma_{\max}\left\{\Delta_L(j\omega)\right\} &= \max_i \sigma_{\max}\left\{(\mathrm{e}^{-j\omega\Delta_{L_i}} - 1)I_{n_i}\right\} = 2\max_i\left\{\left|\sin\left(\frac{\omega\Delta_{L_i}}{2}\right)\right|\right\} \\ &\le 2W_L(\omega\Delta_L). \end{aligned} \tag{4.83}$$

Finally, we obtain Theorem 4.1 from the inequalities (4.81), (4.82) and (4.83).

Using Theorem 4.1, we can obtain a stability region on the plane whose axes are the magnitude of mismatches on system matrices and the maximum mismatch on delay lengths. When the maximum delay mismatch Δ_L satisfies an inequality $\Gamma(\Delta_L) < 1$, we can easily draw the region of $||\Delta_C||$ and $||\Delta_A||$ for which the closed-loop system is stable, since the factors γ_C and γ_A are constant and the factor $\Gamma(\Delta_L)$ is a function of a single factor Δ_L. However, if the maximum delay mismatch Δ_L meets an inequality $\Gamma(\Delta_L) \ge 1$, we cannot obtain a stability region from Theorem 4.1, because the inequality (4.70) does not hold.

Note that Theorem 4.1 gives a sufficient condition and seems to be conservative, since the operations of the norms are not so strict. The closed-loop system is possibly stable if the condition (4.70) does not hold. However, this condition is helpful in practical applications required to be safe rather than to be high-performance, such as medical applications.

4.3 Numerical example

Here, we design a robust state-predictive servo controller for a multivariable system whose output paths have different time delays, and analyze robust stability of the closed-loop system that consists of the controller and the controlled process.

Consider a fourth-order two-input two-output system (4.1)–(4.3), where

$$A = \left[\begin{array}{cc|cc} 0 & -0.05 & 0 & 0 \\ 1 & -0.2 & 0 & 0 \\ \hline -0.2 & 0 & 0 & -0.02 \\ 0 & 0 & 1 & -0.3 \end{array}\right], \; B = \left[\begin{array}{cc} 1 & 0 \\ 0 & -1 \\ \hline 0 & 1 \\ 0 & 0 \end{array}\right], \; C = \left[\begin{array}{cc|cc} 0 & 1 & 0 & 0 \\ \hline 0 & 0 & 0 & 1 \end{array}\right], \quad (4.84)$$

$$L_1 = 3, \; L_2 = 13. \quad (4.85)$$

The eigenvalues of A_{11} and A_{22} are $\{-0.1 \pm 0.2i\}$ and $\{-0.1, -0.2\}$, respectively.

First, we construct a state-predictive servo controller that makes the output track a step reference. Using `MATLAB` standard function *place*, we determine the observer gain K and the feedback gain F_w and F_x in order to assign the poles of the nominal closed-loop system as follows (Design A):

- Poles of the observer (eigenvalues of $(A^* - KC)$) to $\{-0.15 \pm 0.15i, -0.25 \pm 0.05i\}$.
- Poles of the augumented system (eigenvalues of $(\bar{A} - \bar{B}\bar{F})$) to $\{-0.45 \pm 0.45i, -0.30 \pm 0.35i, -0.25, -0.30\}$.

The nominal response of the closed-loop system is shown in Fig. 4.4. Here, initial values of the controlled process, the integral compensator and the predictor are set to 0. The reference is given by $r(t) = [1 \; 2]^{\mathrm{T}}$. In Fig. 4.4, each output converges to the reference at an appropriate rate after delay time elapses.

Next, we analyze the robust stability of the closed-loop system. The values $||\Delta_C||$ and $||\Delta_A||$ are treated together as one value $\delta = ||\Delta_C|| + \gamma_A/\gamma_C||\Delta_A||$. The values Δ_{L_i} for $i = 1, \cdots, p$ are treated by $\Delta_L = \max_i(|\Delta_{L_i}|)$. Figure 4.5 demonstrates the stability region on the plane whose vertical axis and horizontal axis represent the values of δ and Δ_L, respectively. Namely, if the pair (δ, Δ_L) of the actual controlled process is included in the hatched region of Fig. 4.5, then the closed-loop system is stable. Here, γ_A/γ_C equals to 19.3. The stability margin in Fig. 4.5 may be conservative. However, this gives a useful guideline of the closed-loop robustness in practical use.

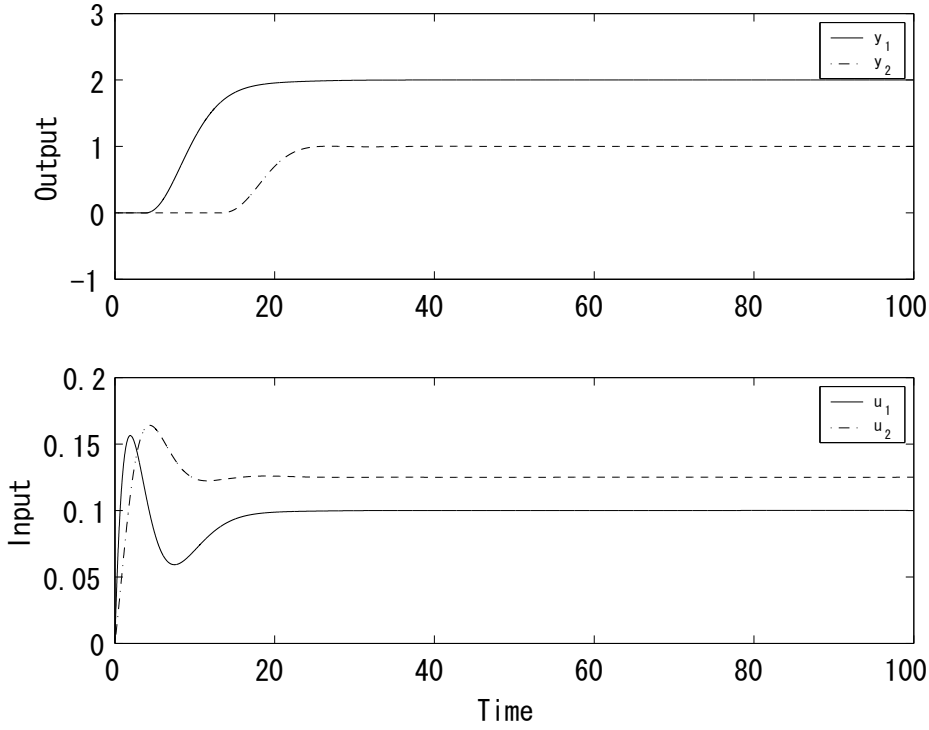

Figure 4.4: Nominal response to step reference (Design A)

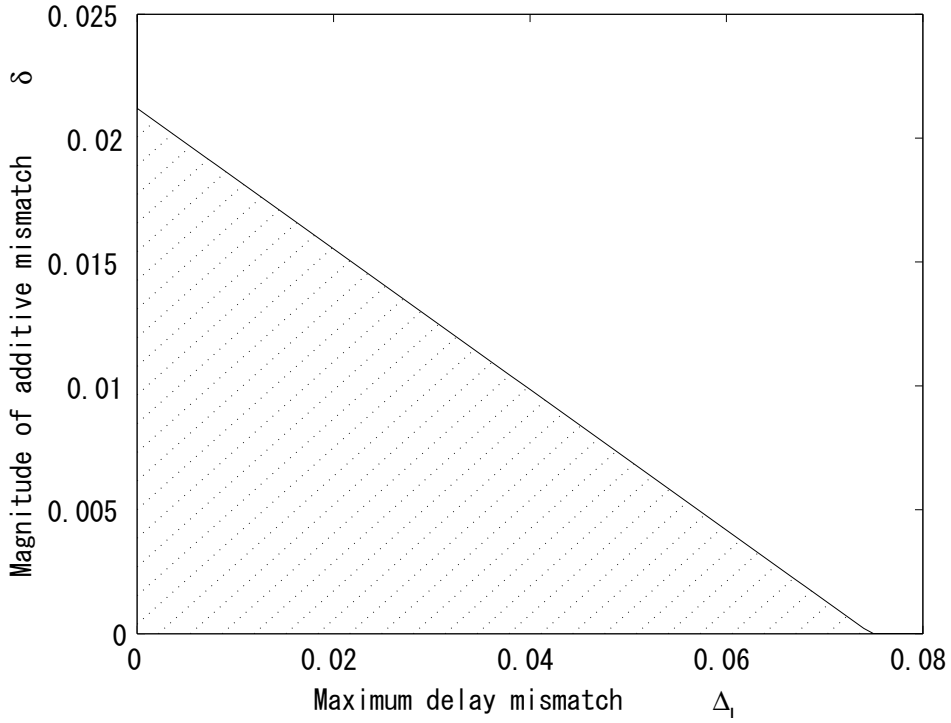

Figure 4.5: Robust stability region (Design A)

Figures 4.6 and 4.7 show the nominal response to step references and the robust stability region, respectively, of the state-predictive servo control system whose observer gain K and state feedback gain F_w and F_p are set to assign the poles as follows (Design B):

- Poles of the observer (eigenvalues of $(A^* - KC)$) to $\{-0.3 \pm 0.3i, -0.5 \pm 0.1i\}$.
- Poles of the augumented system (eigenvalues of $(\bar{A} - \bar{B}\bar{F})$) to $\{-0.9 \pm 0.9i, -0.6 \pm 0.7i, -0.5, -0.6\}$.

In this case, the ratio γ_A/γ_C becomes 8.3. In Fig. 4.6, the nominal response to the step references is approximately twice faster than the case of Fig. 4.4.

However, the robust stability region in Fig. 4.7 is extremely smaller than that of Fig. 4.5. This shows the trade-off between robustness and response speed of the closed-loop system in the control system design. In practical cases, this trade-off must be considered adequately in order to construct an appropriate closed-loop system. The stability analysis method proposed in this chapter would be useful to carry out such design procedure.

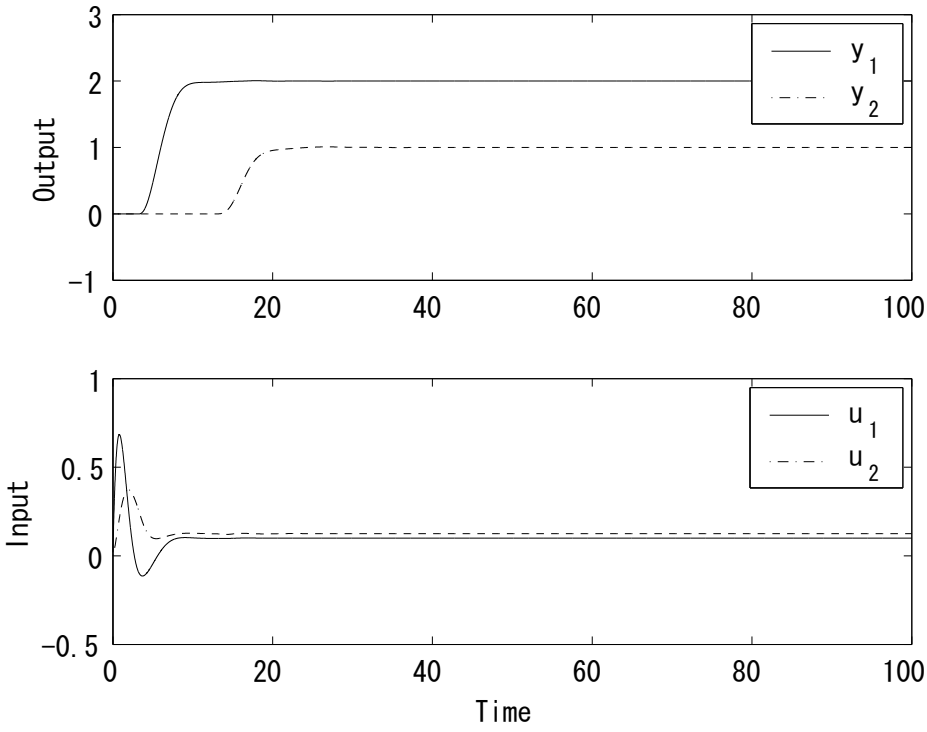

Figure 4.6: Nominal response to step reference (Design B)

4.4 Concluding remarks

In this chapter, a design method of a state-predictive servo control system and a robust stability analysis method of the control system are given for multivariable systems whose output paths have different time delays. First, we construct a controller which consists of an observer, an integral compensator, a prediction mechanism for an augmented system and a state feedback controller. Second, a characteristic equation of the closed-loop system is derived, with consideration of parameter mismatches on system matrices and lengths of the delays. Then we derive a sufficient condition for robust stability of the closed-loop system using the characteristic equation. This condition enables us to draw a stability region on the plane whose axes mean the magnitudes of mismatches on the system matrices and the delay lengths. This condition may be conservative, but gives appropriate guidelines to construct state-predictive servo control systems. Numerical examples show the procedure of the proposed design and analysis method of the proposed state-predictive servo control system and a trade-off between robustness and response speed of the closed-loop system.

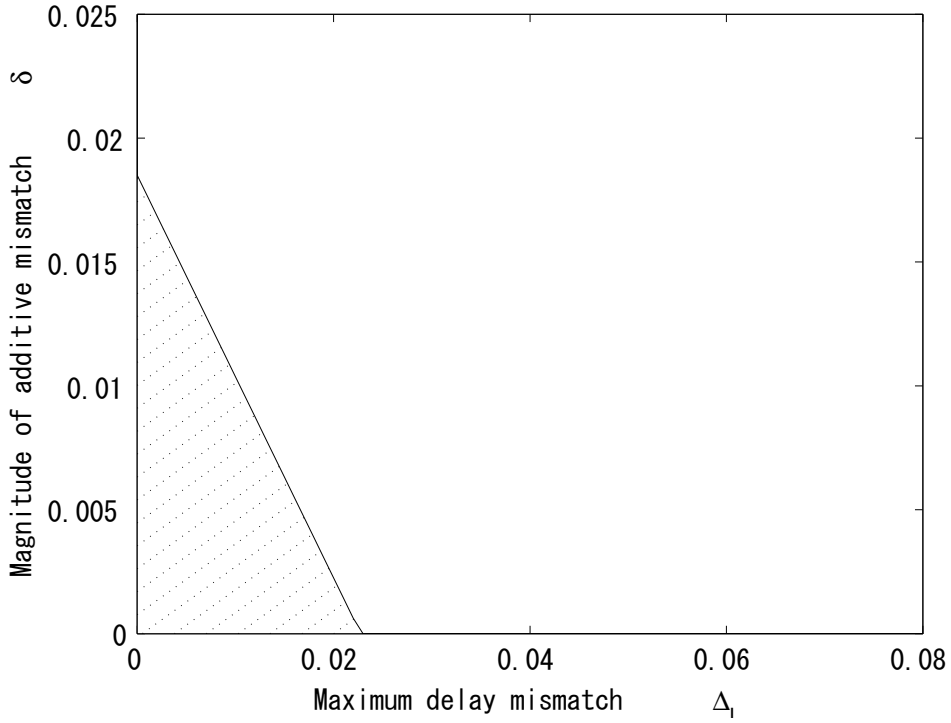

Figure 4.7: Robust stability region (Design B)

4.5 Derivations

4.5.1 Preliminaries

Here, we introduce some notations and lemmas utilized in the following subsections.

First we introduce a notation $[X]_i$ which means a row block matrix consisting of the $(\hat{n}_{(i-1)}+1)$-st through $\hat{n}_i$-th row vectors of the matrix $X \in R^{n\times k}$, where k is an arbitrary positive integer and

$$\hat{n}_0 \;=\; 0, \quad \hat{n}_i = \sum_{j=1}^{i} n_j \quad (i = 1, \cdots, p). \tag{4.86}$$

Namely,

$$[X]_i \;=\; \left[\; 0_{n_i\times\hat{n}_{(i-1)}+1} \quad I_{n_i} \quad 0_{n_i\times(n-\hat{n}_i)} \;\right] X. \tag{4.87}$$

Obviously,

$$[XY]_i \;=\; [X]_i\, Y, \tag{4.88}$$

for an arbitrary matrix Y with an appropriate size. Similarly, we use a notation $\langle X\rangle_i$ to extract the i-th row vector of the matrix $X \in R^{p\times k}$, where k is an arbitrary positive

integer. Obviously,

$$\langle X \rangle_i = \left[\begin{array}{ccc} 0_{1\times(i-1)} & 1 & 0_{1\times(p-i)} \end{array} \right] X, \tag{4.89}$$

and

$$\langle XY \rangle_i = \langle X \rangle_i Y. \tag{4.90}$$

Lemma 4.1 For an arbitrary real number ξ, the following equation holds.

$$E(\xi)S(\xi) = B, \tag{4.91}$$

where

$$E(\xi) = \left[\begin{array}{ccc} E_{11}(\xi) & & 0 \\ \vdots & \ddots & \\ E_{p1}(\xi) & \cdots & E_{pp}(\xi) \end{array} \right], \tag{4.92}$$

$$S(\xi) = \left[\begin{array}{c} S_1(\xi) \\ \vdots \\ S_p(\xi) \end{array} \right]. \tag{4.93}$$

Proof. The definition of $S_i(\xi)$ is as follows:

$$S_i(\xi) = \mathrm{e}^{-A_{ii}(L_i+\xi)} \left\{ B_i - \sum_{j=1}^{i-1} E_{ij}(\xi) S_j(\xi) \right\}. \tag{4.94}$$

Noting that $\mathrm{e}^{-A_{ii}(L_i+\xi)} = E_{ii}^{-1}(\xi)$, we obtain the following equation by multiplying $E_{ii}(\xi)$ from the left side of the above equation.

$$E_{ii}(\xi)S_i(\xi) = B_i - \sum_{j=1}^{i-1} E_{ij}(\xi) S_j(\xi). \tag{4.95}$$

Transposing the sum from the right side to the left side, we obtain

$$\sum_{j=1}^{i} E_{ij}(\xi) S_j(\xi) = B_i, \quad [E(\xi)S(\xi)]_i = [B]_i. \tag{4.96}$$

Arranging the each side of the above equation for $i = 1, \cdots, p$ in one column, we find that Eq. (4.91) holds. Q.E.D.

Lemma 4.2 For arbitrary real numbers α and β,

$$E(\alpha)E^{-1}(\beta) = \mathrm{e}^{A(\alpha-\beta)}. \tag{4.97}$$

Proof. As shown in Eq. (3.21), $E_{ij}(\tau)$ is the state transition matrix that maps $x_j(t-L_j)$ to $x_i(t+\tau)$. Therefore $E(\alpha)$ is the state transition matrix that maps $x^P(t) = \left[\begin{array}{ccc} x_1^{\mathrm{T}}(t-L_1) & \cdots & x_p^{\mathrm{T}}(t-L_p) \end{array}\right]^{\mathrm{T}}$ to $x(t+\alpha)$. Similarly, $E^{-1}(\beta)$ maps $x(t+\beta)$ to $x^P(t)$. Thus the composite mapping $E(\alpha)E^{-1}(\beta)$ maps $x(t+\beta)$ to $x(t+\alpha)$. On the other hand, the state transition from $x(t+\beta)$ to $x(t+\alpha)$ is given by the state transition matrix $\mathrm{e}^{A(\alpha-\beta)}$. Consequently, we conclude that Eq. (4.97) holds. Q.E.D.

Lemma 4.3

$$\left[E^{-1}\right]_i = \left[\mathrm{e}^{-AL_i}\right]_i . \tag{4.98}$$

Proof. As shown in the proof of the preceding lemma, E^{-1} means the state transition matrix that maps $x(t)$ to $x^P(t)$. Thus the i-th block row $[E^{-1}]_i$ maps $x(t)$ to $x_i(t-L_i)$. This mapping coincides with the i-th block row $\left[\mathrm{e}^{-AL_i}\right]_i$ of the state transition matrix e^{-AL_i} that maps $x(t)$ to $x(t-L_i)$. Therefore Eq. (4.98) holds. Q.E.D.

Lemma 4.4

$$A^* E^{-1} \;=\; E^{-1} A. \tag{4.99}$$

Proof. Using Lemmas 4.2 and 4.3, we obtain the following equations for all $i \in \{1, \cdots, p\}$:

$$\begin{aligned} \left[A^* E^{-1}\right]_i &= [A^*]_i E^{-1} = \left[\begin{array}{ccccccc} A^*_{i1} & \cdots & A^*_{ii} & 0 & \cdots & 0 \end{array}\right] E^{-1} \\ &= \left[\begin{array}{ccccccc} \sum_{k=1}^{i} A_{ik} E_{k1}(-L_i) & \cdots & \sum_{k=i}^{i} A_{ik} E_{ki}(-L_i) & 0 & \cdots & 0 \end{array}\right] E^{-1} \\ &= [AE(-L_i)]_i E^{-1} = \left[AE(-L_i)E^{-1}\right]_i = \left[A\mathrm{e}^{-AL_i}\right]_i = \left[\mathrm{e}^{-AL_i} A\right]_i \\ &= \left[\mathrm{e}^{-AL_i}\right]_i A = \left[E^{-1}\right]_i A = \left[E^{-1} A\right]_i . \end{aligned} \tag{4.100}$$

Thus we have derived Eq. (4.99). Q.E.D.

Lemma 4.5

$$\left\langle \tilde{C} E^{-1} \right\rangle_i \;=\; \left\langle C \int_{-L_i}^{0} \mathrm{e}^{A\lambda} d\lambda \right\rangle_i . \tag{4.101}$$

Proof. From the definitions of $\langle\cdot\rangle_i$, $\tilde{C}$, $E(\lambda)$ and Lemma 4.2, we obtain

$$\begin{aligned}
\left\langle \tilde{C}E^{-1} \right\rangle_i &= \left[\begin{array}{cccccc} \tilde{C}_{i1}(0) & \cdots & \tilde{C}_{ii}(0) & 0 & \cdots & 0 \end{array} \right] E^{-1} \\
&= C_{ii} \left[\begin{array}{cccccc} \int_{-L_i}^0 E_{i1}(\lambda)d\lambda & \cdots & \int_{-L_i}^0 E_{ii}(\lambda)d\lambda & 0 & \cdots & 0 \end{array} \right] E^{-1} \\
&= \left\langle C \int_{-L_i}^0 E(\lambda)d\lambda E^{-1} \right\rangle_i = \left\langle C \int_{-L_i}^0 E(\lambda)E^{-1}(0)d\lambda \right\rangle_i \\
&= \left\langle C \int_{-L_i}^0 \mathrm{e}^{A\lambda}d\lambda \right\rangle_i . \qquad (4.102)
\end{aligned}$$

Q.E.D.

Lemma 4.6

$$S_i(\xi) = \left[\mathrm{e}^{-(L_i+\xi)A}B\right]_i . \qquad (4.103)$$

Proof. Substituting $\xi = -L_i$ into Eq. (4.92), we obtain

$$[E(-L_i)]_i = \left[\begin{array}{ccc} 0_{n_i \times \hat{n}_i} & I_{n_i} & 0_{n_i \times \check{n}_i} \end{array} \right] . \qquad (4.104)$$

Using the above equation and Lemmas 4.1 and 4.2, we have

$$S_i(\xi) = [E(-L_i)S(\xi)]_i = \left[E(-L_i)E^{-1}(\xi)E(\xi)S(\xi)\right]_i = \left[\mathrm{e}^{-(L_i+\xi)A}B\right]_i . \qquad (4.105)$$

Q.E.D.

Using these notations and lemmas, we show the details of the derivation of Eqs. (4.51), (4.58) and (4.64).

4.5.2 Derivation of Eq. (4.51)

The Laplace transform of Eq. (4.18) is obtained as

$$s\tilde{X}(s) - \tilde{x}^0 = A_o\tilde{X}(s) + KY(s) + \mathcal{L}\left[B^*(u,t)\right], \qquad (4.106)$$

where $\mathcal{L}$ means an operator of Laplace transformation. From the definition of Laplace transformation, the i-th row block of $\mathcal{L}\left[B^*(u,t)\right]$ is

$$\mathcal{L}\left[B^*(u,t)\right]_i = \int_0^\infty \mathrm{e}^{-st} \left\{ B_i u(t-L_i) - \sum_{j=1}^{i} A_{ij}^* \int_{-L_i}^{-L_j} S_j(\xi)u(t+\xi)d\xi \right\} dt$$

$$
\begin{aligned}
&= \mathrm{e}^{-sL_i}B_iU(s) - \sum_{j=1}^{i} A^*_{ij} \int_{-L_i}^{-L_j} S_j(\xi)\mathrm{e}^{s\xi}d\xi U(s) \\
&\quad + \int_{-L_i}^{0} \mathrm{e}^{-s(L_i+\tau)}B_iu(\tau)d\tau + \sum_{j=1}^{i} A^*_{ij} \int_{-L_i}^{-L_j} \int_{0}^{\xi} S_j(\xi)\mathrm{e}^{s(\xi-\tau)}u(\tau)d\tau d\xi.
\end{aligned} \tag{4.107}
$$

In the above equation, the last two terms are determined only by the initial values of the input. We refer to the coefficient matrix to $U(s)$ in the above equation as $\tilde{B}_i(s)$, and we obtain

$$
\tilde{B}_i(s) = \mathrm{e}^{-sL_i}B_i - \sum_{j=1}^{i} A^*_{ij} \int_{-L_i}^{-L_j} \mathrm{e}^{s\xi}S_j(\xi)d\xi. \tag{4.108}
$$

From Lemma 4.6, $\tilde{B}_i(s)$ becomes

$$
\begin{aligned}
\tilde{B}_i(s) &= \mathrm{e}^{-sL_i}B_i - \sum_{j=1}^{i} A^*_{ij} \int_{-L_i}^{-L_j} \mathrm{e}^{s\xi} \left[\mathrm{e}^{-(L_j+\xi)A}B\right]_j d\xi \\
&= \mathrm{e}^{-sL_i}B_i - \sum_{j=1}^{i} A^*_{ij} \left[\mathrm{e}^{-sL_j}(sI_n - A)^{-1}B\right]_j \\
&\quad + \mathrm{e}^{-sL_i} \sum_{j=1}^{i} A^*_{ij} \left[\mathrm{e}^{-A(L_j-L_i)}(sI_n - A)^{-1}B\right]_j \\
&= \mathrm{e}^{-sL_i}B_i - \left[A^*\tilde{L}(s)(sI_n - A)^{-1}B\right]_i \\
&\quad + \mathrm{e}^{-sL_i} \sum_{j=1}^{i} A^*_{ij} \left[\mathrm{e}^{-AL_j}\right]_j \mathrm{e}^{AL_i}(sI_n - A)^{-1}B.
\end{aligned} \tag{4.109}
$$

Here we focus on the factor $\left\{\sum_{j=1}^{i} A^*_{ij} \left[\mathrm{e}^{-AL_j}\right]_j \mathrm{e}^{AL_i}\right\}$ in the third term of the above equation. Referring to Lemmas 4.3 and 4.4, we find that

$$
\begin{aligned}
\sum_{j=1}^{i} A^*_{ij} \left[\mathrm{e}^{-AL_j}\right]_j \mathrm{e}^{AL_i} &= \sum_{j=1}^{i} A^*_{ij} \left[E^{-1}\right]_j \mathrm{e}^{AL_i} = \left[A^*E^{-1}\right]_i \mathrm{e}^{AL_i} = \left[E^{-1}A\mathrm{e}^{AL_i}\right]_i \\
&= \left[E^{-1}\right]_i \mathrm{e}^{AL_i}A = \left[\mathrm{e}^{-AL_i}\right]_i \mathrm{e}^{AL_i}A = \left[\mathrm{e}^{-AL_i}\mathrm{e}^{AL_i}A\right]_i \\
&= [A]_i .
\end{aligned} \tag{4.110}
$$

Thus

$$
\tilde{B}_i(s) = \mathrm{e}^{-sL_i}B_i - \left[A^*\tilde{L}(s)(sI_n - A)^{-1}B\right]_i + \mathrm{e}^{-sL_i}\left[A(sI_n - A)^{-1}B\right]_i . \tag{4.111}
$$

Obviously, $B_i = [B]_i$ and $\mathrm{e}^{-sL_i}[X]_i = \left[\tilde{L}(s)X\right]_i$. Hence we obtain

$$
\begin{aligned}
\tilde{B}_i(s) &= \left[\tilde{L}(s)\left\{I_n + A(sI_n - A)^{-1}\right\}B\right]_i - \left[A^*\tilde{L}(s)(sI_n - A)^{-1}B\right]_i \\
&= \left[(sI_n - A^*)\tilde{L}(s)(sI_n - A)^{-1}B\right]_i .
\end{aligned} \tag{4.112}
$$

Consequently, we have

$$\begin{aligned}\mathcal{L}\left[B^*(u,t)\right]_i &= \left[(sI_n - A^*)\tilde{L}(s)(sI_n - A)^{-1}B\right]_i U(s) + \int_{-L_i}^{0} \mathrm{e}^{-s(L_i+\tau)} B_i u(\tau) d\tau \\ &\quad + \sum_{j=1}^{i} A_{ij}^* \int_{-L_i}^{-L_j} \int_{0}^{\xi} S_j(\xi) \mathrm{e}^{s(\xi-\tau)} u(\tau) d\tau d\xi. \end{aligned} \tag{4.113}$$

Stacking the each side of the above equation for $i = 1, \cdots, p$ in one column, we see that

$$\begin{aligned}\mathcal{L}\left[B^*(u,t)\right] &= (sI_n - A^*)\tilde{L}(s)(sI_n - A)^{-1}BU(s) \\ &\quad + \begin{bmatrix} \int_{-L_1}^{0} \mathrm{e}^{-s(L_1+\tau)} B_1 u(\tau) d\tau + A_{11}^* \int_{-L_1}^{-L_1} \int_{0}^{\xi} S_1(\xi) \mathrm{e}^{s(\xi-\tau)} u(\tau) d\tau d\xi \\ \int_{-L_2}^{0} \mathrm{e}^{-s(L_2+\tau)} B_2 u(\tau) d\tau + \sum_{j=1}^{2} A_{2j}^* \int_{-L_2}^{-L_j} \int_{0}^{\xi} S_j(\xi) \mathrm{e}^{s(\xi-\tau)} u(\tau) d\tau d\xi \\ \vdots \\ \int_{-L_p}^{0} \mathrm{e}^{-s(L_p+\tau)} B_p u(\tau) d\tau + \sum_{j=1}^{p} A_{pj}^* \int_{-L_p}^{-L_j} \int_{0}^{\xi} S_j(\xi) \mathrm{e}^{s(\xi-\tau)} u(\tau) d\tau d\xi \end{bmatrix}. \end{aligned} \tag{4.114}$$

Substituting the above equation into Eq. (4.106), we obtain Eq. (4.51).

4.5.3 Derivation of Eq. (4.58)

The Laplace transform of Eq. (4.33) becomes

$$U(s) = -\begin{bmatrix} F_w & F_p \end{bmatrix} \begin{bmatrix} W(s) - \mathcal{L}\left\{S_w(u,t)\right\} \\ \tilde{X}(s) - \mathcal{L}\left\{S_x(u,t)\right\} \end{bmatrix}. \tag{4.115}$$

First, we analyze the i-th element of $\mathcal{L}\left\{S_w(u,t)\right\}$.

$$\begin{aligned}\left\langle \mathcal{L}\left\{S_w(u,t)\right\} \right\rangle_i &= \int_0^{\infty} \mathrm{e}^{-st} \left\{ \int_{-L_i}^{0} \sum_{j=1}^{i} \tilde{C}_{ij}(\xi) S_j(\xi) u(t+\xi) d\xi \right\} dt \\ &= \int_{-L_i}^{0} \sum_{j=1}^{i} \tilde{C}_{ij}(\xi) S_j(\xi) \left\{ \int_0^{\infty} \mathrm{e}^{-st} u(t+\xi) dt \right\} d\xi \\ &= \int_{-L_i}^{0} \mathrm{e}^{s\xi} \sum_{j=1}^{i} \tilde{C}_{ij}(\xi) S_j(\xi) d\xi U(s) \\ &\quad - \int_{-L_i}^{0} \int_{0}^{\xi} \mathrm{e}^{s(\xi-\tau)} \sum_{j=1}^{i} \tilde{C}_{ij}(\xi) S_j(\xi) u(\tau) d\tau d\xi. \end{aligned} \tag{4.116}$$

The coefficient vector of $U(s)$ is

$$\int_{-L_i}^{0} \mathrm{e}^{s\xi} \sum_{j=1}^{i} \tilde{C}_{ij}(\xi) S_j(\xi) d\xi = \int_{-L_i}^{0} \mathrm{e}^{s\xi} \sum_{j=1}^{i} \left\{ C_{ii} \int_{-L_i}^{\xi} E_{ij}(\lambda) d\lambda \right\} S_j(\xi) d\xi$$

$$
\begin{aligned}
&= \left\langle C \int_{-L_i}^{0} \int_{-L_i}^{\xi} \mathrm{e}^{s\xi} E(\lambda) E^{-1}(\xi) E(\xi) S_j(\xi) d\lambda d\xi \right\rangle_i \\
&= \left\langle C \int_{-L_i}^{0} \mathrm{e}^{A\lambda} \int_{\lambda}^{0} \mathrm{e}^{(sI_n - A)\xi} d\xi d\lambda B \right\rangle_i \\
&= \left\langle C \int_{-L_i}^{0} \mathrm{e}^{A\lambda} \left\{ I_n - \mathrm{e}^{(sI_n - A)\lambda} \right\} d\lambda (sI_n - A)^{-1} B \right\rangle_i \\
&= \left\langle C \left\{ \int_{-L_i}^{0} \mathrm{e}^{A\lambda} d\lambda - \left[s^{-1} \mathrm{e}^{s\lambda} I_n \right]_{-L_i}^{0} \right\} (sI_n - A)^{-1} B \right\rangle_i \\
&= \left\langle \left\{ \tilde{C} E^{-1} - s^{-1} C + s^{-1} L(s) C \right\} (sI_n - A)^{-1} B \right\rangle_i .
\end{aligned}
\tag{4.117}
$$

The last equality is derived from Lemma 4.5. Thus we obtain

$$
\begin{aligned}
\mathcal{L}\{S_w(u,t)\} &= \left\{ \tilde{C} E^{-1} - s^{-1} C + s^{-1} L(s) C \right\} (sI_n - A)^{-1} B U(s) \\
&\quad - \begin{bmatrix} \int_{-L_1}^{0} \int_{0}^{\xi} \mathrm{e}^{s(\xi-\tau)} \sum_{j=1}^{1} \tilde{C}_{1j}(\xi) S_j(\xi) u(\tau) d\tau d\xi \\ \vdots \\ \int_{-L_p}^{0} \int_{0}^{\xi} \mathrm{e}^{s(\xi-\tau)} \sum_{j=1}^{p} \tilde{C}_{pj}(\xi) S_j(\xi) u(\tau) d\tau d\xi \end{bmatrix} .
\end{aligned}
\tag{4.118}
$$

Second, we examine the i-th row block of $\mathcal{L}\{S_x(u,t)\}$.

$$
\begin{aligned}
[\mathcal{L}\{S_x(u,t)\}]_i &= \int_0^{\infty} \mathrm{e}^{-st} \left\{ \int_{-L_i}^{0} S_i(\xi) u(t+\xi) d\xi \right\} dt \\
&= \int_{-L_i}^{0} \mathrm{e}^{s\xi} S_i(\xi) d\xi U(s) - \int_{-L_i}^{0} \int_{0}^{\xi} \mathrm{e}^{s(\xi-\tau)} S_i(\xi) u(\tau) d\tau d\xi .
\end{aligned}
\tag{4.119}
$$

Here, we examine the coefficient matrix to $U(s)$ in the first term of the above equation. From Lemma 4.6,

$$
\begin{aligned}
\int_{-L_i}^{0} \mathrm{e}^{s\xi} S_i(\xi) d\xi &= \int_{-L_i}^{0} \mathrm{e}^{s\xi} \left[\mathrm{e}^{-A(L_i+\xi)} B \right]_i d\xi \\
&= \left[\mathrm{e}^{-AL_i} \int_{-L_i}^{0} \mathrm{e}^{(sI_n - A)\xi} d\xi B \right]_i \\
&= \left[\left\{ \mathrm{e}^{-AL_i} - \mathrm{e}^{-sL_i} I_n \right\} (sI_n - A)^{-1} B \right]_i \\
&= \left[E^{-1} - \tilde{L}(s) \right]_i (sI_n - A)^{-1} B .
\end{aligned}
\tag{4.120}
$$

Consequently, the Laplace transform of $S_x(u,t)$ is obtained as

$$
\begin{aligned}
\mathcal{L}\{S_x(u,t)\} &= \left\{ E^{-1} - \tilde{L}(s) \right\} (sI_n - A)^{-1} B U(s) \\
&\quad - \begin{bmatrix} \int_{-L_1}^{0} \int_{0}^{\xi} \mathrm{e}^{s(\xi-\tau)} S_1(\xi) u(\tau) d\tau d\xi \\ \vdots \\ \int_{-L_p}^{0} \int_{0}^{\xi} \mathrm{e}^{s(\xi-\tau)} S_p(\xi) u(\tau) d\tau d\xi \end{bmatrix} .
\end{aligned}
\tag{4.121}
$$

Substituting Eqs. (4.118) and (4.121) into Eq. (4.115), we find Eq. (4.58).

4.5.4 Derivation of Eq. (4.64)

As in Eq. (4.63), the characteristic function of the closed-loop system is $\det R(s) = 0$ where

$$R(s) = \begin{bmatrix} sI_p & \bar{C}^r(s) & 0_{p\times n} & 0_{p\times p} \\ 0_{n\times p} & sI_n - A - \Delta_A & 0_{n\times n} & -B \\ 0_{n\times p} & -K\bar{C}^r(s) & sI_n - A_o & -\tilde{B}(s) \\ F_w & 0_{p\times n} & F_p & I_p + f_u(s) \end{bmatrix}. \tag{4.122}$$

In the following, we apply fundamental operations to the matrix $R(s)$ in order to make it block lower triangular, then calculate a determinant of it as a product of determinants of its diagonal blocks.

First, multiplying the first column block from right side by $s^{-1}\bar{C}^r(s)$ and the fourth column block from right side by F_x, and subtracting them from the second column block, we obtain

$$\det R(s) = \begin{vmatrix} sI_p & 0_{p\times n} & 0_{p\times n} & 0_{p\times p} \\ 0_{n\times p} & sI_n - A_F^\Delta & 0_{n\times n} & -B \\ 0_{n\times p} & -K\bar{C}^r(s) + \tilde{B}(s)F_x & sI_n - A_o & -\tilde{B}(s) \\ F_w & -s^{-1}F_w\tilde{C}^r(s) - F_x - f_u(s)F_x & F_p & I_p + f_u(s) \end{vmatrix}, \tag{4.123}$$

where $A_F^\Delta = A + \Delta_A - BF_x$. Next, multiplying the second column from right by $(sI_n - A_F^\Delta)^{-1}B$ and adding them to the fourth column, we have

$$\det R(s) = \begin{vmatrix} sI_p & 0_{p\times n} & 0_{p\times n} & 0_{p\times p} \\ 0_{n\times p} & sI_n - A_F^\Delta & 0_{n\times n} & 0_{n\times p} \\ 0_{n\times p} & -K\bar{C}^r(s) + \tilde{B}(s)F_x & sI_n - A_o & G_{34}(s) \\ F_w & -s^{-1}F_w\tilde{C}^r(s) - F_x - f_u(s)F_x & F_p & G_{44}(s) \end{vmatrix}, \tag{4.124}$$

where

$$G_{34}(s) = -\tilde{B}(s) - K\bar{C}^r(s)(sI_n - A_F^\Delta)^{-1}B + \tilde{B}(s)F_x(sI_n - A_F^\Delta)^{-1}B, \tag{4.125}$$

$$G_{44}(s) = I_p + f_u(s) - \left\{s^{-1}F_w\bar{C}^r(s) + F_x + f_u(s)F_x\right\}(sI_n - A_F^\Delta)^{-1}B. \tag{4.126}$$

Then multiplying the third column from right by $(sI_n - A_o)^{-1}G_{34}(s)$ and subtracting it from the fourth column, we find that

$$\det R(s) = \begin{vmatrix} sI_p & 0_{p\times n} & 0_{p\times n} & 0_{p\times p} \\ 0_{n\times p} & sI_n - A_F^\Delta & 0_{n\times n} & 0_{n\times p} \\ 0_{n\times p} & -K\bar{C}^r(s) + \tilde{B}(s)F_x & sI_n - A_o & 0_{n\times p} \\ F_w & -s^{-1}F_w\tilde{C}^r(s) - F_x - f_u(s)F_x & F_p & G_U(s) \end{vmatrix}, \tag{4.127}$$

where

$$G_U(s) = G_{44}(s) - F_p(sI_n - A_o)^{-1}G_{34}(s). \tag{4.128}$$

Consequently, we obtain

$$\det R(s) = s^p \det\left\{sI_n - A_F^{\Delta}\right\} \det\left\{sI_n - A_o\right\} \det\left\{G_U(s)\right\}. \tag{4.129}$$

Now we analyze the determinant of $G_U(s)$. From the definitions of $G_U(s)$, $G_{34}(s)$ and $G_{44}(s)$, we have

$$\begin{aligned} G_U(s) &= I_p + f_u(s) - \left\{s^{-1}F_w\bar{C}^r(s) + F_x + f_u(s)F_x\right\}(sI_n - A_F^{\Delta})^{-1}B \\ &\quad + F_p(sI_n - A_o)^{-1}\tilde{B}(s)\left\{I_p - F_x(sI_n - A_F^{\Delta})^{-1}B\right\} \\ &\quad + F_p(sI_n - A_o)^{-1}K\bar{C}^r(s)(sI_n - A_F^{\Delta})^{-1}B \\ &= \left\{I_p + f_u(s) + F_p(sI_n - A_o)^{-1}\tilde{B}(s)\right\}\left\{I_p - F_x(sI_n - A_F^{\Delta})^{-1}B\right\} \\ &\quad - \left\{s^{-1}F_w - F_p(sI_n - A_o)^{-1}K\right\}\bar{C}^r(s)(sI_n - A_F^{\Delta})^{-1}B. \end{aligned} \tag{4.130}$$

Substituting Eqs. (4.59) and (4.54) into the term $\left\{I_p + f_u(s) + F_p(sI_n - A_o)^{-1}\tilde{B}(s)\right\}$, we have

$$\begin{aligned} &\left\{I_p + f_u(s) + F_p(sI_n - A_o)^{-1}\tilde{B}(s)\right\} \\ &\quad = I_p + F_w\left\{\tilde{C}E^{-1} - s^{-1}C + s^{-1}L(s)C\right\}(sI_n - A)^{-1}B + F_pE^{-1}(sI_n - A)^{-1}B \\ &\quad\quad - F_p\tilde{L}(s)(sI_n - A)^{-1}B + F_p(sI_n - A_o)^{-1}(sI_n - A^*)\tilde{L}(s)(sI_n - A)^{-1}B \\ &\quad = I_p + \left[F_x - s^{-1}F_w\left\{C - L(s)C\right\} - F_p(sI_n - A_o)^{-1}KC\tilde{L}(s)\right](sI_n - A)^{-1}B, \end{aligned} \tag{4.131}$$

because $A^* = A_o + KC$ (Eq. (4.53)) and $F_x = F_w\tilde{C}E^{-1} + F_pE^{-1}$ (Eq. (4.34)). Therefore we obtain

$$\begin{aligned} G_U(s) &= \left\{I_p + f_A(s)(sI_n - A)^{-1}B\right\}\left\{I_p - F_x(sI_n - A_F^{\Delta})^{-1}B\right\} \\ &\quad - f_C(s)\bar{C}^r(s)(sI_n - A_F^{\Delta})^{-1}B, \end{aligned} \tag{4.132}$$

where

$$f_A(s) = F_x - s^{-1}F_w\left\{C - L(s)C\right\} - F_p(sI_n - A_o)^{-1}KC\tilde{L}(s), \tag{4.133}$$

$$f_C(s) = s^{-1}F_w - F_p(sI_n - A_o)^{-1}K. \tag{4.134}$$

For terms in Eq. (4.132), the following equations hold:

$$\begin{aligned} &\left\{I_p + f_A(s)(sI_n - A)^{-1}B\right\}\left\{I_p - F_x(sI_n - A_F^{\Delta})^{-1}B\right\} \\ &\quad = I_p + f_A(s)(sI_n - A)^{-1}B - \left\{I_p + f_A(s)(sI_n - A)^{-1}B\right\}F_x(sI_n - A_F^{\Delta})^{-1}B \\ &\quad = I_p + f_A(s)(sI_n - A)^{-1}\left\{(sI_n - A) + BF_x - \Delta_A\right\}(sI_n - A_F^{\Delta})^{-1}B \\ &\quad\quad - \left\{F_x + f_A(s)(sI_n - A)^{-1}BF_x\right\}(sI_n - A_F^{\Delta})^{-1}B \\ &\quad = I_p + \left\{f_A(s) - F_x\right\}(sI_n - A_F^{\Delta})^{-1}B - f_A(s)(sI_n - A)^{-1}\Delta_A(sI_n - A_F^{\Delta})^{-1}B, \\ &f_C(s)\bar{C}^r(s)(sI_n - A_F^{\Delta})^{-1}B \\ &\quad = f_C(s)L(s)\left\{C + CL_{\Delta}(s) + C_{\Delta}(s)\right\}(sI_n - A_F^{\Delta})^{-1}B \\ &\quad = f_C(s)L(s)C(sI_n - A_F^{\Delta})^{-1}B + f_C(s)L(s)\Delta(s)(sI_n - A_F^{\Delta})^{-1}B. \end{aligned} \tag{4.135}$$

Therefore $G_U(s)$ is given by

$$\begin{aligned} G_U(s) &= I_p + \{f_A(s) - F_x - f_C(s)L(s)C\}(sI_n - A_F^\Delta)^{-1}B \\ &\quad - \left\{f_A(s)(sI_n - A)^{-1}\Delta_A + f_C(s)L(s)\Delta(s)\right\}(sI_n - A_F^\Delta)^{-1}B. \end{aligned} \tag{4.136}$$

From the definitions of $f_A(s)$ and $f_C(s)$, the following equations hold:

$$\begin{aligned} &\{f_A(s) - F_x - f_C(s)L(s)C\} \\ &\quad = F_x - s^{-1}F_w\{C - L(s)C\} - F_p(sI_n - A_o)^{-1}KC\tilde{L}(s) - F_x - s^{-1}F_wL(s)C \\ &\qquad + F_p(sI_n - A_o)^{-1}KL(s)C \\ &\quad = -s^{-1}F_wC - F_p(sI_n - A_o)^{-1}K\left\{C\tilde{L}(s) - L(s)C\right\} = -s^{-1}F_wC. \end{aligned} \tag{4.137}$$

The last equation is due to the block diagonality of C. Thus $G_U(s)$ is given by

$$G_U(s) = I_p - G_1(s)(sI_n - A_F^\Delta)^{-1}B, \tag{4.138}$$

where

$$G_1(s) = s^{-1}F_wC + f_A(s)(sI_n - A)^{-1}\Delta_A + f_C(s)L(s)\Delta(s). \tag{4.139}$$

We have

$$\begin{aligned} \det\{G_U(s)\} &= \det\left\{I_p - G_1(s)(sI_n - A_F^\Delta)^{-1}B\right\} = \det\left\{I_n - (sI_n - A_F^\Delta)^{-1}BG_1(s)\right\} \\ &= \det\left\{(sI_n - A_F^\Delta)^{-1}\right\}\det\left\{sI_n - A_F^\Delta - BG_1(s)\right\}. \end{aligned} \tag{4.140}$$

The second factor of the above equation is given by

$$\begin{aligned} &\det\left\{sI_n - A_F^\Delta - BG_1(s)\right\} \\ &\quad = \det\left\{sI_n - A_F^\Delta - s^{-1}BF_wC - Bf_A(s)(sI_n - A)^{-1}\Delta_A - Bf_C(s)L(s)\Delta(s)\right\} \\ &\quad = \det\left\{sI_n - \hat{A}_F(s) - G_3(s)\Delta_A - Bf_C(s)L(s)\Delta(s)\right\}, \end{aligned} \tag{4.141}$$

where $G_3(s) = \{I_n + Bf_A(s)(sI_n - A)^{-1}\}$. From Eq. (4.137), the term $G_3(s)$ becomes

$$\begin{aligned} G_3(s) &= I_n + B\left\{F_x + f_c(s)L(s)C - s^{-1}F_wC\right\}(sI_n - A)^{-1} \\ &= \left\{(sI_n - A) + BF_x - s^{-1}BF_wC + Bf_c(s)L(s)C\right\}(sI_n - A)^{-1} \\ &= \left\{sI_n - \hat{A}_F(s)\right\}\{I_n + G_\Delta(s)C\}(sI_n - A)^{-1}. \end{aligned} \tag{4.142}$$

Substituting the above equation into Eq. (4.141), we obtain

$$\det\left\{sI_n - A_F^\Delta - BG_1(s)\right\} = \det\left\{sI_n - \hat{A}_F(s)\right\}\det\{I_n - G_A(s)\Delta_A - G_\Delta(s)\Delta(s)\}. \tag{4.143}$$

Furthermore, we have

$$s^p\det\left\{sI_n - \hat{A}_F(s)\right\} = \det\left\{sI_n - \bar{A} + \bar{B}\bar{F}\right\}, \tag{4.144}$$

because Eq. (4.10) holds.

Substituting Eqs. (4.140), (4.143) and (4.144) into Eq. (4.129), we find that Eq. (4.64) holds.

Chapter 5

A model predictive hypnosis control system under total intravenous anesthesia

In the preceding chapters, we discussed on identification and control of multivariable systems including multiple delays. As an actual controlled process of such systems, we refer to a patient receiving general anesthesia. In this controlled process, outputs are considered to be hypnosis, analgesia, muscle relaxation, elimination of autonomic reflexes, and so forth [37]. The manipulated input of the controlled process is administration of various drugs. Administering these drugs, an anesthesiologist maintains the outputs at their desired level. In the following chapters, control systems for maintaining these outputs are developed, utilizing the results of the preceding chapters.

In this chapter, noticing only hypnosis of the patient, a hypnosis control system during general anesthesia is developed. This system regulates only hypnosis level and regards the controlled process as a single-input single-output process. A multivariable control system for general anesthesia is studied in the next chapter.

During general anesthesia, hypnotic drugs must be administered adequately to prevent intra-operative arousal and post-operative adverse reactions. This requirement is crucial in ambulatory surgery because patients must stay in the hospital overnight if the adverse reactions are severe. To satisfy this requirement, an intravenous hypnotic drug, propofol, is widely used for ambulatory anesthesia because propofol possesses favorable pharmacokinetic profiles [38] and shows reduced frequency of post-operative adverse reactions such as post-operative nausea and vomiting (PONV) [39]. The infusion rate of propofol during general anesthesia must be adjusted carefully to realize these merits. For that reason, numerous studies of automatic administration of propofol have been done [40–50]. Among them, "Target Controlled Infusion (TCI)" system [40] is well known and now widely accepted. The TCI system estimates propofol concentration in plasma or in the effect site of propofol using a pharmacokinetic model of propofol as a dynamic model, and administers propofol to regulate the concentration close to a target

level. Some researchers have advocated that the TCI system has sufficient performance for clinical use [41]. However, from the viewpoint of control engineering, the TCI system works as an open-loop controller and does not have tracking ability to a target. Consequently, anesthesiologists should adjust the target concentration suitably to cope with individual differences and noxious stimuli during surgery.

On the other hand, some quantitative indices derived from spontaneous electroencephalogram (EEG) for assessing the depth of hypnosis have been proposed in recent years [51]. Among them, the Bispectral Index (BIS) [52] is the most widely investigated and used [53]. The BIS is indicated as a number between 0 to 100, where the value 100 corresponds to an awake state and a lower value means a higher hypnotic state. The BIS is derived from a proprietary algorithm [52] including bispectral analysis, power spectral analysis and time domain analysis. These analyzes are performed on the EEG obtained from three electrodes. The first electrode is placed on the center of the forehead, the second electrode is set at 1.1 in. lateral to the first electrode, and the third electrode is placed on either temporal area between the corner of the eye and the hairline. The sampling frequency of the EEG measurement is 128Hz. In October 1996, the original BIS monitors (A-1000 and A-1050) were approved by the U. S. (United States) Food and Drug Administration (FDA) as the first device for monitoring of anesthetic depth [54]. In January 2004, the improved BIS monitor (A-2000) was approved by the FDA for the indication of reducing the incidence of intraoperative awareness during general anesthesia [55]. The manufacturer (Aspect Medical Systems Inc., Norwood, MA) states that in April 2007, the BIS monitor has been adopted in 55% of all operating rooms in the U. S., 71% of the largest 1000 U. S. hospitals, and 86% of the U. S. teaching hospitals [56]. Although the BIS occasionally indicates an incorrect hypnotic state [57], the BIS monitor is the most reliable and widely accepted device among currently available devices, and utilized for titrating hypnotic drug dose [58].

Utilizing the BIS, automatic infusion systems with feedback mechanisms have been studied [42–50] to handle the individual differences and the noxious stimuli adequately. In these systems, proportional-derivative or proportional-integral-derivative controllers [42–47], a model-based controller [48, 49], or a nonlinear adaptive controller [50] were used. However, most of those studies did not take into account for delays caused by the movement of propofol in an intravenous line, the distribution of propofol in blood vessels, and the signal processing time within the BIS monitor [59]. Struys et al. [48] took the delays into account in estimation of patient-specific parameters, but that system required much time for the estimation, and the control strategy was unable to cope adequately with the delays. Bailey and Haddad [50] pointed out the need for consideration of the delays, because an undershoot of the BIS at the induction of anesthesia occurred in their nonlinear adaptive control system.

We have developed a hypnosis control system using the BIS as the index of hypnosis and propofol as the intravenous hypnotic drug. The system uses a model predictive controller [10], which can rigorously take the delay into account. Moreover, it has a function of short-time estimation of individual pharmacodynamic parameters from the

BIS response during the induction of anesthesia. With the approval of the Ethics Committee on Human Research of the Kyoto University Graduate School of Medicine, we applied the system to various kinds of ambulatory surgery at Kyoto University Hospital (Kyoto, Japan) and confirmed its accuracy in hypnosis control and effects of drug reduction. This chapter describes the details of a model of BIS response to propofol infusion, the parameter estimation function, the control law and the risk-control function. Furthermore, the results of clinical trials are compared with those of other hypnosis control systems [44–48] and anesthesiologist's manual adjustment.

This chapter is organized as follows. Section 5.1 is devoted to description of the model of the BIS response to propofol infusion. Individual differences in model parameters are also considered. In Section 5.2, a function for estimation of the individual parameters, strategy and design of model predictive controller, and a risk-control function of the system are explained. In Section 5.3, the clinical system and the results of the clinical trials are presented. Evaluation of the controller performance and discussion are made in Section 5.4.

5.1 Model of hypnosis change to drug infusion

To design an appropriate controller for a specific process, a mathematical model of the process is required. The accuracy of the model strongly influences the performance of the control system, especially when a model-based controller is used. In this section, we introduce a model of the BIS response to propofol infusion. The model is a series connection of three elements: a pharmacokinetic model, a time delay, and a pharmacodynamic model. In the following subsections, detailed descriptions of respective elements are presented.

5.1.1 Pharmacokinetic model

Pharmacokinetic models describe the dynamics of drug concentration in human body. We construct a pharmacokinetic model based on the population pharmacokinetic model given through a large-scale multicenter study by Schüttler and Ihmsen [20], because the patient's age and body weight are incorporated in this model and this model seems to be sufficiently reliable. However, the Schüttler-Ihmsen model does not include the effect site [60] that relates directly to the BIS. Furthermore, the model parameters for continuous infusion of the Schüttler-Ihmsen model differ from those for a bolus. Considering these factors, we propose a unified model that can deal with both bolus and continuous infusion and has the effect site compartment.

The original Schüttler-Ihmsen model is given by

$$\frac{d}{dt}\begin{bmatrix} x_1(t) \\ x_2(t) \\ x_3(t) \end{bmatrix} = \begin{bmatrix} -\frac{k_1+k_2+k_3}{V_1} & \frac{k_2}{V_1} & \frac{k_3}{V_1} \\ \frac{k_2}{V_2} & -\frac{k_2}{V_2} & 0 \\ \frac{k_3}{V_3} & 0 & -\frac{k_3}{V_3} \end{bmatrix} \begin{bmatrix} x_1(t) \\ x_2(t) \\ x_3(t) \end{bmatrix} + \begin{bmatrix} \frac{1}{V_1} \\ 0 \\ 0 \end{bmatrix} u(t). \tag{5.1}$$

Table 5.1: Pharmacokinetic parameter values given by Schüttler and Ihmsen [20]

V_1^{con}	$1.72\mathrm{BW}^{0.71}\mathrm{age}^{-0.39}$ L	V_1^{bol}	$4.49\mathrm{BW}^{0.71}\mathrm{age}^{-0.39}$ L
V_2^{con}	$3.32\mathrm{BW}^{0.61}$ L	V_2^{bol}	$5.74\mathrm{BW}^{0.61}$ L
V_3^{con}	266 L	V_3^{bol}	the same as V_3^{con}
k_1^{con}	$0.0595\mathrm{BW}^{0.75}$ L/min (age ≤ 60) $(0.0595\mathrm{BW}^{0.75} - 0.045\mathrm{age} + 2.7)$ L/min (age > 60)	k_1^{bol}	the same as k_1^{con}
k_2^{con}	$0.0969\mathrm{BW}^{0.62}$ L/min	k_2^{bol}	$0.293\mathrm{BW}^{0.62}$ L/min
k_3^{con}	$0.0889\mathrm{BW}^{0.55}$ L/min	k_3^{bol}	$0.0462\mathrm{BW}^{0.55}$ L/min

Here x_i is the concentration of propofol in compartment i; compartments 1, 2 and 3 correspond respectively to the central, shallow peripheral, and deep peripheral compartment. In addition, u is the infusion rate of propofol, and k_i and V_i are the clearance and volume of compartment i, respectively, given by functions of the patient's age and body weight, as in Table 5.1. The superscripts "bol" and "con" of the parameters in Table 5.1 respectively designate administration by bolus and continuous infusion.

Based on Eq. (5.1), we construct a unified model under the following considerations.

- The parameter values of the unified model for continuous infusion, except for those of the effect site, are given by the parameter values for continuous infusion in Table 5.1, because anesthesia is usually maintained by continuous infusion.

- In the bolus case, infused propofol moves directly to the shallow peripheral compartment and to the central compartment, as shown in Fig. 5.1.

  Physiologically, a bolus of propofol reduces hepatic blood flow [61], which decreases the clearance of the central compartment. Consequently, the bolused propofol remains in the patient's body for a longer time than in continuous-infusion cases. Although this phenomenon might be considered by a nonlinear clearance, such nonlinearity increases the model complexity. Furthermore, the exact form of the nonlinearity has never been shown. For these reasons, we introduce a linear model which imitates this phenomenon by assuming that a fraction of the bolused propofol accumulates in the shallow peripheral compartment, and fades after the transition to the central compartment.

- The volume V_4 of the effect site compartment is one hundredth of the central compartment. Namely, V_4 is set to $V_4 = V_1^{\mathrm{con}}/100$.

  Many studies have presumed that this volume is negligible. However, that consideration relies on the assumption that the drug is metabolized or eliminated in the effect site. That assumption seems to be irrelevant to hypnotic drugs. Furthermore, the assumption changes the relative degree of a transfer function of the process. For those reasons, we do not neglect the volume of the effect site compartment, and regard it to one-hundredth of the central compartment.

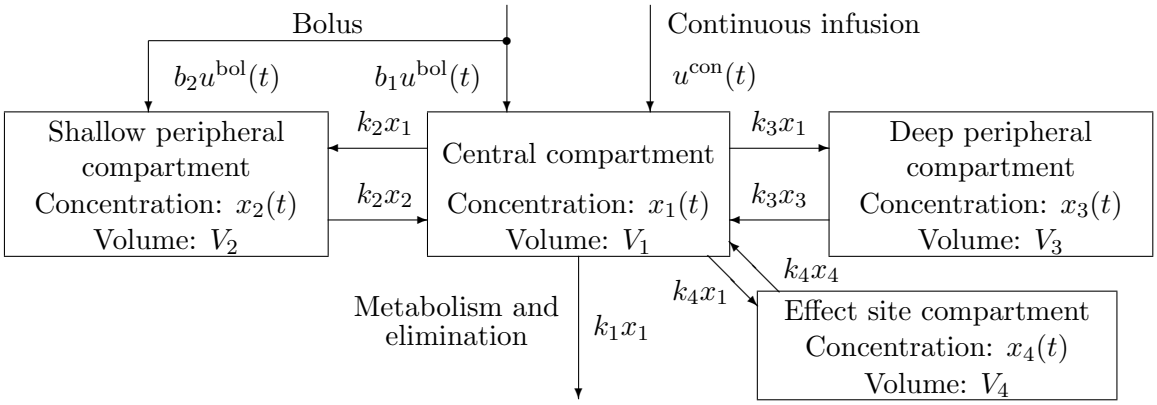

Figure 5.1: Three-compartment pharmacokinetic model with the effect site and a direct route to a shallow peripheral compartment for a bolus.

The constructed pharmacokinetic model is given by

$$\frac{dx(t)}{dt} = \begin{bmatrix} -\frac{k_1^{\mathrm{con}}+k_2^{\mathrm{con}}+k_3^{\mathrm{con}}+k_4}{V_1^{\mathrm{con}}} & \frac{k_2^{\mathrm{con}}}{V_1^{\mathrm{con}}} & \frac{k_3^{\mathrm{con}}}{V_1^{\mathrm{con}}} & \frac{k_4}{V_1^{\mathrm{con}}} \\ \frac{k_2^{\mathrm{cdn}}}{V_2^{\mathrm{con}}} & -\frac{k_2^{\mathrm{con}}}{V_2^{\mathrm{con}}} & 0 & 0 \\ \frac{k_3^{\mathrm{con}}}{V_3^{\mathrm{con}}} & 0 & -\frac{k_3^{\mathrm{con}}}{V_3^{\mathrm{con}}} & 0 \\ \frac{k_4}{V_4} & 0 & 0 & -\frac{k_4}{V_4} \end{bmatrix} x(t) + \begin{bmatrix} \frac{1}{V_1^{\mathrm{con}}} & b_1 \\ 0 & b_2 \\ 0 & 0 \\ 0 & 0 \end{bmatrix} \begin{bmatrix} u^{\mathrm{con}}(t) \\ u^{\mathrm{bol}}(t) \end{bmatrix}, \tag{5.2}$$

with $x(t) = [x_1(t)\ x_2(t)\ x_3(t)\ x_4(t)]^{\mathrm{T}}$, where x_4 is the propofol concentration in the effect site compartment, $u^{\mathrm{bol}}(t)$ is the bolus rate, and $u^{\mathrm{con}}(t)$ is the continuous infusion rate. Constants b_1 and b_2 are input coefficients for the bolus, and are given by solving the minimization problem of the quadratic error between $x_1(t)$ after a single bolus (an impulse input) of the Schüttler-Ihmsen model and that of Eq. (5.2). The clearance k_4 of the effect site compartment is determined from preliminary data collected from 47 patients (M/F 16/31, Age 48 ± 18 yr.(mean ± SD), body weight 57 ± 11 kg) under various kinds of ambulatory surgery. In these measurements, propofol was administered at the rate of 120 mg/kg/h for the first 1 min, then at the rate of 10 mg/kg/h for the subsequent 2 or 3 min. Thereafter, the rate was adjusted to maintain the BIS within the range of 40–60 [62] until surgery was completed. The values of the BIS and infusion rate were obtained in every one second. Using these measurements, k_4 is set to 0.12L/min so that the median peak time [63] of the effect site concentration, calculated using Eq. (5.2), coincides with the time between the beginning and the peak of the BIS decrease averaged among the patients.

In the following, we treat the infusion whose rate is greater than u^{th}, the threshold rate of the continuous infusion, as a bolus. That is, we define $u^{\mathrm{con}}(t)$ and $u^{\mathrm{bol}}(t)$ as

$$u^{\mathrm{con}}(t) = \begin{cases} u(t), & (u(t) \leq u^{\mathrm{th}}), \\ 0, & (\text{otherwise}), \end{cases} \quad u^{\mathrm{bol}}(t) = \begin{cases} 0, & (u(t) \leq u^{\mathrm{th}}), \\ u(t), & (\text{otherwise}). \end{cases} \tag{5.3}$$

The threshold rate u^{th} is set to 20 mg/kg/h, which is twice of the upper bound of the adequate infusion rate recommended by the supplier (AstraZeneca, Osaka, Japan), because the rate u^{th} is sufficiently large for maintenance of anesthesia in most situations. In all preliminary data, the continuous infusion rate of propofol was less than u^{th}.

Figure 5.2 shows responses of $x_1(t)$ to a bolus and continuous infusion for the Schüttler-Ihmsen model and the constructed unified model for a 40-year-old patient whose body weight is 60 kg. This figure shows that the unified model provides adequate responses both to the bolus and continuous infusion over the whole time domain. Similar results were obtained for patients of all ages and body weights.

5.1.2 Time delays and the pharmacodynamic model

In this subsection, we give a detailed description of delays and a pharmacodynamic model, and estimate their parameter values from preliminary measurements. Furthermore, the necessity for consideration of individual differences and the validity of the model are evaluated.

The response of the BIS to propofol infusion includes considerable time delays, which are caused by movement of propofol from a three-way stopcock to the patient's body in an intravenous fluid line, distribution of propofol in blood vessels (the central compartment), and calculation time of the BIS in the BIS monitor (approximately 15–60 s [59]).

The process is a single-input single-output system. Therefore, we consider a single output delay L_c whose length is the sum of the delays described above. That is, the present BIS value $\mathrm{BIS}(t)$ is determined by the past value of the effect site concentration,

$$y(t) = Cx(t - L_c), \tag{5.4}$$

where $C = [\ 0\ 0\ 0\ 1]$.

A pharmacodynamic model describes the relationship between the propofol concentration in the effect site compartment and the BIS. We use the sigmoidal $E_{\max}$ model [64] because it is widely accepted in pharmacodynamic studies of propofol [21,22]. This model is given by

$$\mathrm{BIS}^{\mathrm{model}}(t) = E_0 - E_{\max}\frac{y^{\gamma}(t)}{y^{\gamma}(t) + c_{50}^{\gamma}}, \tag{5.5}$$

where $\mathrm{BIS}^{\mathrm{model}}(t)$ is the present BIS, E_0 is the BIS in the waking state, $E_{\max}$ is the maximum effect intensity, c_{50} is the propofol concentration corresponding to the BIS value of $E_{\max}/2$, and γ is the Hill coefficient.

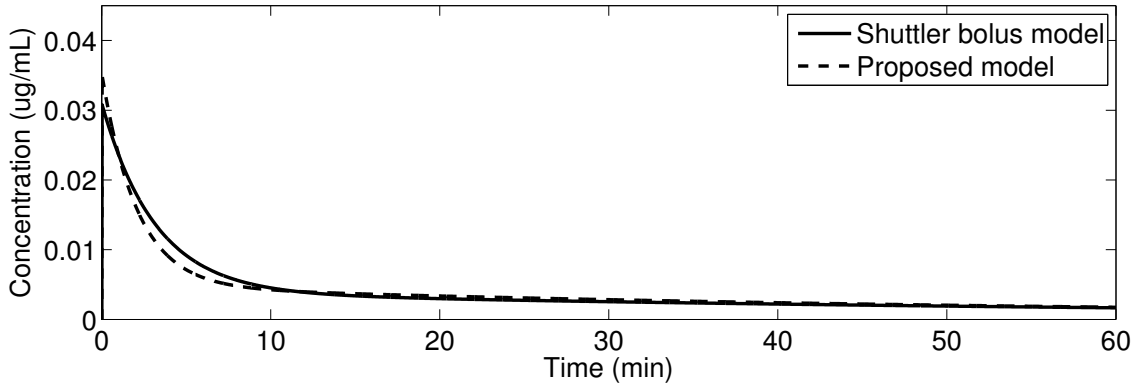

(a) Plasma propofol concentration to 1 mg/kg bolus

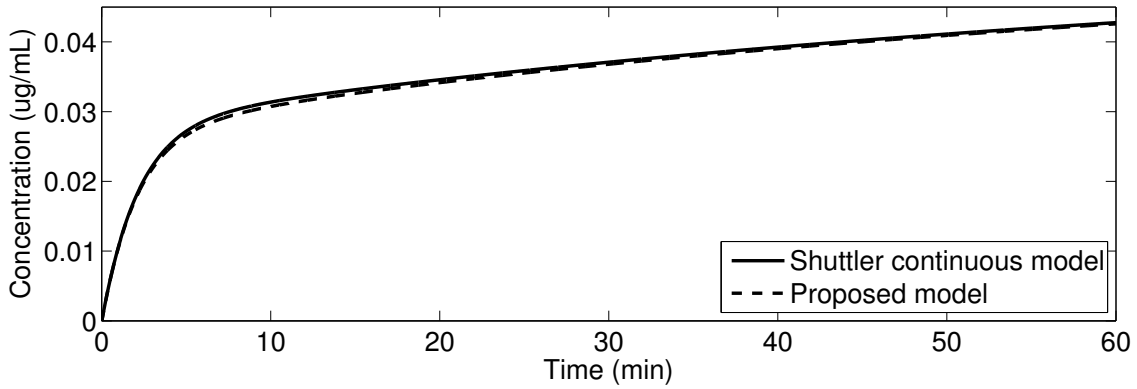

(b) Plasma propofol concentration to 10 mg/kg/h continuous infusion

Figure 5.2: Plasma propofol concentration of the conventional pharmacokinetic model given by Schüttler and Ihmsen [20] and the proposed model.

Next, we estimate the actual values of the delay length and pharmacodynamic parameters from the 47 data sets described in the preceding subsection.

To begin with, the delay length is estimated for each data. First, propofol concentration in the effect-site compartment is calculated from the propofol infusion rate $u(t)$ and Eq. (5.2). Then the estimate of the delay length $\hat{L}_c$ is determined by trial and error so that the relation between $y(t)$ and BIS(t) during the induction (the first 120 s after the start of infusion) approaches to the relation during the awakening period (time period after the stop of infusion). As an example of this procedure, the relationships between the propofol concentration in the effect site compartment and the BIS are shown in Figs. 5.3(a) and 5.3(b), without and with consideration of the delay.

Under the assumption that $E_{\max} = E_0$, which means the BIS tends to 0 when propofol concentration in the effect site becomes infinite, other parameters are estimated as follows. E_0 is set to the maximum BIS value before the start of infusion. The constants c_{50} and γ are determined to minimize a model fitness measure

$$J = \sum_{i=1}^{3} \sum_{t \in T_i} \frac{1}{\text{length}(T_i)} \left\{ \text{BIS}^{\text{model}}(t + \hat{L}_c) - \text{BIS}(t + \hat{L}_c) \right\}^2, \tag{5.6}$$

where T_1, T_2 and T_3 mean the induction, awakening and maintenance period that are defined, respectively, as the period up to 120 s from the start of infusion, the period after the end of infusion, and the period between induction and awakening periods. Moreover, length(T_i) represents the number of data points in T_i $(i = 1, 2, 3)$.

In the preliminary 47 data sets, the estimates of L_c, E_0, c_{50} and γ are 68 ± 34 s (mean$\pm$SD), 97.3 ± 0.8, 3.90 ± 1.05 μg/mL and 1.81 ± 0.67, respectively. The mean and standard deviation of the measure J for each measurement are 95.7 and 52.9, respectively.

The measure with fixed parameter values is calculated to evaluate the effect of individual differences. Substituting the mean values of the estimates into L_c, E_0, c_{50} and γ, the mean and standard deviation of measure J are 266.2 and 151.9, respectively. The mean is significantly larger than that with the individualized parameters. Therefore, we should consider the individual differences of these parameters.

Additionally, to evaluate the validity of the nonlinear pharmacodynamic model Eq. (5.5), we compare the model fitness of the nonlinear model with that of a linear model

$$\text{BIS}^{\text{lin}}(t) = k^{\text{lin}} y(t) + \text{BIS}^0. \tag{5.7}$$

The parameters k^{lin} and BIS^0 are identified individually using least-squares method under the same measure of model fitness. The identified values of k^{lin} and BIS^0 are, respectively, -11.5 ± 3.9 and 94.7 ± 11.7. The mean and standard deviation of the measure J are 112.6 and 57.3, respectively. The mean is larger than that of the nonlinear model with individualized parameters. Therefore, the nonlinear pharmacodynamic model, Eq. (5.5), is more adequate than the linear one. Based on the above considerations, we utilize the nonlinear pharmacodynamic model with individualized parameters.

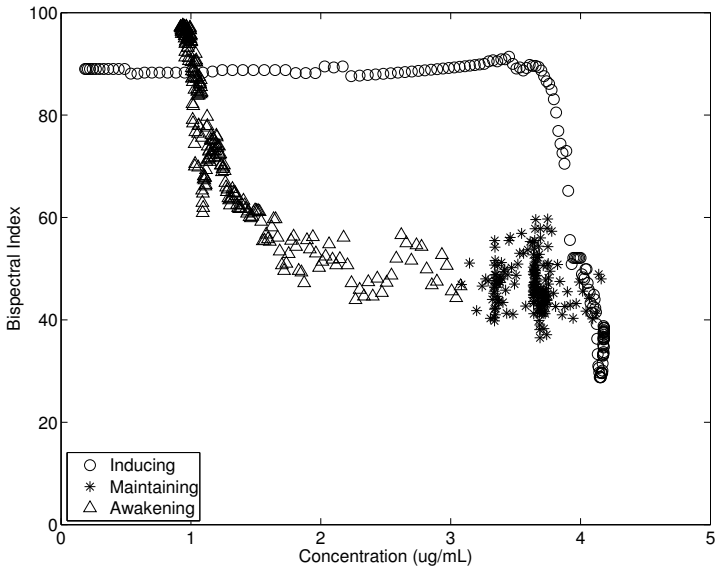

(a) When the delay is not considered ($\hat{L}_c$=0), the relation between BIS and the effect site concentration shows a hysteresis loop

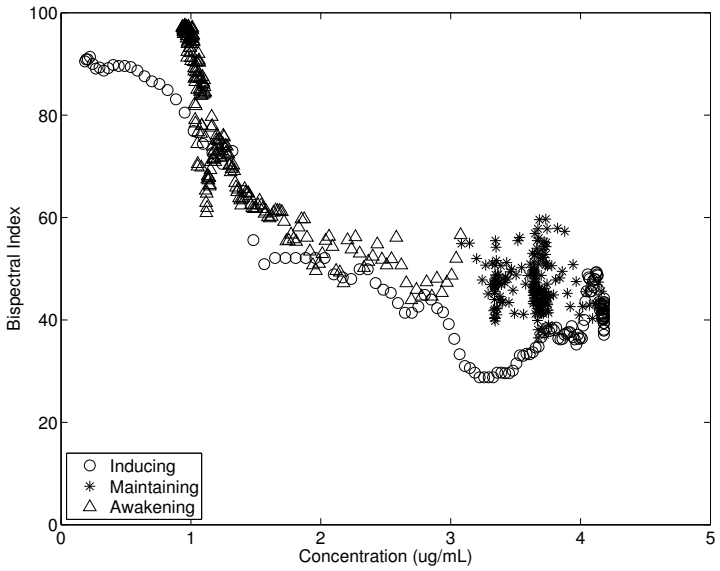

(b) When the delay is considered adequately ($\hat{L}_c$=60s), the relation between BIS and the effect site concentration during the induction period approaches to the relation during the awakening period

Figure 5.3: BIS values vs. effect site concentrations.

5.2 Hypnosis control system

In this section, the hypnosis control system is explained in detail. The main components of the control system are an estimation function of individual parameters during induction of anesthesia, a model predictive controller and a risk-control function for prevention of undesired states. These components act as follows: first, a bolus and subsequent continuous infusion of propofol is administered to anesthetize patients quickly. From the response of the BIS to this bolus, individual parameters are obtained by the estimation function. Then the model predictive controller starts to adjust the continuous infusion rate, coping with undesired states by the risk-control function. In the following subsections, the detailed descriptions of these components are given.

5.2.1 Parameter estimation during induction

As presented in the preceding section, the individual differences in the pharmacodynamic parameters and the delay length are quite large. The differences may degrade the performance of hypnosis control if they are not treated adequately. Therefore, the author developed a parameter estimation function that estimates the pharmacodynamic parameters and the delay length from the response of the BIS to propofol infusion during induction of anesthesia.

For induction of propofol anesthesia, propofol is usually administered as sequential bolus and continuous infusion [65] to anesthetize patients quickly. According to the widely accepted procedure for propofol-induced anesthesia, the hypnosis control system administers propofol at the rates of 120 mg/kg/h for the first 1 min and 10 mg/kg/h for the subsequent 2 or 3 min. At the end of this induction period, the individual delay length L_c and pharmacodynamic parameters E_0, $E_{\max}$, c_{50} and γ are estimated from the response of the BIS and the calculated effect site concentration. After the completion of parameter estimation, parameters of the controller are adjusted using the estimation result, and feedback control starts.

In the following, we explain the details of this parameter estimation function. First, E_0 and $E_{\max}$ are determined as the maximum value of the BIS before the bolus of propofol. Next, the delay length L_c is determined using an estimation equation

$$L_c = 0.932T_{30} - 41.5\text{s}, \tag{5.8}$$

where T_{30} is the time when BIS(t) reaches $(E_0 - 30)$. Equation (5.8) is derived by least-squares fitting of T_{30} and estimated delay $\hat{L}_c$ in the preliminary 47 data sets. We utilize Eq. (5.8) because the correlation coefficient between T_{30} and $\hat{L}_c$ is high (0.956). The standard deviation of the estimation error $(L_c - \hat{L}_c)$ in the preliminary 47 data sets is 13.8 s. Then c_{50} and γ are identified by least-squares fitting based on the equation

$$\log\left(\frac{E_0 - \text{BIS}(t)}{\text{BIS}(t) + E_{\max} - E_0}\right) = \gamma \log y(t) - \gamma \log c_{50}, \tag{5.9}$$

Table 5.2: Permissible ranges and default values for parameter estimation

	E_0	$E_{\max}$	γ	c_{50} (μg/mL)	L_c (s)
Upper bound	98.0	98.0	4.20	7.70	170
Lower bound	87.0	87.0	0.70	1.70	30
Default value	97.0	97.0	1.87	3.75	73

using measurements during the BIS descending period from the start of infusion to $(L_c + 120)$ s. The equation presented above is derived from Eq. (5.5), as in Section 5.6. Using this method, the delay length and pharmacodynamic parameters of each individual are estimated during the induction period.

In the practice, we occasionally meet device failures or severely abnormal measurements. Even for such cases, the parameters must be selected appropriately. Therefore rule-based actions are implemented for the parameter estimation as follows: if any obtained parameter value is out of the range shown in Table 5.2, the parameter is set at the upper or lower bound of the range. If the measured data are unreliable, in other words, if the signal quality of electroencephalogram is fatally low or the BIS remains higher than $(E_0 - 30)$ during 180 s after the start of the bolus, the parameters are set to the default values shown in Table 5.2. The upper and lower bounds and default values are determined to guarantee the robust stability of control system under possible parameter differences estimated from the preliminary measurements.

5.2.2 Model predictive controller

In this section, we introduce a model predictive controller [10] for controlling the hypnosis level of patients during general anesthesia. As described in the preceding section, the model of the BIS response to propofol infusion includes a delay. Furthermore, the infusion rate must be nonnegative. Thus a model predictive controller is applied to handle the delay and the input constraint appropriately.

In model predictive control, the controller acts in discrete time, and determines the manipulated input so that the future output predicted by the model of the process approaches a desirable output trajectory as closely as possible [10]. In the following, we explain the details of the model predictive controller used in the hypnosis control system.

Linearization of model

The model of the BIS response to propofol infusion includes the nonlinear pharmacodynamic model. To simplify computation in the model predictive controller, the model is linearized by connecting an inverse function of the pharmacodynamic model to the output. Namely, we regard the effect site concentration of propofol estimated from the

measured BIS by

$$y^{\text{measured}}(t) = c_{50}\left[\frac{E_0 - \text{BIS}(t)}{E_{\max} - E_0 + \text{BIS}(t)}\right]^{1/\gamma}, \tag{5.10}$$

as the controlled variable. In a similar way, the target value of the control system is set to

$$y^{\text{target}} = c_{50}\left[\frac{E_0 - \text{BIS}^{\text{target}}}{E_{\max} - E_0 + \text{BIS}^{\text{target}}}\right]^{1/\gamma}, \tag{5.11}$$

where $\text{BIS}^{\text{target}}$ is the target value of the BIS. Although the nominal values of the parameters used in Eqs. (5.10) and (5.11) might differ from the actual value of the process, the BIS converges with its target value when the controlled variable $y^{\text{measured}}(t)$ reaches to its target value y^{target} because the pharmacodynamic model and its inverse are one-to-one mappings.

Control law

The control law of the model predictive controller is shown here. First, we introduce some notations and assumptions. We respectively describe the starting time of propofol infusion and the present time as $t = 0$ and $t = kT$, where T is the sampling period of the controller. We assume that the initial state is zero, i.e. $x(\tau) = 0$ for $\tau \leq 0$, because no propofol exists in the patient's body before the start of propofol infusion. Furthermore, we assume that the bolus of propofol will not be administered after the present time and that the infusion rate of propofol will be changed N_M times at every sampling instant. That is, the future inputs are assumed to be

$$\begin{aligned} u(t) &= u_l, \quad lT \leq t < (l+1)T, \quad l = k, k+1, \cdots, && (5.12)\\ 0 &\leq u_l \leq u^{\text{th}}, \quad l = k, k+1, \cdots, k+N_M-1, && (5.13)\\ u_l &= u_{k+N_M-1}, \quad l = k+N_M, k+N_M+1, \cdots, && (5.14) \end{aligned}$$

where u_l for $l = k, k+1, \cdots$ is the infusion rate of propofol during the future period $[lT, (l+1)T)$. The integer N_M is referred as the length of control horizon [10].

Under these assumptions, the future output is predicted by the model. From the initial condition $x(0) = 0$ and the past input $u(t)$ for $t \in [0, kT)$, the future output $y^{\text{model}}(kT+\tau)$ of the nominal model for $\tau \geq 0$ is predicted as a function of future inputs u_k, u_{k+1}, $\cdots$, using Eqs. (5.2) and (5.4). Additionally, a constant disturbance

$$e_k = y^{\text{measured}}(kT) - y^{\text{model}}(kT), \tag{5.15}$$

is introduced, in order to suppress the output disturbance and the error resulting from model mismatches [10]. Therefore the predicted output is given by

$$\hat{y}(kT+\tau) = y^{\text{model}}(kT+\tau) + e_k, \ \tau \geq 0. \tag{5.16}$$

Next, we introduce the reference trajectory that the predicted output should track as closely as possible. Using the target value y^{target} and the predicted output $\hat{y}(kT + L_c)$ at time point $kT + L_c$, the reference trajectory $y^{\text{ref}}(kT + \tau)$ for $\tau \geq L_c$ is set as

$$y^{\text{ref}}(kT + \tau) = (1 - e^{(\tau - L_c)/T^{\text{ref}}})y^{\text{target}} + e^{(\tau - L_c)/T^{\text{ref}}}\hat{y}(kT + L_c), \tag{5.17}$$

where T^{ref} is a time constant of the reference trajectory.

Then, future input values u_k, u_{k+1}, $\cdots$ are calculated as the solution of an optimization problem

$$\min_{u_k, \cdots, u_{k+N_M-1}} J = \lambda \sum_{l=k}^{k+N_M-1} u_l^2 + \sum_{l=k+1}^{k+N_P} \left\{ y^{\text{ref}}(lT + L_c) - \hat{y}(lT + L_c) \right\}^2, \tag{5.18}$$

$$\text{subject to} \quad 0 \leq u_l \leq u^{\text{th}}, \quad l = k, k+1, \cdots, k+N_M-1, \tag{5.19}$$

$$u_l = u_{k+N_M-1}, \quad l = k+N_M, k+N_M+1, \cdots, \tag{5.20}$$

where N_P is a positive integer and λ is a real number. The integer N_P means the length of the prediction horizon [10] where the tracking error of the predicted output to the reference trajectory is evaluated. λ is a weighting coefficient for the input to the output error.

Finally, the controller applies the first element u_k of the future inputs, which can be obtained by solving the optimization problem (5.18), to the controlled process, and repeats this procedure at every sampling time.

Controller design

Here we present a specification of the hypnosis control system and design a model predictive controller. The hypnosis level of the patient should approach quickly to the target value and then be maintained around the target. Furthermore, the control system must be robustly stable for individual differences among patients, although the effect of the differences might be suppressed partly by the parameter estimation function. Taking these requirements into account, the specification of the hypnosis control system is given for patients whose age, body weight and delay length are in the ranges of 18–80 yr., 40–100 kg and 30–150 s, respectively. First, the 5% settling time of the model predictive control system should be less than 15 min to provide clinically acceptable responses. Second, the control system should be stable for $\bar{L}_c \in [0.1L_c, 1.9L_c]$ and $K \in [0, 2.1]$, where $\bar{L}_c$ and L_c are actual and nominal delay lengths and K is the relative gain between the actual and nominal processes. These ranges are given by the three-sigma limits of relative mismatch of delay estimate in the preceding subsection and those of linear gain estimated in the preceding section, respectively.

To satisfy the above specification for every patient model in the targeted characteristic group, the controller parameters T, N_P, N_M, T^{ref} and λ are set. The sampling period T of the controller is set to 10 s under a mechanical restriction of a syringe pump. The length of the control horizon N_M is set to 1 because the control system must have

sufficient robustness. The time constant T^{ref} of the reference trajectory is set to 245 s so that the settling time of the reference trajectory meets the specification on settling time. The length of the prediction horizon N_P and the weighting coefficient λ are set to $N_P = 30$ and $\lambda = 10^{-4}(\mu\mathrm{g/mL})^2/(\mathrm{mg/kg/h})^2$ by trial and error to provide a sufficient robust stability margin of the closed-loop system.

Typical nominal responses are shown in Fig. 5.4, which shows the nominal step response of the closed-loop system and the nominal closed-loop response after the sequential bolus and continuous infusion for a 40-year-old, 60-kg patient with the mean pharmacodynamic parameter values and the mean delay described in the preceding section. We can confirm that adequate control is achieved and that the settling time is less than 15 min. A typical result of robust stability analysis for the same patient model is shown in Fig. 5.5. This figure is obtained from the Nyquist stability condition with the assumption that the modeling errors exist only in the linear gain and the delay length [66]. We can confirm that the robust stability region is sufficiently large to satisfy the specified requirement.

The author repeated simulations and analysis for various patients' models without or with model mismatches on pharmacokinetic and pharmacodynamic parameters and delay length. The mismatches were given as normally distributed random values, whose mean and standard deviation were the nominal values and 20% of the nominal values for pharmacokinetic parameters, and the mean and standard deviation of the estimates in the preliminary 47 data sets for pharmacodynamic parameters and delay length, in order to simulate individual differences among actual patients. Under these model mismatches, it is confirmed that the hypnosis control system satisfies the given specifications.

5.2.3 Risk-control function

In the usual mode, the infusion rate of propofol is adjusted by the model predictive controller to maintain the BIS around the target value. However, unmodeled surgical disturbances and sensitive autonomic nervous system might cause undesirable states, such as intra-operative arousal, hypotension, and bradycardia. To prevent these undesirable states as well as over-infusion of propofol, a rule-based risk-control function that imitates countermeasures taken by anesthesiologists for such states is implemented, because the model predictive controller cannot respond quickly to such unmodeled factors. In the following, we explain risk-avoiding actions.

Prevention of propofol over-infusion

To avoid adverse reactions of propofol over-infusion, such as PONV and a delay of arousal, the upper bound of the infusion rate is set to 20 mg/kg/h, except the bolus for a countermeasure to intra-operative arousal. Moreover, the maximum bolus dose $U_{\max}$ for the countermeasure to intra-operative arousal is set to $U_{\max} = 1$ mg/kg.

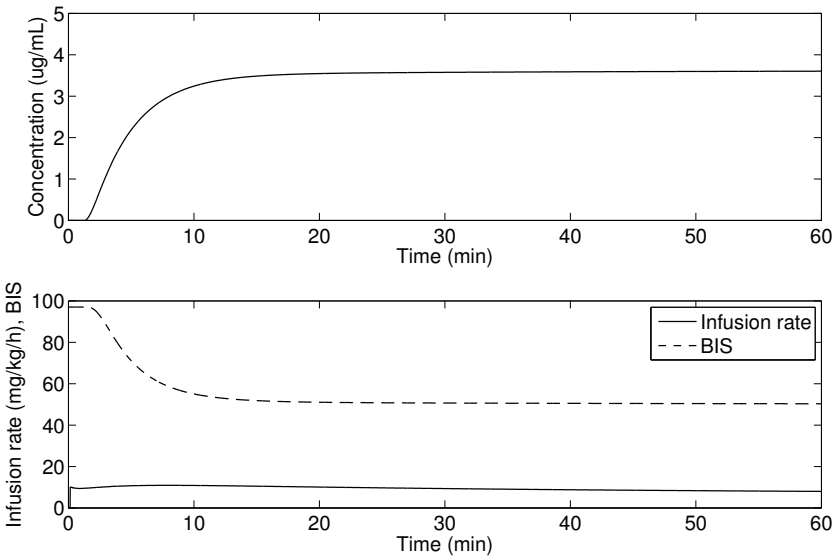

(a) Nominal step response

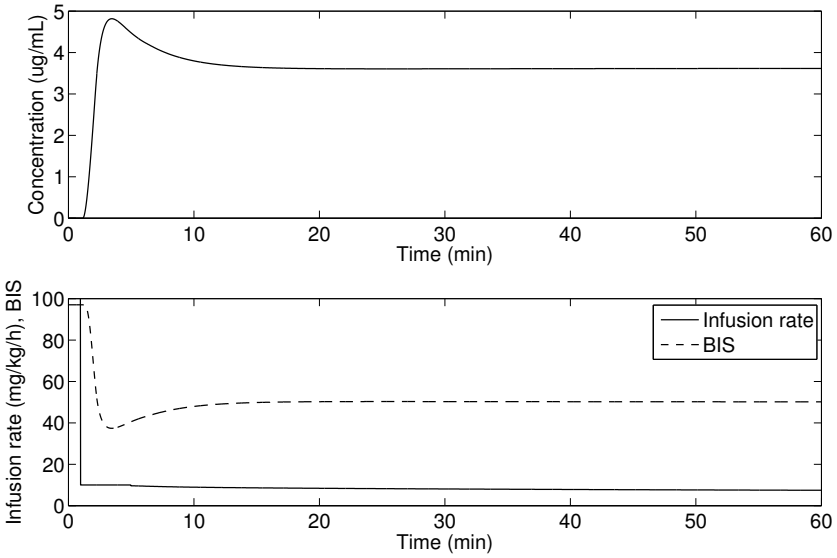

(b) Nominal response after the sequential bolus and continuous infusion

Figure 5.4: Simulation results of the closed-loop system with a model of patient whose age, BW and delay length are 40 yr., 60 kg, and 70 s. In each subfigure, the upper plot shows propofol concentrations in the effect site, and the lower plot shows the infusion rate of the propofol (solid line), and the BIS (dashed line). The setpoints of the concentration and the BIS are set respectively to 3.6 μg/mL and 50.

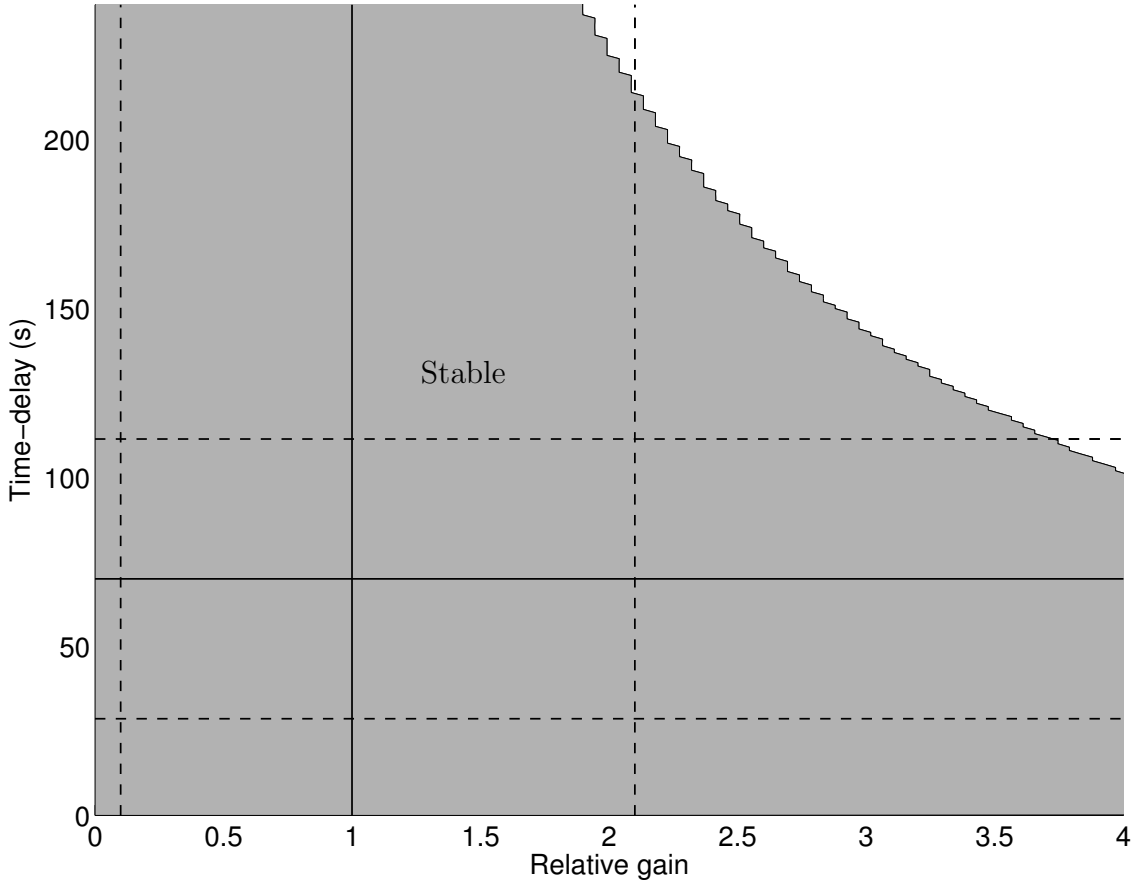

Figure 5.5: Stability region of the closed-loop system in the gain – time-delay plane for a model of patient whose age, BW and delay length are 40 yr., 60 kg and 70 s, respectively. Solid lines mean the nominal values and dashed lines mean the three sigma limits.

Countermeasure to intra-operative arousal

The system administers a bolus of propofol to prevent intra-operative arousal when the BIS rises abnormally. The dose and rate of the bolus are determined based on the BIS rise, $\Delta\mathrm{BIS}(t) = (\mathrm{BIS}(t) - \mathrm{BIS}^{\mathrm{target}})$, by the following procedure:

- When the bolus at the induction is completed, U_{sum} is set to 2 mg/kg. Here, U_{sum} is a fictitious dosage which corresponds to the effect of past boluses.
- During continuous infusion, U_{sum} is decreased exponentially with a time constant of 195 s, which approximately equals to the time constant of the plasma propofol concentration to a bolus of the pharmacokinetic model (Fig. 5.2(a)).
- When $\Delta\mathrm{BIS}(t)$ is greater than 15, the system sets a limit dose U_{bol} of the following bolus to $(U_{\mathrm{max}} - U_{\mathrm{sum}})$, and starts a bolus at the rate of 30 mg/kg/h.
- During the bolus, the bolus rate is increased to 60, 90, and 120 mg/kg/h if the $\Delta\mathrm{BIS}(t)$ are greater than 25, 35, and 45, respectively. On the other hand, the rate is decreased to 90, 60, and 30 mg/kg/h if $\Delta\mathrm{BIS}(t)$ falls under 40, 30, and 20, respectively. If $\Delta\mathrm{BIS}(t)$ falls below 10 or the bolus dose reaches U_{bol}, the bolus is terminated, and the bolus dose is added to U_{sum}.

Management of hypotension and bradycardia

To cope with adverse reactions of propofol to the patient's cardiovascular system, the hypnosis control system continuously monitors the non-invasive systolic pressure and pulse rate. When one of these values falls below 70 mmHg or 40 bpm, the system sounds an alarm and decreases the propofol infusion rate according to a predicted awakening time. The predicted awakening time is calculated from Eqs. (5.2) and (5.4) as the time for $y(t)$ to reach y_{80}, which is the effect site propofol concentration corresponding to BIS=80, under the assumption that $u(t+\tau) = 0$ $(\tau \geq 0)$. The propofol infusion rate is set to zero if the predicted awakening time is longer than 4 min. Otherwise, the propofol infusion rate is set to a half of the calculated rate by the model predictive controller.

Countermeasure to BIS noise

The BIS is calculated from the measured EEG. When an electric knife is used, a signal quality of the EEG worsens because of electrical noise; sometimes the BIS output is suspended. Moreover, when the myogenic potential appears frequently on the EEG, the BIS output is also suspended. During the suspension, the model predictive controller cannot obtain the measured output. In such cases, the controller determines the propofol infusion rate assuming that the step disturbance e_k in Eq. (5.16) is the same as that at one step before, namely, $e_k = e_{k-1}$.

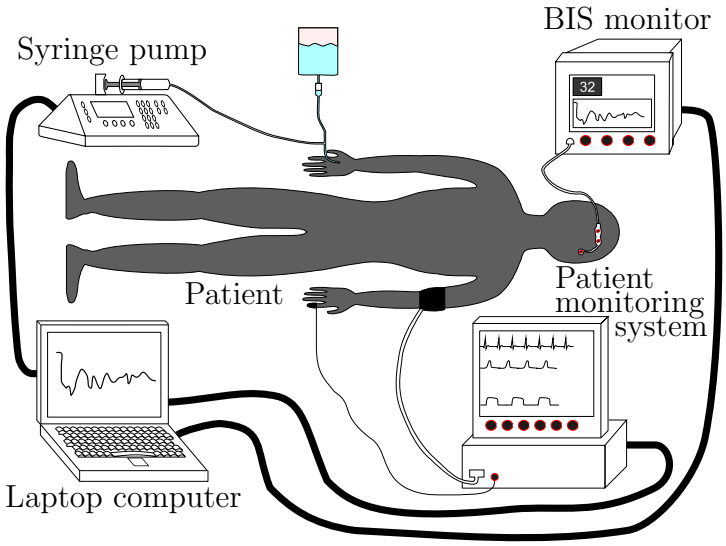

Figure 5.6: The structure of the clinical trial system. The system is comprised of a BIS monitor, a patient monitoring system, a syringe pump and a laptop computer. These devices are connected using RS-232 serial cables.

5.3 Clinical trials

5.3.1 Implementation

Implementation of the hypnosis control system is shown in Fig. 5.6. This system measures the BIS, the non-invasive systolic blood pressure, and the pulse rate. The BIS is calculated by a BIS Monitor (A-2000; Aspect Medical Systems Inc., Norwood, MA, USA). The non-invasive systolic blood pressure and the pulse rate are measured using a Central Monitoring System (Agilent Technologies, Palo Alto, CA, USA). Propofol is administered by a syringe pump (Graseby 3500; Graseby Medical Ltd., Walford, UK) via an intravenous fluid line. An IBM-compatible laptop computer is used to calculate the infusion rate of propofol. These instruments are connected via RS-232 serial connections, and driven by software written in a commonly used computer language (Microsoft Visual C++ Ver. 6; Microsoft Corp., Redmond, WA, USA).

5.3.2 Clinical protocols

After obtaining the approval of the Ethics Committee on Human Research of the Kyoto University Graduate School of Medicine, 160 adult patients (American Society of Anesthesiologists [ASA] physical status [PS] class I–II; age, 18–80 years; body mass index [BMI], 15–36 kg m^{-2}) undergoing elective various kinds of ambulatory surgery were included in this study. They were assigned randomly to either group A (automatic control) or M (manual adjustment) using the envelope method.

Before induction, all patients were instructed to close their eyes. In group A, patients' hypnosis was controlled by the hypnosis control system, whereas patients in the group M received propofol administration whose infusion rate was adjusted manually by an anesthesiologist after 2 mg/kg initial bolus and 10 mg/kg/h continuous infusion at an induction period. In both group, the target value of the BIS was set to 50 because the desired level of the BIS during surgery is 40–60 [62].

Supplemental IV fentanyl and vecuronium, local infiltration anesthetics and rectal diclofenac were administered for pain relief and muscle relaxation during anesthesia. Boluses of fentanyl (25 μg each) were administered at the start of propofol infusion, before and 30 min after skin incision, and before skin closure. Vecuronium and rectal diclofenac were administered after loss of consciousness. The initial dose of vecuronium was 0.06–0.12 mg/kg, depending on the estimated duration of anesthesia. Additional administration of vecuronium was done if insufficient muscle relaxation was observed. Local infiltration anesthetics were administered by surgeons before the start and at the end of the operation. In all cases, anesthesia care was provided by one anesthesiologist.

After each surgery, propofol infusion was terminated by the anesthesiologist. The recovery time from the stop of infusion to tracheal extubation or laryngeal mask airway (LMA) removal and the time required for the BIS to be above 80 after the stop of infusion were recorded.

In all cases, the BIS and infusion rate of propofol were recorded on a computer every second. Episodes of hypotension (systolic blood pressure < 70 mmHg) and bradycardia (pulse rate < 40 bpm) were also recorded. Evaluation and comparison of results were performed after all trials. Statistical analyzes were performed using Student's t-test. Differences of $P < 0.05$ were inferred to be statistically significant.

5.3.3 Results

In one case of automatic control, a misuse of the syringe pump engendered device failure. Consequently, that case was excluded from subsequent analyzes.

Between the two groups, no statistically significant differences were found in patient characteristic data, type of surgery, duration of propofol infusion, or consumption of drugs aside from propofol, as shown in Table 5.3. In both groups, adequate anesthesia was achieved in all cases.

The BIS and the infusion rate in typical cases of automatic control and manual adjustment are shown respectively in Figs. 5.7(a) and 5.7(b). Figure 5.7(a) shows the BIS and infusion rate for a 46-year-old male who underwent oral surgery. In this case, the parameter estimation was completed at 2.7 min after the start of infusion. The infusion was terminated at 138.8 min. During the control period, defined as the period between the completion of the parameter estimation and the termination of infusion, the averages of the BIS and of the propofol infusion rate were 49.2 and 5.8 mg/kg/h, respectively. The settling time, defined as the time that the BIS reaches and is maintained within 40–60 for 5 min, was 10.0 min. The rate in the target zone, defined by the percentage of

time when the BIS is within 40–60 during the control period, was 90.8%. The recovery time until extubation and the time required for the BIS to be above 80 after the stop of infusion were, respectively, 6.9 min and 3.0 min.

Figure 5.7(b) also represents the BIS and infusion rate for a 57-year-old female patient who had oral surgery under manually adjusted propofol anesthesia which lasted 123.5 min. For manually adjusted cases, we define the control period as the period from 4 min after the start of propofol infusion to the stop of infusion. The averages of the BIS and infusion rate during the control period were 51.7 and 9.8 mg/kg/h. The settling time, the rate in target zone and the recovery time to extubation and to BIS=80 were, respectively, 22.8 min, 82.4%, 5.0 min, and 12.3 min.

The aggregated results of each group are shown in Fig. 5.8 and Table 5.3. Figure 5.8 presents the average and standard deviation of all time courses of the BIS and infusion rate before the stop of infusion. In Fig. 5.8(b), boluses for prevention of intraoperative arousal stand out because their infusion rates were extremely high. The averaged BIS is clearly closer to the setpoint, and the standard deviation of infusion rate is larger in the system. This means that the system can make the BIS closer to the setpoint taking individual differences of propofol requirement into account. In Table 5.3 the mean values and standard deviations of the averaged BIS during the control period, the averaged infusion rate, the settling time, the rate in target zone and the recovery time to BIS=80 and tracheal extubation/LMA removal of each group are shown. Between the two groups, the averaged BIS, the averaged infusion rate and the rate in target zone differ significantly. In group A, abnormal BIS rise and propofol bolus occurred more frequently than in group M, whereas the frequency of hypotension and bradycardia did not differ between the two groups.

5.4 Discussion

In this study, a model predictive controller was developed for closed-loop control of hypnosis using propofol. The system is applied to ambulatory surgery because adverse reactions of propofol overdose are severe problems, especially in ambulatory surgery. The proposed control framework combines 1) a new description of propofol pharmacokinetics based on the result of Schüttler and Ihmsen [20], 2) a fast and reliable estimation of individual pharmacodynamic parameters and delay length, 3) a model predictive controller that can easily deal with the time delay and input constraints, and 4) a risk-control function as a countermeasure to undesirable states. The model predictive control strategy is a powerful method for controlling propofol anesthesia; it achieves stable control in the presence of mismatches on the delay length and the gain. In the clinical trials, the model predictive hypnosis control system can maintain patients' hypnosis adequately. nHereafter, we compare the results of clinical trials with those of previous works [44–48] and anesthesiologist's manual adjustment.

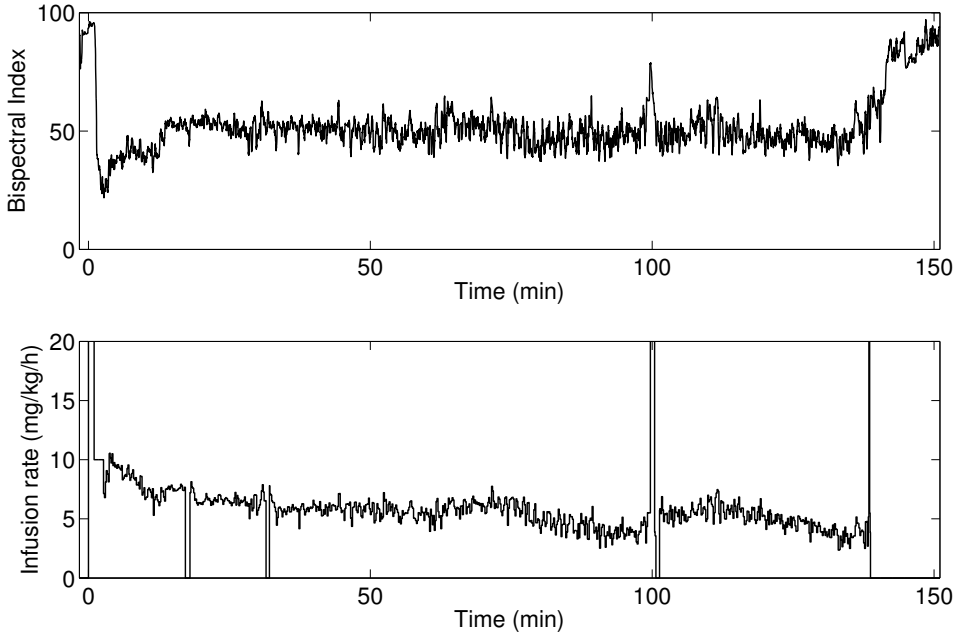

(a) Typical result of automatic control (group A)

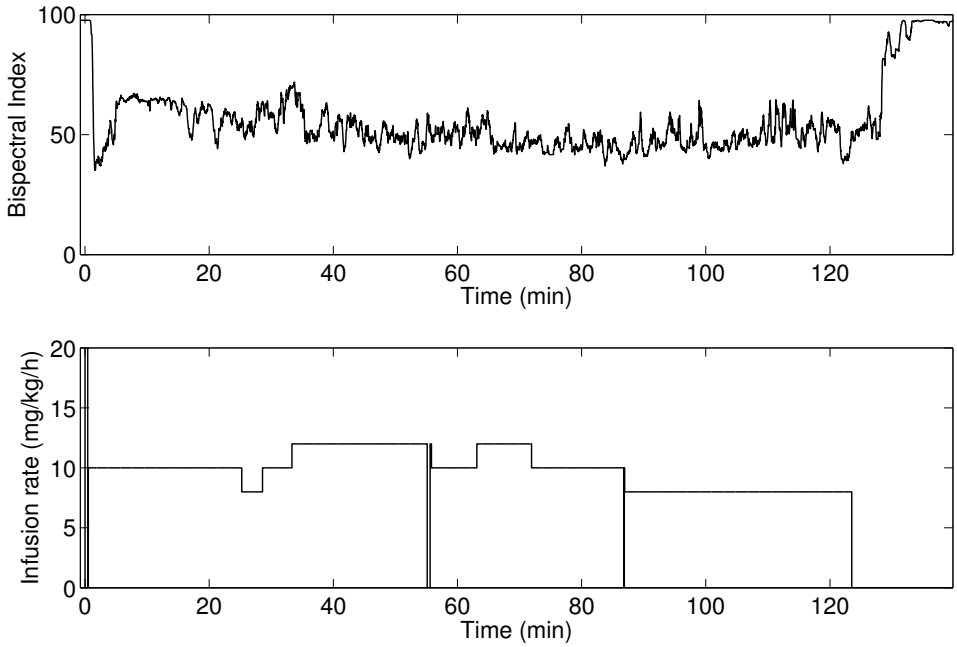

(b) Typical result of manual adjustment (group M)

Figure 5.7: Representative plots of both groups. In each figure, the upper and lower plots respectively show the BIS and infusion rate of propofol.

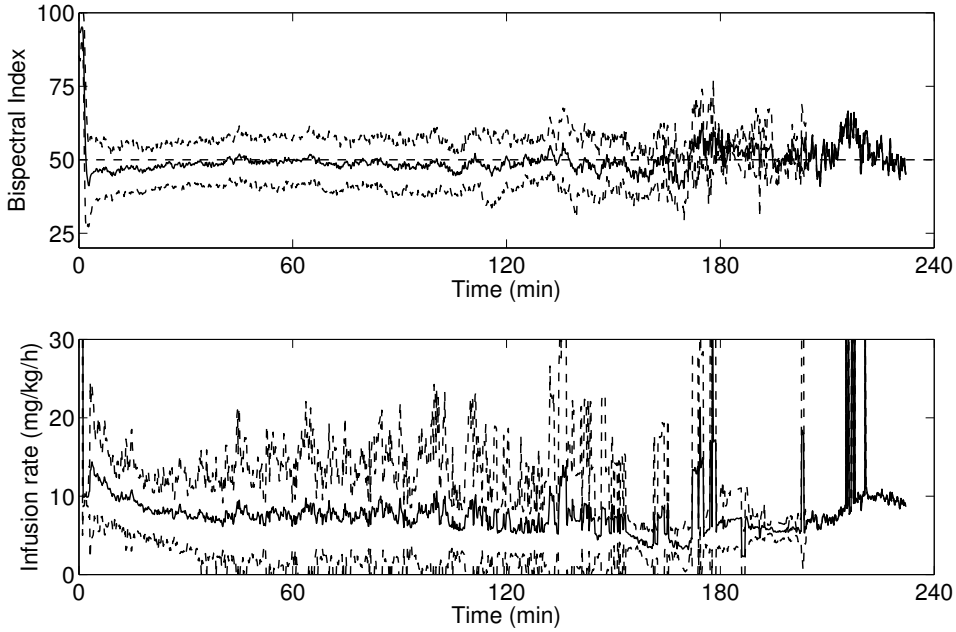

(a) Automatic control (group A)

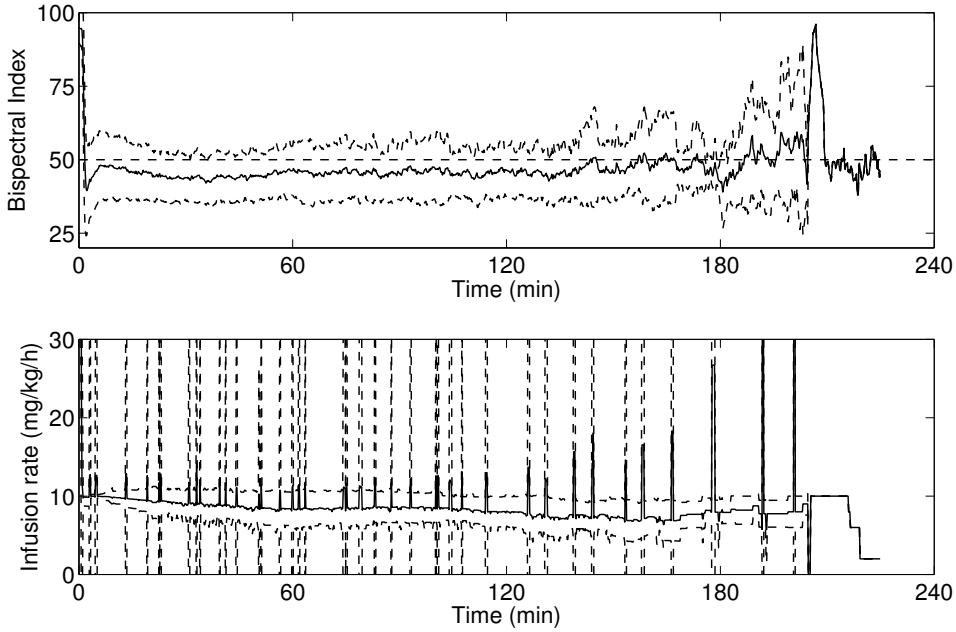

(b) Manual adjustment (group M)

Figure 5.8: The BIS and infusion rate from induction to discontinuation of infusion for automatic control and manual adjustment groups. Average values (solid line) are presented with standard deviation values (dashed line).

Table 5.3: Patient characteristics, performance indices, drug consumption, and occurrence of abnormal state of automatic control and manual adjustment

Group	A ($n = 79$)	M ($n = 80$)
Age (yr.)	45.6±16.2	47.4±16.4
Height (cm)	160.1±8.2	160.9±9.65
Body weight (kg)	57.2±11.3	56.0±11.2
Sex m/f (n)	19/60	16/64
ASA PS I/II (n)	52/27	44/36
Tracheal tube/LMA (n)	33/46	28/52
Duration of propofol infusion (min)	107±45	116±49
Type of surgery		
Breast surgery (n)	23	26
Oral surgery (n)	19	19
Hysteroscopic surgery (n)	17	16
Arthroscopic surgery (n)	8	6
Hernioplasty (n)	6	6
Dermatologic surgery (n)	4	3
Otolaryngologic surgery (n)	2	4
Averaged BIS	48.4 ± 2.5	45.7 ± 6.2**
Averaged infusion rate (mg/kg/h)	8.28 ± 2.0	8.97 ± 1.4*
Settling time (min)	24.8 ± 34.8	37.1 ± 49.8
Rate in target zone (%)	78.1 ± 15.3	62.1 ± 25.3**
Time to BIS=80 after stop of infusion	8.45 ± 5.56	7.46 ± 3.86
Time to extubation/LMA removal	10.0 ± 5.3	8.75 ± 3.98
Drugs used during the maintenance period		
Fentanyl (μg/kg)	1.29±0.59	1.18±0.82
Vecuronium (μg/kg)	125±44	114±53
Diclofenac (n)	62	64
Atropine (n)	1	0
Ephedrin (n)	0	1
Intraoperative episodes		
Abnormal BIS rise[a](n)	71	51**
Propofol bolus (n)	71	23**
Hypotension[b](n)	4	3
Bradycardia[c](n)	2	1

Values are mean ± SD or numbers (n)

[a] BIS > 65, [b] Systolic blood pressure < 70 mmHg, [c] Pulse rate < 40 bpm,

* $p < 0.05$, ** $p < 0.01$.

5.4.1 Comparison with other closed-loop systems

In most previous works, median performance error (MDPE) and median absolute performance error (MDAPE) were used to indicate the performance of the controller [44–48]. The MDPE and MDAPE are measures of performance error (PE), which are obtained by

$$\mathrm{PE}(t) = \frac{\mathrm{BIS}(t) - \mathrm{BIS}^{\mathrm{target}}}{\mathrm{BIS}^{\mathrm{target}}} \times 100(\%). \tag{5.21}$$

The MDPE is a median of the PE, and the MDAPE is a median of the absolute values of the PE.

Table 5.4 shows the MDPE and MDAPE of the developed system and those of previous works [44–48]. The table shows that the MDPE and the MDAPE of the developed system were not so good. A main reason for this is probably the difference of pain relief methods. In the previous closed-loop systems, patients received epidural anesthesia [46], or higher-dose opioids [44, 46–48] than in the developed system. For example, Absalom et al. [46] administered epidural anesthesia with 0.5% bupivacaine 10 mL and Liu et al. [47] and Struys et al. [48] respectively used remifentanil infusion at the rates of about 0.22μg/kg/min and at least 0.25μg/kg/min. In general, fluctuations of the BIS caused by painful stimulus depend on the level of analgesia [67]. Epidural anesthesia can produce dense sensory blockage; consequently, perturbation of the BIS during surgery can be suppressed. Intra-operative administration of opioid similarly suppresses the perturbation of the BIS [68]. However, epidural anesthesia requires a preparation time, causes delay of post-operative recovery, and possesses risks of failure and accidental dural puncture. The high-dose administration of opioids causes adverse reactions such as PONV [69], which delays discharge from the hospital. Therefore, these analgesic methods are inappropriate for ambulatory surgery. On the other hand, intermittent fentanyl infusion was used for analgesia: its total amount was less than 100 μg. Therefore the MDAPE of the system was larger than others. For an appropriate comparison of the MDAPE, similar analgesic regimens must be used.

The MDPE of the developed system is not good, perhaps because of the use of the propofol bolus as a countermeasure to intraoperative arousal. The bolus was stopped when the BIS fell under 60. However, the BIS continued to decrease after the stop of the bolus because of the time delay. Sometimes undershooting of the BIS to the target value of 50 occurred due to too large bolus dose. To prevent an unnecessary BIS decrease, the effect of the delay must be considered adequately and the bolus dose should be determined based on the future BIS predicted by a model with the consideration of disturbances.

Another possible reason for the worse performance is the inaccuracy of the model. In this study, a custom-made pharmacokinetic-pharmacodynamic (PK-PD) model is utilized. Although the proposed PK-PD model has worked well, the model is not necessarily the best for prediction of the BIS response. This is because the model always has

Table 5.4: Median of the performance error (MDPE) and Median of the absolute values of the performance error (MDAPE) of the developed system and other published hypnosis control systems

Developers	Analgesia	N	MDPE	MDAPE
The author	Fentanyl	79	−4.1	11.4
Morley et al. [44]	Alfentanil	30	–	13.6
Absalom et al. [46]	Epidural	10	2.2	8.0
Absalom and Kenny [45]	Remifentanil	20	−0.42	5.63
Liu et al. [47]	Remifentanil	83	−3.3	9.9
Struys et al. [48]	Remifentanil	10	−6.6	7.7

mismatches, which include individual differences in the PK-PD parameter values and estimation error in the pharmacodynamic parameters. These mismatches yield bias and fluctuation of the BIS if the model is utilized in an open loop controller. The closed-loop system can attenuate the effects of these mismatches. However, more accurate model improves the tracking ability and robust stability of the closed-loop control system. A possible candidate is a combined PK-PD model [22], whose plasma effect-site equilibration rate constant was derived in a more rigorous way.

5.4.2 Comparison with manual adjustment

As described above, the control system can maintain the BIS accurately and reduce the amount of propofol when compared with manual adjustments. These results are attributable to the accurate and adequate consideration of individual differences, the effect of time delays and complex pharmacokinetics of propofol. However, some future directions of the control system are suggested by comparison with manual adjustments.

Before clinical trials, we anticipated that strict control of the BIS would decrease the propofol consumption and facilitate faster recovery from anesthesia. The averaged infusion rate is decreased as expected. However, the recovery profiles are almost identical to those of the manual adjustment cases, as shown in Table 5.3.

A main reason for this lack of difference is the lack of consideration of the progress of the surgery. In the cases of manual adjustment, an anesthesiologist carefully monitors the patient state and the progress of the surgery. For example, the infusion rate is not increased in the last stage of the surgery, even if a sudden rise of the BIS were to occur from the pain of skin sutures. On the other hand, the developed system only monitors the BIS, non-invasive systolic pressure, and pulse rate, and was unable to collect or use information about the progress of the surgery. In each clinical trial, the instructions to the controller given by the anesthesiologist were only two: “start infusion” and “stop infusion”. Moreover, the target value, the control law, and the risk-control rules during the control period were the same for all cases. Therefore, when a sudden BIS

increase occurred because of skin sutures in the last stage of the surgery, the controller administered a bolus of propofol until the BIS fell to 60. This BIS fall might have caused a delay of awakening. Changing the target point and risk-control rules according to instructions about the progress of the surgery might bring about less drug consumption and earlier awakening.

5.5 Concluding remarks

In this chapter, a hypnosis control system was developed using a model predictive controller. The system uses the BIS as the index of hypnosis and propofol as a hypnotic drug. It has a parameter estimation function of individual differences, in addition to a risk-control function. Results of clinical trials show the potential of the system in reducing the amount of propofol infusion and maintaining the BIS more accurately.

To improve the system effectiveness, we must consider the following topics:

- developing a more accurate model;
- improving a more reliable method for parameter estimation; and
- optimizing rules for the risk-control function.

5.6 Derivation of Eq.(5.9)

Subtracting each side of Eq. (5.5) from E_0 and multiplying them by $(y^\gamma(t) + c_{50}^\gamma)$, we obtain

$$(E_0 - \mathrm{BIS}(t))(y^\gamma(t) + c_{50}^\gamma) = E_{\max} y^\gamma(t). \tag{5.22}$$

Transposing some terms, we get

$$(\mathrm{BIS}(t) - E_0 + E_{\max}) y^\gamma(t) = (E_0 - \mathrm{BIS}(t)) c_{50}^\gamma. \tag{5.23}$$

The logarithm of each side yields

$$\log\{(\mathrm{BIS}(t) - E_0 + E_{\max}) y^\gamma(t)\} = \log\{(E_0 - \mathrm{BIS}(t)) c_{50}^\gamma\}, \tag{5.24}$$

$$\log(\mathrm{BIS}(t) - E_0 + E_{\max}) + \gamma \log y(t) = \log(E_0 - \mathrm{BIS}(t)) + \gamma \log c_{50}, \tag{5.25}$$

$$\log(\mathrm{BIS}(t) - E_0 + E_{\max}) - \log(E_0 - \mathrm{BIS}(t)) = \gamma \log c_{50} - \gamma \log y(t). \tag{5.26}$$

Consequently, we obtain

$$\log\left(\frac{E_0 - \mathrm{BIS}(t)}{\mathrm{BIS}(t) + E_{\max} - E_0}\right) = \gamma \log y(t) - \gamma \log c_{50}. \tag{5.27}$$

Chapter 6

A state-predictive servo control system of hypnosis and muscle relaxation under total intravenous anesthesia

An invasive surgical operation requires adequate anesthesia for the patient's safety. General anesthesia is a common technique used for the relief purposes. In the preceding section, the author have developed a control system which regulates only hypnosis level with only a hypnotic agent during general anesthesia. However, general anesthesia consists of four elements [37] — hypnosis, analgesia, muscle relaxation and elimination of autonomic reflexes, and several drugs with different actions are administered to the patient during general anesthesia, because target levels of the four elements are different among each surgical procedure.

The development of pharmacological agents has provided short-acting drugs that have more specific effects and lower adverse reactions than traditional ones [70]. These drugs allow physicians to provide good anesthesia and fast recovery, thus these agents have been used widely in ambulatory surgery. Regardless their favorable pharmacological profiles, an overdosage of these drugs must still be avoided. Especially in the cases of ambulatory surgery, the overdosage is a big problem because it postpones postoperative recovery and discharge. Sometimes an unscheduled hospitalization is required if the ill effects of the overdosed drugs are severe. On the other hand, insufficient administration of the drugs causes more severe problems, such as intra-operative arousal, unexpected somatic movements, hypertension, tachycardia, and so on. Therefore a physician must observe the patient's state and the surgical procedure carefully, and decide the dosage of drugs adequately and swiftly. Since this task is hard and fatiguing, automatic control systems for multiple elements of anesthesia have been studied extensively [71, 72]. However, almost all of them have aimed at regulation of a single element of anesthesia using a single drug. Few have attempted to treat multiple elements using multiple drugs [73, 74].

However, they used obscure indices of the elements, such as mean arterial pressure or heart rate as an index of analgesia. These indices are affected by several factors [70], thus detectability of analgesia is not enough.

Until now, reliable indices of the elements of anesthesia have been developed for only muscle relaxation and hypnosis. Thus simultaneous control system of muscle relaxation and hypnosis is realizable and may be useful for anesthesia management. Janda et al. [75] reported briefly about such a system and its clinical application to 22 adult patients. Although details are not shown in the abstract [75], probably they constructed the controller by combining two independent controllers, and ignored possible interaction between a hypnotic agent and a muscle relaxant. If the interaction is treated exactly, more suitable control will be achieved.

Therefore possible interaction and simultaneous control of hypnosis and muscle relaxation during general anesthesia are studied in this chapter. To the best knowledge of the author, a theoretical model of the interaction between a hypnotic agent and a muscle relaxant have not been appeared. Thus such model is identified from measurements during general anesthesia. Delays caused by drug movement in an intravenous line and index calculation are also taken into account in the identification procedure. Using the identified model, a state-predictive servo controller is constructed. We also perform the robust stability analysis of the closed-loop system, and confirm that the constructed controller satisfies specifications of the control system.

The contents of this chapter are as follows. In Section 6.1, a multivariable model of hypnosis and muscle relaxation is identified using the method proposed in Chapter 2. In Section 6.2, a robust servo controller with a state predictor proposed in Chapter 3 is designed as in Chapter 4. The performance of the robust servo control system is evaluated in Section 6.3.

6.1 Identification of model of hypnosis and muscle relaxation to drug infusion

In this section a mathematical model of the changes of hypnosis and muscle relaxation caused by administration of anesthetic drugs is identified from measurements during general anesthesia.

In ambulatory surgery, patient's hypnosis and muscle relaxation are mainly maintained by the administration of propofol and vecuronium, respectively. These intravenous agents have superior characteristics of recovery, a low incidence of adverse reactions and favorable pharmacokinetic profiles [70].

The effects of these drugs, hypnosis and muscle relaxation, were evaluated by means of the Bispectral Index (BIS) [52] and single twitch height [70], respectively. The detailed explanation of the BIS is given in the preceding chapter. The single twitch height is defined by the magnitude of an evoked response to single electric stimulus to a peripheral

nerve. Usually, the stimulus is applied to an ulnar nerve and the evoked response is measured as acceleration of a thumb.

For these drugs and indices, many models have been proposed in pharmacological literature. However, almost all of them are single-input single-output models. Some investigators [76–84] have been studied the interactions between propofol and vecuronium, and have reported contradictory results.

The effect of propofol on muscle relaxation was analyzed in [76–82]. Among them, [76–78] reported that propofol enhances the effect of vecuronium on muscle relaxation. On the other hand, [79–81] and [82] advocated that propofol has no effect on muscle relaxation. Although these researchers inferred contradictory results, all of them assumed static interactions and did not take dynamic interactions into account.

The effect of vecuronium on the BIS were studied in [83] and [84]. They reported that the bolus of vecuronium decreases the BIS during light and moderate sedation, because the bolus suppresses patient's electromyogram, which affects BIS calculation. However, these studies also missed the consideration of possible dynamic interactions. Therefore a novel model of effects of propofol and vecuronium infusion is required for design a closed-loop controller.

In the following, a novel multivariable model of hypnosis and muscle relaxation is identified from measurements during general anesthesia, using the method proposed in Chapter 2. This method cannot take into account nonlinearities such as saturation and a switchover between moderate and deep sedation. However, the characteristics of the target system around the interested equilibrium point would be modeled reasonably as a linear model. Moreover, the possible dynamic interactions is also taken into account in the model.

6.1.1 Subjects and method

Ten adult patients who were scheduled for short stay surgery at the day surgery unit of Kyoto University Hospital (Kyoto, Japan) were included in the study. Anesthesia was induced with 2 mg/kg bolus of propofol, then 10 mg/kg/h continuous infusion of propofol was administered. After loss of consciousness and calibration of a muscle relaxation monitor, $0.07 \sim 0.10$ mg/kg bolus of vecuronium was given. Tracheal intubation or laryngeal mask insertion was performed when sufficient muscle relaxation was achieved. After that, infusion rate of propofol was adjusted by a physician so as to regulate the BIS within the range $[40, 60]$. Vecuronium was administered intermittently when needed. Analgesia was achieved with intermittent fentanyl, diclofenac and local anesthetics. At the end of surgery, the propofol infusion was terminated. When sufficient recovery was obtained, tracheal tube or laryngeal mask was removed, and the patient left the operation room.

During each procedure, drug infusion rates and indices of their effects were recorded as follows: The infusion rates of propofol and vecuronium were recorded by a laptop computer and by hand, respectively, because propofol was infused continuously by com-

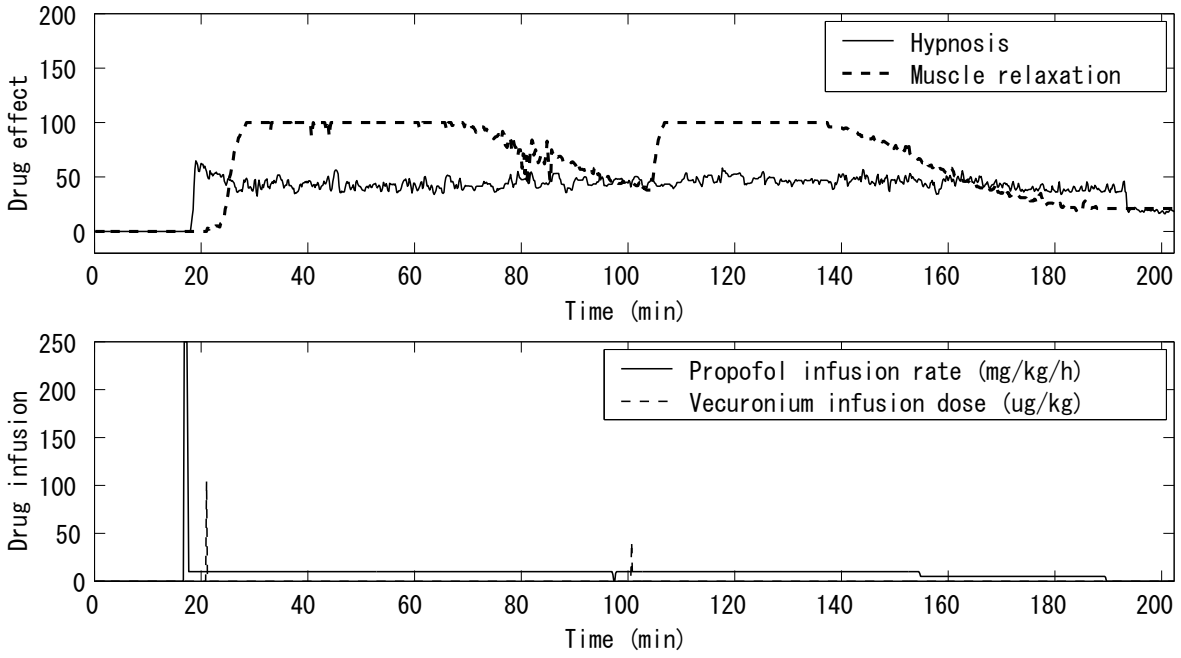

Figure 6.1: Typical input and output sequences during general anesthesia. The inputs are infusion rates of propofol and vecuronium. The outputs are decreases of the BIS and twitch height from initial values.

puterized syringe pump and vecuronium was administered intermittently by the physician. The BIS was stored on the computer at every one second. The twitch height between the end of its calibration and the removal of tube or mask was also stored on the computer at every ten seconds. In this way, ten measurements of input and output (I/O) sequences were obtained. Typical I/O sequences are shown in Fig. 6.1. In Fig. 6.1, hypnosis and muscle relaxation are displayed as decreases of the BIS and twitch height from their initial values.

From these measurements, a model of the decreases of the indices to drug infusion rates, which is shown in Fig. 6.2, was identified using the method proposed in Chapter 2. First, each I/O measurement was resampled with sampling period $T_s = 10$ seconds. Second, using the resampled sequences of the i-th patient, block Hankel matrices $U^i_{0|k}$ and $Y^i_{0|k}$ were formed as defined in Eq. (2.19). Then the block Hankel matrices were rowed up, and lengths of delays in I/O paths and system matrices of a delay-free part were identified.

6.1.2 Result

The demographic data of the ten patients were shown in Table. 6.1.

First, lengths of the delays in I/O paths were estimated. The parameter k, the size

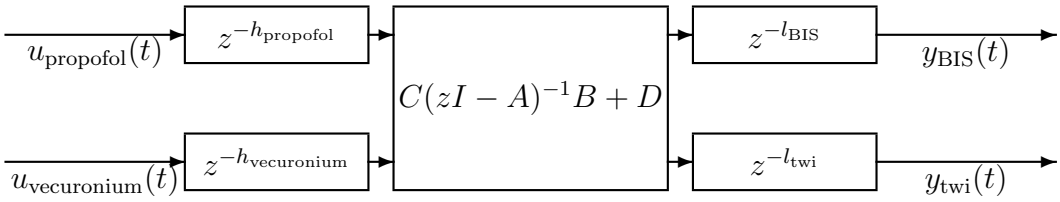

Figure 6.2: Model of decreases of the BIS and twitch height to infusion of propofol and vecuronium

Table 6.1: Demographic data of subjects whose measurements are utilized for identification of the model

Number of subjects	10
Age (yr.)	45.7 ± 11.0
Body weight (kg)	62.1 ± 12.1
Height (cm)	164 ± 8
Sex (m/f)	2/8
Duration of anesthesia (min)	104 ± 47

Values are mean ± SD or numbers (n)

of a block Hankel matrices, was set to $k = 28$. An integer $\tilde{n}$, the size of an augmented observability matrix, was set to $\tilde{n} = 12$. The estimate of impulse response matrix was as in Fig. 6.3. The delays in propofol input path, in vecuronium input path, in BIS output path and in twitch output path were estimated as $h_{\text{propofol}} = 0$, $h_{\text{vecuronium}} = 0$, $l_{\text{BIS}} = 4$ and $l_{\text{twi}} = 6$, respectively.

Next, the system matrices of the delay-free part were identified. Since the impulse response from the vecuronium infusion rate u_{vecu} to the index y_{BIS} of hypnosis was relatively small than others and the output delay l_{BIS} of the BIS was smaller than the delay l_{twi} of the twitch height, the model was assumed to be the following form:

$$\begin{aligned}
\begin{bmatrix} x_{\text{BIS}}(k+1) \\ x_{\text{twi}}(k+1) \end{bmatrix} &= \begin{bmatrix} A_{\text{BIS,BIS}} & 0 \\ A_{\text{twi,BIS}} & A_{\text{twi,twitch}} \end{bmatrix} \begin{bmatrix} x_{\text{BIS}}(k) \\ x_{\text{twi}}(k) \end{bmatrix} \\
&\quad + \begin{bmatrix} B_{\text{BIS}} \\ B_{\text{twi}} \end{bmatrix} \begin{bmatrix} u_{\text{propofol}}(k) \\ u_{\text{vecuronium}}(k) \end{bmatrix}, \qquad (6.1) \\
y_{\text{BIS}}(k) &= C_{\text{BIS}} x_{\text{BIS}}(k - l_{\text{BIS}}), \qquad (6.2) \\
y_{\text{twi}}(k) &= C_{\text{twi}} x_{\text{twi}}(k - l_{\text{twi}}). \qquad (6.3)
\end{aligned}$$

The triplet $(A_{\text{BIS,BIS}}, B_{\text{BIS}}, C_{\text{BIS}})$ was identified from y_{BIS} and the input sequence. Then the triplet $(A_{\text{twi,twitch}}, [A_{\text{twi,BIS}}\ B_{\text{twi}}], C_{\text{twi}})$ was identified from y_{twi}, the input sequence and the estimate of x_{BIS}, which was calculated from $A_{\text{BIS,BIS}}$, B_{BIS} and u_{propofol}. Following this procedure, the matrices $A_{\text{BIS,BIS}}$, $A_{\text{twi,BIS}}$, $A_{\text{twi,twitch}}$, B_{BIS}, B_{twi}, C_{BIS} and C_{twi} were

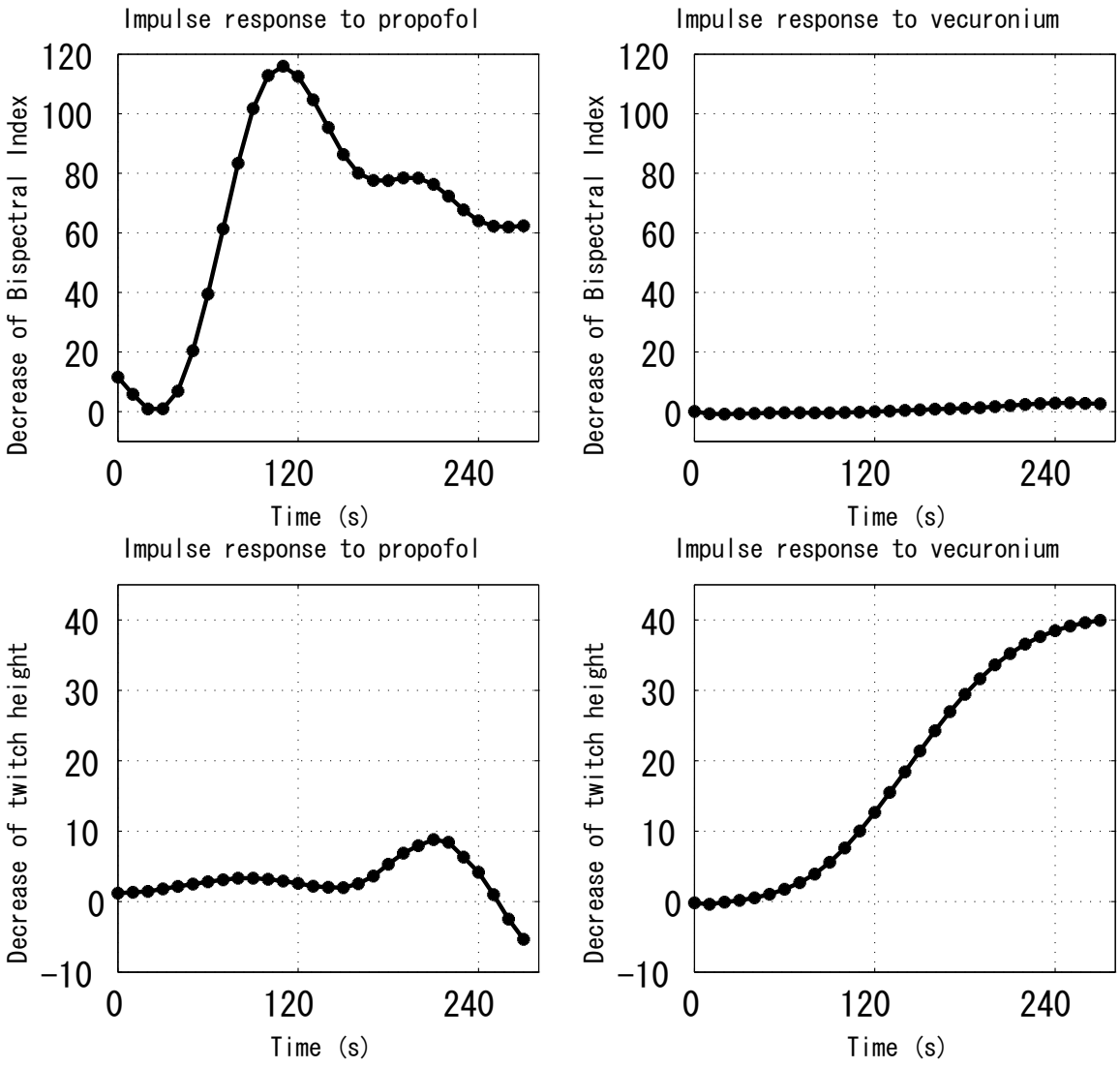

Figure 6.3: Estimate of impulse response matrix for delay estimation. Subfigures show the impulse responses of the decreases of the BIS and twitch height to infusion of propofol and vecuronium.

obtained. Finally, the discrete-time system (6.1) $\sim$ (6.3) was converted to a continuous-time model by `MATLAB` *d2c* function assuming zero-order hold on the inputs.

The identified system matrices and delay lengths of continuous system are as follows:

$$A = \left[\begin{array}{c|cc} -0.0357 & 0 & 0 \\ \hline 0.0491 & 0.0103 & -0.4422 \\ -0.0025 & 0.0449 & -0.1664 \end{array}\right] (\mathrm{min}^{-1}), \tag{6.4}$$

$$B = \left[\begin{array}{cc} 8.6153 & 0.4534 \\ \hline -0.5705 & 1.1575 \\ 1.0879 & -1.8869 \end{array}\right] (\mathrm{kg} \cdot \mathrm{mg}^{-1}), \tag{6.5}$$

$$C = \left[\begin{array}{c|cc} 7.1691 & 0 & 0 \\ 0 & 11.5625 & 6.5187 \end{array}\right], \ L_{\mathrm{BIS}} = 0.667(\mathrm{min}), \ L_{\mathrm{twi}} = 1.0(\mathrm{min}). \tag{6.6}$$

The impulse response matrix of the identified model is shown in Fig. 6.4. Figure 6.5 shows measurements of I/O sequences and the model output. For almost all measurements, the model output approximates fairly well the output measurements. Thus we conclude that the identified model is acceptable and can be utilized for the design of a control system of hypnosis and muscle relaxation.

6.2 Construction of control system of hypnosis and muscle relaxation

In this section, a state-predictive servo controller for controlling the hypnosis and muscle relaxation during general anesthesia is designed. First specification of the closed-loop system is given. Next the gain matrices of a servo controller and of an observer are determined using a standard linear-quadratic (LQ) design method. Then countermeasures against input constraint and output saturation are shown.

6.2.1 Specification of control system

In this subsection, specification of the hypnosis and muscle relaxation control system is given. First, an initial action at induction of anesthesia is explained. Second, the target values of indices during maintenance of anesthesia are shown. Then performance specification of control system is given as a settling time, a disturbance rejection ability and a robust stability range.

According to the widely accepted procedure, the designed control system provides an initial action at induction of anesthesia, in order to anesthetize patients quickly and safely. The initial action of the control system is a bolus and continuous infusion of propofol followed by a bolus of vecuronium. In clinical routine, 2 mg/kg bolus of propofol is administered at the induction of anesthesia so as to eliminate anxiety of the patient quickly. Following this bolus, propofol is infused continuously at the rate of 10 mg/kg/h,

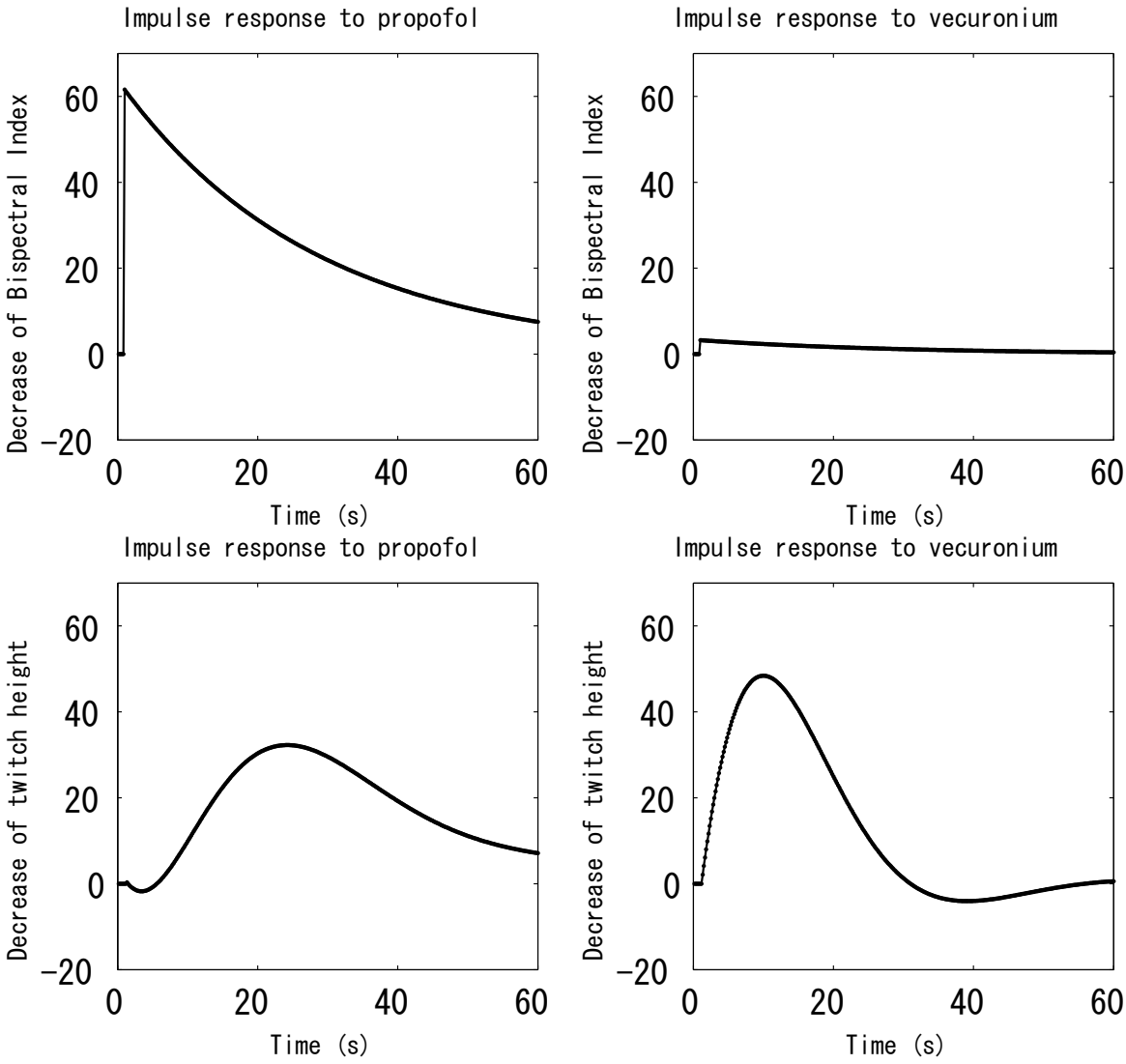

Figure 6.4: Impulse response matrix of identified model

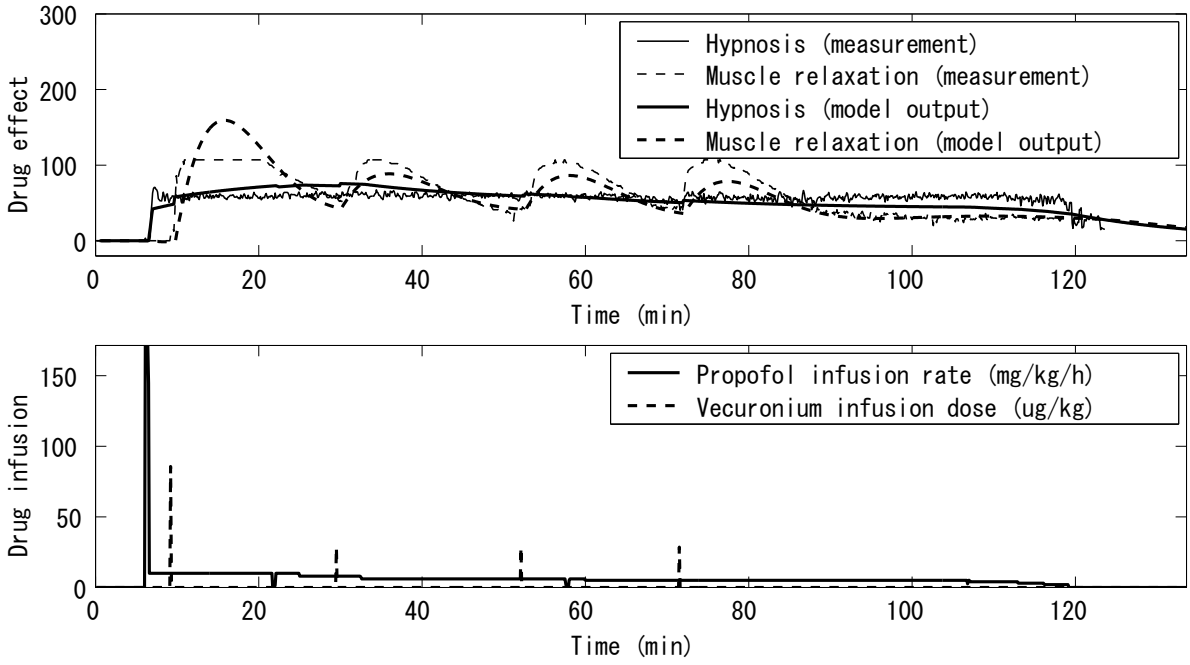

Figure 6.5: An example of measurements and corresponding model outputs

so as to avoid awakening caused by intubation stimulus. Then after the loss of consciousness of the patient, vecuronium is given as 0.10 mg/kg bolus to prevent laryngospasm during the intubation. Therefore the same administration of these drugs is provided as the initial action in the designed control system. The feedback control begins when the bolus of vecuronium is administered. An interval between the propofol bolus and the vecuronium bolus is set to 3 minutes.

Next, the target values of indices during feedback control are given. An adequate range of the BIS during maintenance of anesthesia is from 40 to 60 [62]. Thus the target value of the BIS is set to 50. The twitch height value higher than 25 means insufficient muscle relaxation that allows somatic movement obstructing the surgical procedure. On the other hand, the twitch height value lower than 5 may be a symptom of excessive muscle relaxation that delays a recovery after the surgery. Thus the target value of twitch height is set to 15. Consequently, the purpose of the closed-loop control is to regulate the indices of hypnosis and muscle relaxation, the decreases of the BIS and the twitch height, to 50 and 85, respectively.

The performance specification of the closed-loop control system is given as follows.

Settling time The 5% settling time for a step change of the hypnosis reference should be less than 15 minutes. The 5% settling time for a step change of the muscle relaxation reference also should be less than 15 minutes.

Disturbance rejection Here a disturbance rejection property is specified for an asyn-

chronous step output disturbance during steady state. The decay rate of the disturbance effect is quantified by time constant, and should be less than 15 minutes.

Robust stability Parameter mismatches only on the output matrix C and the delay lengths L_{BIS} and L_{twi} are considered. The required stability range is given as:

$$||C^r - C|| \leq 0.25||C||, \tag{6.7}$$

$$|L^r_{\mathrm{BIS}} - L_{\mathrm{BIS}}| \leq 0.75\mathrm{min}, \quad |L^r_{\mathrm{twi}} - L_{\mathrm{twi}}| \leq 0.75\mathrm{min}, \tag{6.8}$$

where C^r, L^r_{BIS} and L^r_{twi} are actual values of the output matrix, the length of delay of BIS output and that of twitch output.

To satisfy the above-mentioned purpose and specification, gain matrices of an observer and a servo controller are determined in the following subsection.

6.2.2 Design of state-predictive servo control system

In this subsection, the state-predictive servo controller that proposed in Chapter 4 is designed.

First an observer gain matrix for the state predictor shown in Chapter 3 is determined based on an LQ design method. First of all a fictitious system

$$\frac{d\xi_o(t)}{dt} = A^{*\mathrm{T}}\xi_o(t) + C^{\mathrm{T}}v(t), \tag{6.9}$$

is introduced. Here, A^* is a constant matrix defined by Eq. (3.27). For this fictitious system, a feedback gain matrix F_o of a feedback control law

$$v(t) = -F_o\xi_o(t), \tag{6.10}$$

is designed so as to minimize a performance index

$$J_o = \int_0^\infty \left\{\xi_o(t)^{\mathrm{T}}Q_o\xi_o(t) + v(t)^{\mathrm{T}}R_o v(t)\right\} dt, \tag{6.11}$$

where $Q_o = I_3$ and $R_o = 10^7 \times I_2$. Finally K is set to the transpose of F_o, namely, $K = F_o^{\mathrm{T}}$.

Next a feedback gain matrix for the state-predictive servo controller shown in Chapter 4 is also determined. Here, another fictitious system

$$\frac{d\xi_c(t)}{dt} = \bar{A}\xi_c(t) + \bar{B}u(t), \tag{6.12}$$

and a feedback control law

$$u(t) = -\bar{F}\xi_c(t), \tag{6.13}$$

with a feedback gain matrix $\bar{F}$ are introduced. Here, $\bar{A}$ and $\bar{B}$ are given in Eq. (4.14). Then the feedback matrix $\bar{F}$ is determined so as to minimize a performance index

$$J_c = \int_0^\infty \left\{ \xi_c(t)^{\mathrm{T}} Q_c \xi_c(t) + u(t)^{\mathrm{T}} R_c u(t) \right\} dt, \tag{6.14}$$

where $Q_c = \mathrm{diag}(1,\ 50,\ 0,\ 0,\ 0)$ and $R_c = 10^6 \times I_2$.

Using these gain matrices, the state-predictive servo controller is constructed.

6.2.3 Countermeasures against constraint and saturation

In this subsection, an anti-windup mechanism and an output compensation mechanism are introduced as countermeasures against input constraint and output saturation, respectively.

First the anti-windup mechanism is explained. The controller adjusts infusion rates of two drugs. Although these infusion rates must be nonnegative, manipulated input $u_{\mathrm{cal}}(t)$ calculated by the state-predictive controller is not guaranteed to be nonnegative. When the manipulated input $u_{\mathrm{cal}}(t)$ has a negative value, the controller should stop the infusion of the corresponding drug. This restriction is considered as an input constraint. This input constraint worsens closed-loop performance, because control action by the integral compensator in the controller is inhibited by the constraint. In order to cope with this problem, a conventional anti-windup mechanism [85] is added to the control system. Namely, the error $e_u(t)$ between constrained input $u_{\mathrm{real}}(t)$ and input $u_{\mathrm{cal}}(t)$ calculated by the state-predictive controller is subtracted from the integration of the error $e(t)$ between the reference signal and the measured output through a high gain matrix G_{ARW}, as

$$e_u(t) = u_{\mathrm{cal}}(t) - u_{\mathrm{real}}(t), \tag{6.15}$$

$$\frac{dw(t)}{dt} = e(t) - G_{\mathrm{ARW}} e_u(t), \tag{6.16}$$

where $w(t)$ is the state of the integral compensator. The gain matrix G_{ARW} is set to

$$G_{\mathrm{ARW}} = \begin{bmatrix} 10^4 & 0 \\ 0 & 25 \end{bmatrix}, \tag{6.17}$$

by a trial and error procedure. Using this anti-windup mechanism, the controller deals with the problem of input constraint.

Next an output compensation mechanism for output saturation is shown. The output signals of the controlled process saturate when they reach to 100, because both of the BIS and single twitch height lies in the range $[0, 100]$. However, this nonlinear phenomena was not taken into account adequately at the design of the control system. This nonlinearity worsens the controller performance if any output signals reach to the saturating point, since the controller cannot know a "true" output value. To handle this problem adequately, "fictitious" output signals are generated from the state of the observer, and

fed to the state-predictive servo controller. The fictitious outputs $\bar{y}_{\rm BIS}(t)$ and $\bar{y}_{\rm twi}(t)$ are given by

$$\bar{y}_{\rm BIS}(t) = \begin{cases} y_{\rm BIS}(t) & (y_{\rm BIS}(t) < y_{\rm BIS}^{\rm MAX}), \\ \max\{y_{\rm BIS}(t),\ C_{\rm BIS}\bar{x}_{\rm BIS}(t - L_{\rm BIS}|t)\} & (y_{\rm BIS}(t) = y_{\rm BIS}^{\rm MAX}), \end{cases} \tag{6.18}$$

$$\bar{y}_{\rm twi}(t) = \begin{cases} y_{\rm twi}(t) & (y_{\rm twi}(t) < y_{\rm twi}^{\rm MAX}), \\ \max\{y_{\rm twi}(t),\ C_{\rm twi}\bar{x}_{\rm twi}(t - L_{\rm twi}|t)\} & (y_{\rm twi}(t) = y_{\rm twi}^{\rm MAX}), \end{cases} \tag{6.19}$$

where $\bar{x}_{\rm BIS}(t - L_{\rm BIS}|t)$ and $\bar{x}_{\rm twi}(t - L_{\rm twi}|t)$ are the estimated states by the delayed-state observer. $y_{\rm BIS}^{\rm MAX}$ and $y_{\rm twi}^{\rm MAX}$ are the saturating values and set to 100. Using this output compensation mechanism, the controller copes with the problem of output saturation.

6.3 Performance evaluation of control system

In this section, performance of constructed control system is evaluated by computer simulation. First closed-loop responses without and with model mismatches are shown, then robust stability analysis is performed. Throughout this section, the control system is applied to general anesthesia lasting two hours.

First, nominal response of the control system is shown in Fig. 6.6. Following to the bolus of propofol, hypnosis level rose suddenly. Then the bolus of vecuronium raised muscle relaxation level immediately. The hypnosis level was affected by the vecuronium bolus, but approached the setpoint at adequate rates after the feedback control began. On the other hand, the muscle relaxation level reached 100 in 13 minutes, and saturated for 12 minutes. Then the level approached to its setpoint adequately. As seen above, we can confirm that the control system works appropriately in the nominal case.

Next, closed-loop responses with model mismatches are shown. Figures 6.7 and 6.8 indicate closed-loop responses with $+25\%$ and -25% model mismatches on all elements of the output matrix, respectively. The responses with $+75\%$ and -75% mismatches on all delay lengths are presented in Figs. 6.9 and 6.10, respectively. In these results, both hypnosis and muscle relaxant levels approached the respective setpoints without steady state error at adequate rates. These show that the control system has an appropriate tracking ability despite model mismatches.

Next, robust stability analysis of the constructed control system is performed. A stability region on a plane whose axes are the magnitude of mismatches on system matrices and the maximum mismatch on delay lengths is derived using the method proposed in Chapter 4, as Fig. 6.11. In Fig. 6.11, allowable values of $||\Delta_C||$, $||\Delta_A||$, $\Delta L_{\rm BIS}$ and $\Delta L_{\rm twi}$ are demonstrated. Here, Δ_C, Δ_A, $\Delta L_{\rm BIS}$ and $\Delta L_{\rm twi}$ mean additive model mismatches on matrices C, A and the delays $L_{\rm BIS}$, $L_{\rm twi}$, respectively. The model mismatches on matrices are treated by the linear combination $\delta = ||\Delta_C|| + \delta_A||\Delta_A||$ of their norms. In Fig. 6.11, the value δ is assigned in the vertical axis. The model mismatches on the delay lengths $\Delta L_{\rm BIS}$ and $\Delta L_{\rm twi}$ are treated by $\Delta_L = \max(|\Delta L_{\rm BIS}|, |\Delta L_{\rm twi}|)$, and assigned in the horizontal axis. If the pair (δ, Δ_L) of the actual system is included in the hatched region

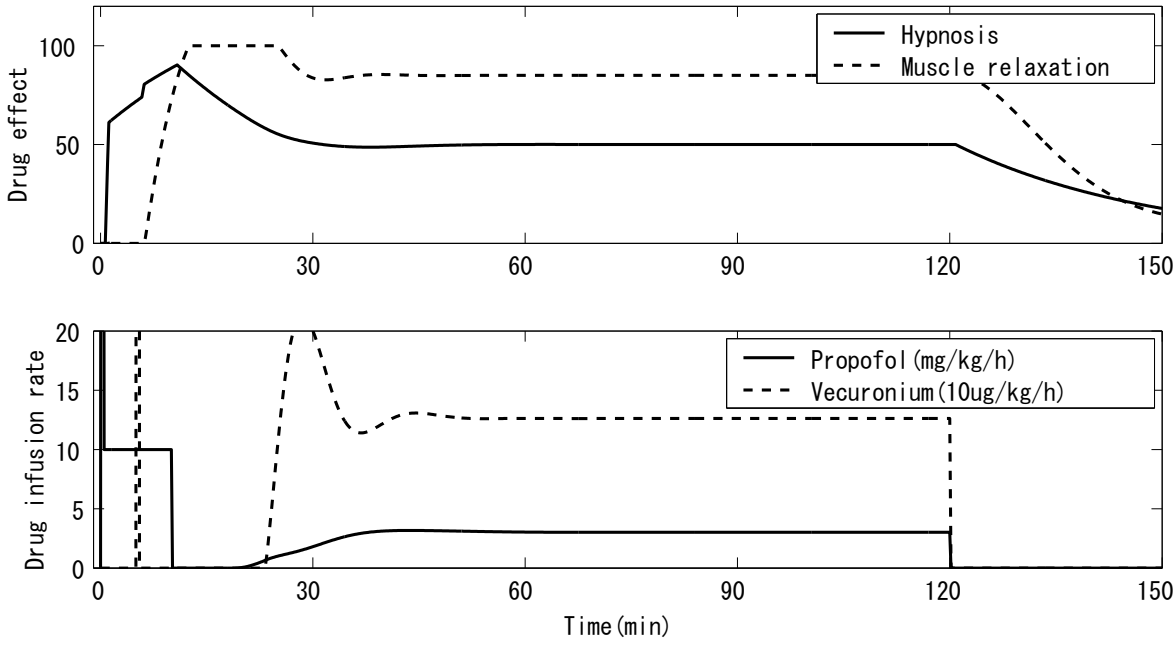

Figure 6.6: Closed-loop response of the multivariable anesthesia control system in the nominal case

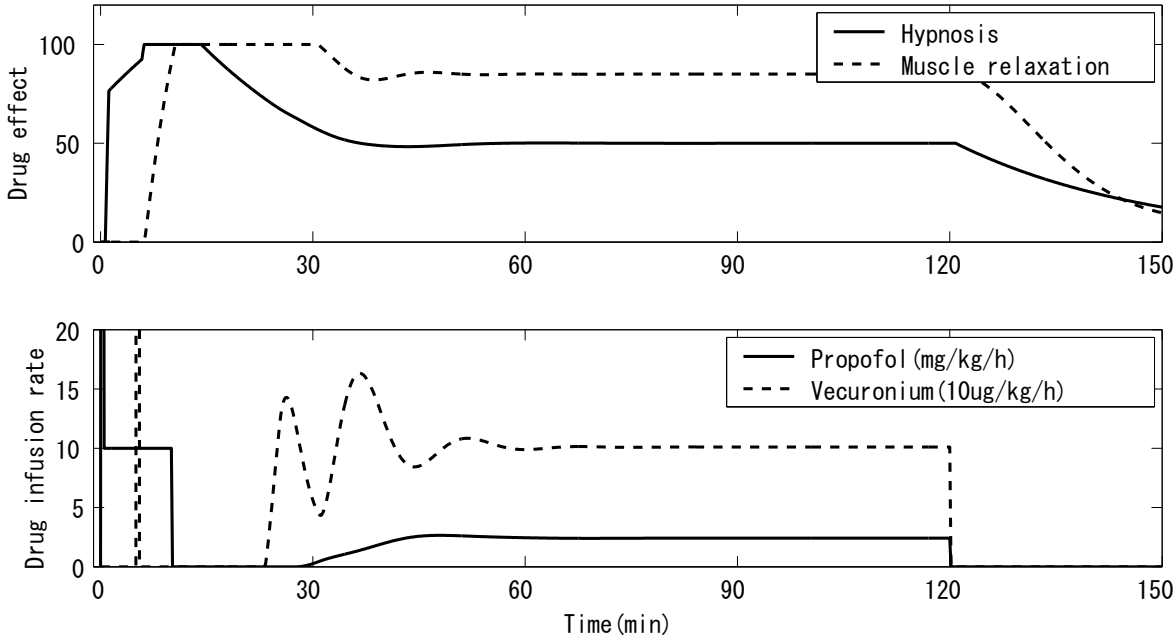

Figure 6.7: Closed-loop response of the multivariable anesthesia control system with +25% mismatch on output matrix

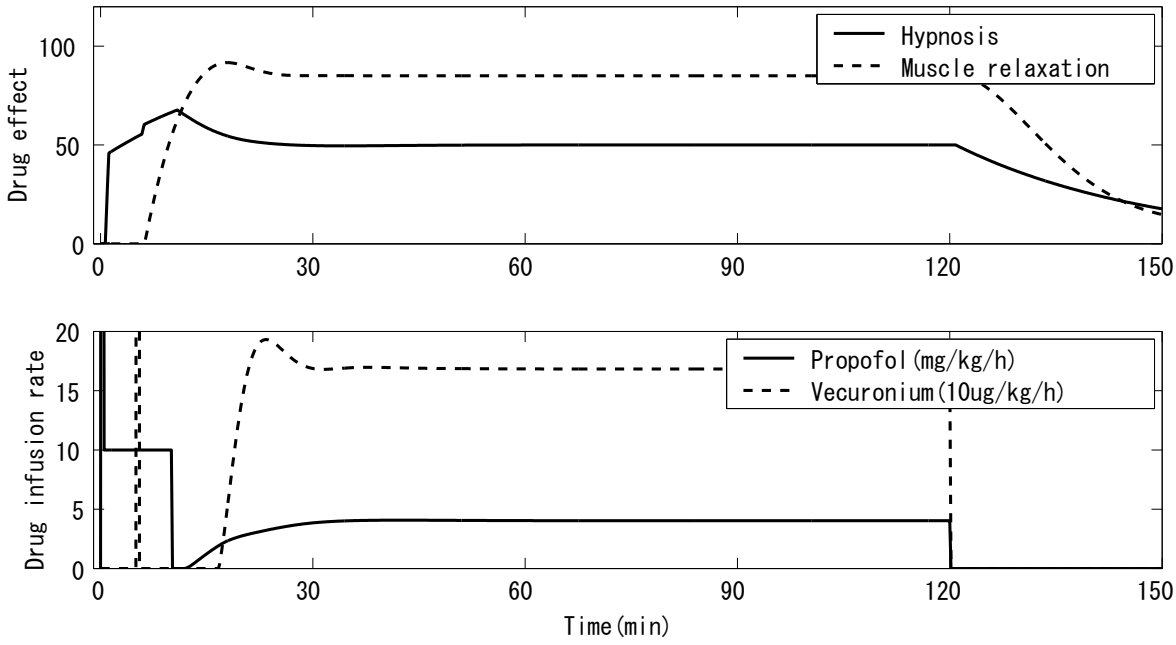

Figure 6.8: Closed-loop response of the multivariable anesthesia control system with -25% mismatch on output matrix

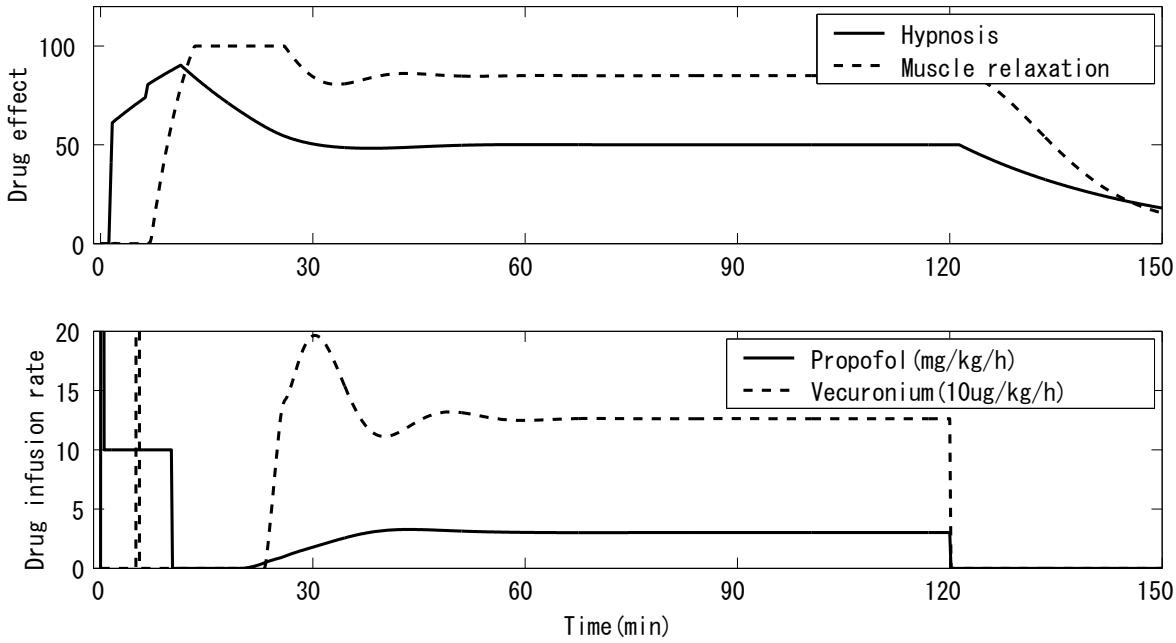

Figure 6.9: Closed-loop response of the multivariable anesthesia control system with $+75\%$ mismatch on all delay lengths

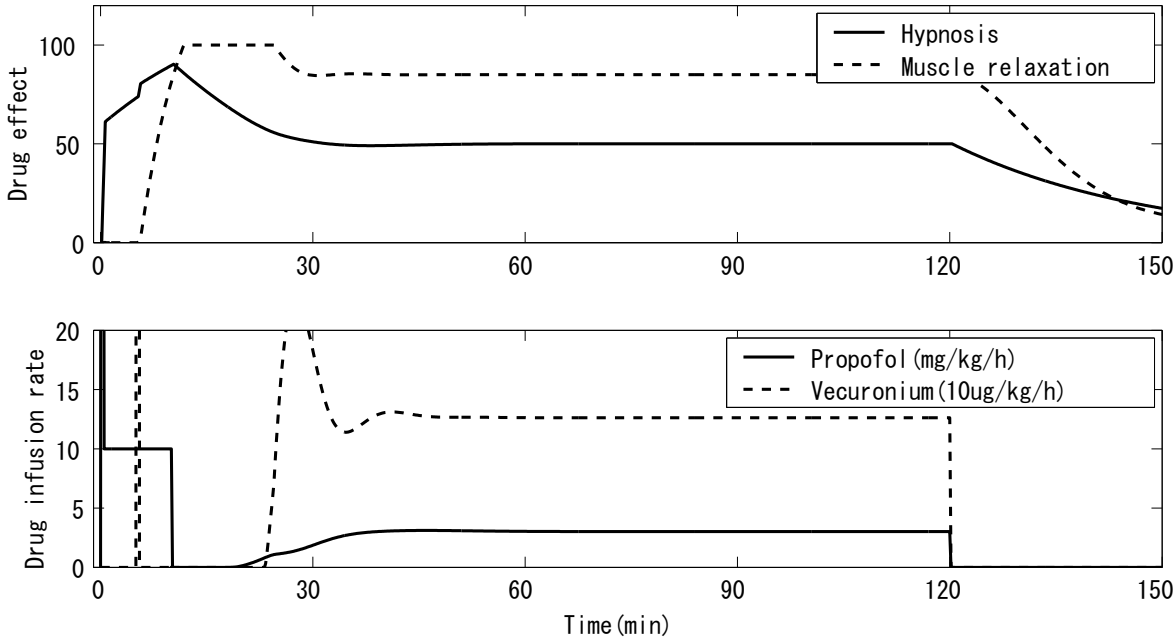

Figure 6.10: Closed-loop response of the multivariable anesthesia control system with -75% mismatch on all delay lengths

in Fig. 6.11, then the closed-loop system remains stable. In this case, the factor δ_A is 129. The stability margin in Fig. 6.11 is probably conservative, but large enough to cover the specification of the control system. Consequently, we conclude that the constructed control system has sufficient robust stability against the mismatches on system matrices and delay lengths.

6.4 Concluding remarks

In this chapter, a multivariable control system of hypnosis and muscle relaxation during general anesthesia is constructed. First a model of responses of hypnosis and muscle relaxation to a hypnotic drug and a muscle relaxant is identified from measurements of them using a subspace identification method proposed in Chapter 2. Then a state-predictive servo controller is constructed as in Chapter 4. Closed-loop responses of the control system with model mismatches are examined. Furthermore, its robust stability is analyzed by the method proposed in Chapter 4. As a result, we can confirm that the constructed control system satisfies specifications of hypnosis and muscle relaxation control during general anesthesia.

Although synthesis and analysis in this chapter are quite preliminary, these show the availability of the proposed identification method, state-predictive servo controller with state predictor and analysis method of robust stability of the control system. For

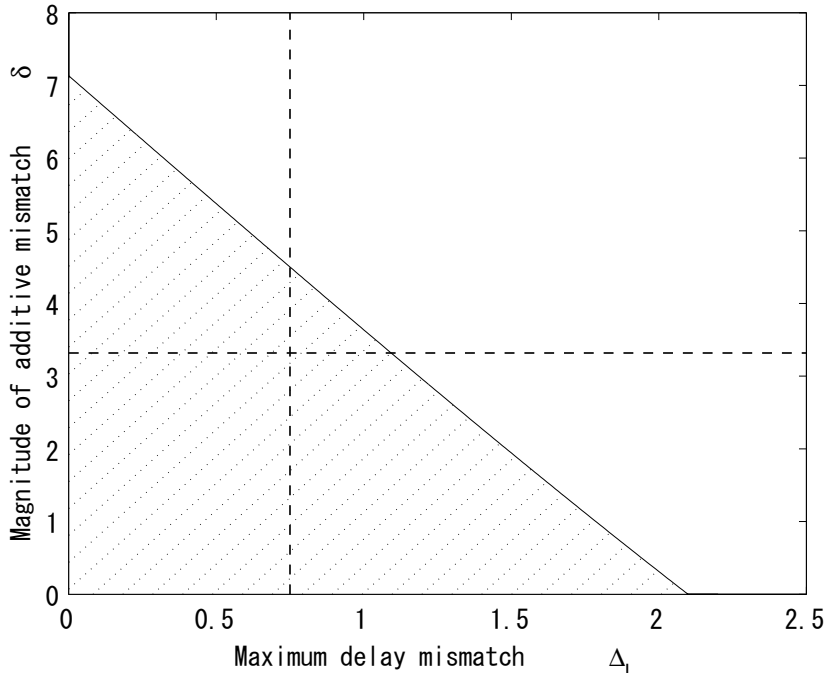

Figure 6.11: Robust stability region of the multivariable anesthesia control system

clinical use of the control system, some improvements are required: identifying more accurate model, redesigning the controller, and integrating a risk-control function and an identification function of individual parameters.

Chapter 7

Conclusion

In this thesis, three theoretical issues related to identification and control of multivariable systems whose input and/or output paths have different time delays were examined. Furthermore, two practical systems for maintaining general anesthesia are developed as applications of these theoretical processes.

The first theoretical issue is identification of multivariable systems whose input and output paths have different time delays. The author proposes a novel subspace identification method for such systems to address this issue. This method has two steps: estimation of delay lengths and identification of system matrices of the system's delay-free part. The delay lengths in the respective input and output paths are estimated from the impulse response matrix that is obtained based on a subspace identification method. The system matrices of the delay-free part are identified from input and output sequences of the delay-free part. Because both steps are based on the subspace identification method, no parameterization is required and computation procedures are numerically stable and efficient.

The second issue is state prediction of multivariable systems whose input and output paths have different time delays. A state predictor is newly proposed for this class of systems. This predictor comprises two blocks: a full-order observer which estimates a vector consisting of past states of delay-free part, and a prediction mechanism which predicts the current state of the delay-free part. The interval length of the finite interval integration in the observer equation is shorter than that of an existing delay-compensating observer [9]. Therefore, the proposed predictor would predict the state of the delay-free part more accurately than the delay-compensating observer, especially for systems with long time delays.

The third issue is servo control of multivariable systems whose output paths have different time delays. Using the state predictor described above, a robust servo controller is developed for this class of systems. The developed controller consists of the state predictor, an integral compensator with a prediction mechanism for robust tracking, and a state feedback controller. An analysis method of robust stability against mismatches on system matrices and lengths of delays is proposed based on the characteristic equation

of the closed-loop system. Using this novel method, one can draw a stability region on a plane whose axes show the magnitudes of parameter mismatches on system matrices and delay lengths.

As applications of these theoretical delay-conscious techniques, two automatic control systems are developed for general anesthesia. The first system administers a hypnotic drug to maintain an index of hypnosis at its target value. The second system controls the hypnosis level and muscle relaxation level simultaneously by administering a hypnotic drug and a muscle relaxant. The respective control performances of these two systems are evaluated through clinical trials and computer simulation.

The former system, the hypnosis control system, has three components: a model predictive controller, a parameter estimator, and a risk-control function. The model predictive controller administers a hypnotic drug to the patient based on prediction of future behavior of the hypnosis index using a pharmacological model of hypnosis. The prediction mechanism enables the control system to achieve high-quality control irrespective of an output delay. The parameter estimator identifies individual parameters at the induction of anesthesia to cope with individual differences. The risk-control function prevents undesirable situations during anesthesia by taking rule-based actions. The results of clinical trials underscore the potential for reducing the amount of drug infusion and maintaining hypnosis more accurately than manual adjustment by physicians.

The latter system, a simultaneous control system of hypnosis and muscle relaxation, is constructed using the three theoretical issues described earlier in this thesis. A model of hypnosis and muscle relaxation is identified as a two-input two-output system including output delays with different length, based on measurements of infusion rates of hypnotic drug and muscle relaxant and indices of hypnosis and muscle relaxation. Then a state-predictive servo controller is designed for the identified model. The closed-loop performance is evaluated using time-domain simulations. A robust stability analysis is also performed for the closed-loop system. The tracking ability and robust stability of the closed-loop system meet the specifications that are predefined for clinical use.

Future directions of research are as follows. The robust stability analysis explained in Chapter 4 might be rather conservative. A less conservative analysis of the robust stability might facilitate the design of an adequate controller. Before clinical trials, the control system of hypnosis and muscle relaxation described in Chapter 6 must show better performance in terms of model accuracy, must include countermeasures for individual patient differences and undesirable situations, and must perform in real time.

Bibliography

[1] K. Gu and S.I. Niculescu; "Survey on recent results in the stability and control of time-delay systems," *Journal of Dynamic Systems, Measurement, and Control*, Vol. 125, pp. 158–165, 2003.

[2] J. P. Richard; "Time-delay systems: an overview of some recent advances and open problems," *Automatica*, Vol. 39, pp. 1667–1694, 2003.

[3] J. G. Ziegler and N. B. Nichols; "Optimum settings for automatic controllers," *Transactions of the American Society of Mechanical Engineers*, Vol. 64, pp. 759–768, 1942.

[4] O. J. M. Smith; "A controller to overcome dead time," *Journal of the Instrument Society of America*, Vol. 6, pp. 28–33, 1959.

[5] E. Furutani, S. Bao and M. Araki; A-TDS: A CADCS package for plants with a pure delay, in *Recent Advances in Computer Aided Control Systems Engineering* (eds. M. Jamshidi and C. J. Herget), pp. 247–272, Elsevier (1992)

[6] A. Z. Manitius and A. W. Olbrot; "Finite spectrum assignment problem for systems with delays," *IEEE Transactions of Automatic Control*, Vol. 24, pp. 541–553, 1979.

[7] E. Furutani, T. Hagiwara and M. Araki; "Two-degree-of-freedom design method of state-predictive LQI servo systems," *IEE proceedings. Control theory and applications*, Vol. 149, pp. 365–378, 2002.

[8] A. Kojima, K. Uchida, E. Shimemura and S. Ishijima; "Robust stabilization of a system with delays in control," *IEEE Transactions of Automatic Control*, Vol. 39, pp. 1694–1698, 1994.

[9] K. Watanabe and M. Ito; "An observer for linear feedback control laws of multivariable systems with multiple delays in controls and outputs," *Systems & control letters*, Vol. 1, pp. 54–59, 1981.

[10] E. F. Camacho and C. Bordons; Model Predictive Control, Springer, 1999.

[11] L. Ljung; System Identification: Theory for the User, Second ed., Prentice-Hall, 1999.

[12] S. Bjorklund and L. Ljung; "A review of time-delay estimation techniques", in Proceedings of the 42nd IEEE Conference on Decision and Control, pp. 2502–2507, Maui, Hawaii, 2003.

[13] C. T. Leondes and E. C. Wong; "An identification algorithm for linear stochastic systems with time delays," *International Journal of Control*, Vol. 36, pp. 445–459, 1982.

[14] Z-J. Yang, H. Iemura, S. Kanae and K. Wada; "Identification of continuous-time systems with multiple unknown time delays by global nonlinear least-squares and instrumental variable methods," *Automatica*, Vol. 43, pp. 1257–1264, 2007.

[15] T. Katayama; Subspace Methods for System Identification: A Realization Approach, Springer-Verlag, 2005,

[16] V. L. Kharitonov; "Robust stability analysis of time delay systems: A survey," *Annual Reviews in Control*, Vol. 23, pp. 185–196, 1999.

[17] Z. Palmor; "Stability properties of Smith dead-time compensator controllers," *International Journal of Control*, Vol. 32, pp. 937–949, 1980.

[18] E. Furutani and M. Araki; "Robust stability of state-predictive and Smith control systems for plants with a pure delay," *International Journal of Robust and Nonlinear Control*, Vol. 8, pp. 907–919, 1998.

[19] M. Verhaegen and P. Dewilde; "Subspace model identification Part 1. The output-error state-space model identification class of algorithms," *International Journal of Control*, Vol. 56, pp. 1187–1210, 1992.

[20] J. Schüttler and H. Ihmsen; "Population pharmacokinetics of propofol – a multicenter study –," *Anesthesiology*, Vol. 92, pp. 727–738, 2000.

[21] J. Vuyk, F. H. Engbers, H. J. Lemmens, A. G.. Burm, A. A. Vletter, M. P. Gladines and J. G. Bovill; "Pharmacodynamics of propofol in female patients," *Anesthesiology*, Vol. 77, pp. 3–9, 1992.

[22] T. W. Schnider, C. F. Minto, S. L. Shafer, P. L. Gambus, C. Andresen, D. B. Goodale and E. J. Youngs; "The influence of age on propofol pharmacodynamics," *Anesthesiology*, Vol. 90, pp. 1502–1516, 1999.

[23] B. C. Juricek, D. E. Seborg and W. E. Larimore; "Identification of multivariable, linear, dynamic models: comparing regression and subspace techniques," *Industrial & Engineering Chemistry Research*, Vol. 41, pp. 2185–2208, 2002.

[24] L. Ljung, System Identification Toolbox for use with MATLAB. User 's Guide, Version 6, The MathWorks, 2004.

[25] P. Van Overschee and B. De Moor, "N4SID: Subspace Algorithms for the Identification of Combined Deterministic-Stochastic Systems," *Automatica*, Vol. 30, pp. 75–93, 1994.

[26] O. Sename; "New trends in design of observers for time-delay systems," *Kybernetika*, Vol. 4, pp. 427–458, 2001.

[27] K. Watanabe; "Finite spectrum assignment and observer for multivariable systems with commensurate delays," *IEEE Transactions of Automatic Control*, Vol. 31, pp. 543–550, 1986.

[28] W. M. Wonham; "On pole assignment in multi-input controllable linear systems," *IEEE Transactions of Automatic Control*, Vol. 12, pp. 660–665, 1967.

[29] V. Van Assche, M. Dambrine, J.-F. Lafay and J.-P. Richard; "Some problems arising in the implementation of distributed-delay control law," in Proceedings of the 38th IEEE Conference on Decision and Control, pp. 4668–4672, Phoenix, Arizona, 1999.

[30] K. Engelborghs, M. Dambrine and D. Roose; "Limitations of a class of stabilization methods for delay systems," *IEEE Transactions of Automatic Control*, Vol. 46, pp. 336–339, 2001.

[31] Q.-C. Zhong; "On distributed delay in linear control laws — Part I: discrete-delay implementations," *IEEE Transactions of Automatic Control*, Vol. 49, pp. 2074–2080, 2004.

[32] Q.-C. Zhong; "On distributed delay in linear control laws — Part II: rational implementations inspired from the δ-operator," *IEEE Transactions of Automatic Control*, Vol. 50, pp. 729–734, 2005.

[33] K. Watanabe, Y. Ishiyama and M. Ito; "Modified Smith predictor control for multivariable systems with delays and unmeasurable step disturbances," *International Journal of Control*, Vol. 37, No. 5, pp. 959–973, 1983.

[34] S. Bao and M. Araki; "On robust stability of state-predictive control systems for plant with pure delay (in Japanese)," *Systems and Control*, Vol. 32, pp. 58–65, 1988.

[35] G. Zames; "On the input-output stability on nonlinear time-varying feedback systems Part one: conditions derived using concepts of loop gain, conicity, and positivity," *IEEE Transactions of Automatic Control*, Vol. 11, pp. 228–238, 1966.

[36] G. C. Goodwin, S. F. Graebe and M. E. Salgado; Control System Design, Prentice-Hall, 2001.

[37] P.H. Tonner; "Balanced anaesthesia today," *Best Practice & Research Clinical Anaesthesiology*, Vol. 19, pp. 475–484, 2005.

[38] E. Gepts, F. Camu, I. D. Cockshott and E. J. Douglas; "Disposition of propofol administered as constant rate intravenous infusions in humans," *Anesthesia and Analgesia*, Vol. 66, pp. 1256–1263, 1987.

[39] M. Tramer, A. Moore and H. McQuay; "Propofol anaesthesia and postoperative nausea and vomiting: quantitative systematic review of randomized controlled studies," *British Journal of Anaesthesia*, Vol. 78, pp. 247–255, 1997.

[40] J. B. Glen; "The development of 'diprifusor': a TCI system for propofol," *Anaesthesia*, Vol. 53 Suppl. 1, pp. 13–21, 1998.

[41] D. Russell, M. P. Wilkes, S. C. Hunter, J. G. Glen, P. Hutton and G. N. Kenny; "Manual compared with target-controlled infusion of propofol," *British Journal of Anaesthesia*, Vol. 75, pp. 562–566, 1995.

[42] T. Sakai, A. Matsuki, P. F. White and A. H. Giesecke; "Use of an EEG-bispectral closed-loop delivery system for administering propofol," *Acta Anaesthesiologica Scandinavica*, Vol. 44, pp. 1007–1010, 2000.

[43] K. Leslie, A. Absalom and G. N. Kenny; "Closed loop control of sedation for colonoscopy using the Bispectral Index," *Anaesthesia*, Vol. 57, pp. 693–697, 2002.

[44] A. Morley, J. Derrick, P. Mainland, B. B. Lee and T. G. Short; "Closed loop control of anaesthesia: an assessment of the Bispectral Index as the target of control," *Anaesthesia*, Vol. 55, pp. 953–959, 2000.

[45] A. R. Absalom and G. N. Kenny; "Closed-loop control of propofol anaesthesia using bispectral index^{tm}: performance assessment in patients receiving computer-controlled propofol and manually controlled remifentanil infusions for minor surgery," *British Journal of Anaesthesia*, Vol. 90, pp. 737–741 2003.

[46] A. R. Absalom, N. Sutcliffe and G. N. Kenny; "Closed-loop control of anesthesia using Bispectral Index: performance assessment in patients undergoing major orthopedic surgery under combined general and regional anesthesia," *Anesthesiology*, Vol. 96, pp. 67–73, 2002.

[47] N. Liu, T. Chazot, A. Genty, A. Landais, K. McGee, P. Laloë, B. Trillat, L. Barvais and M. Fischeler; "Titration of propofol for anesthetic induction and maintenance guided by the Bispectral Index: Closed-loop versus manual control: a prospective, randomized, multicenter study," *Anesthesiology*, Vol. 104, pp. 686–695, 2006.

[48] M. M. Struys, T. De Smet, L. F. Versichelen, S. Van de Velde, R. Van den Broecke and E. P. Mortier; "Comparison of closed-loop controlled administration of propofol using Bispectral Index as the controlled variable versus "standard practice" controlled administration," *Anesthesiology*, Vol. 95, pp. 6–17, 2001.

[49] E. Mortier, M. Struys, T. De Smet, L. Versichelen and G. Rolly; "Closed-loop controlled administration of propofol using bispectral analysis," *Anaesthesia*, Vol. 53, pp. 749–754, 1998.

[50] J. M. Bailey and W. M. Haddad; "Drug dosing control in clinical pharmacology," *IEEE Control Systems Magazine*, Vol. 25, pp. 35–51, 2005.

[51] J. Bruhn, P. S. Myles, R. Sneyd and M. M. R. F. Struys; "Depth of anaesthesia monitoring: what's available, what's validated and what's next?" *British Journal of Anaesthesia*, Vol. 97, pp. 85–94, 2006.

[52] J. C. Sigl and N. G. Chamoun; "An introduction to bispectral analysis for the electroencephalogram," *Journal of Clinical Monitoring*, Vol. 10, pp. 392–404, 1994.

[53] L. Voss and J. Sleigh; "Monitoring consciousness: the current status of EEG-based depth of anaesthesia monitors," *Best Practice & Research Clinical Anaesthesiology*, Vol. 21, pp. 313–325, 2007.

[54] U. S. Food and Drug Administration; "510(k) Premarket Notification Database, #K963644," [Online]. Available: `http://www.accessdata.fda.gov/scripts/cdrh/cfdocs/cfPMN/pmn.cfm?ID=106460` (accessed 2008-02-20).

[55] U. S. Food and Drug Administration; "510(k) Premarket Notification Database, #K030267," [Online]. Available: `http://www.accessdata.fda.gov/scripts/cdrh/cfdocs/cfPMN/pmn.cfm?ID=10728` (accessed 2008-02-20).

[56] Aspect medical systems, Inc.; "BIS adoption quick facts," [Online]. Available: `http://www.aspectms.com/products/bis_quick_facts_popup.mspx`, (accessed 2008-02-20).

[57] A. A. Dahaba; "Different conditions that could result in the Bispectral index indicating an incorrect hypnotic state," *Anesthesia and Analgesia*, Vol. 101, pp. 765–773, 2005.

[58] J. W. Johanson; "Update on Bispectral Index monitoring," *Best Practice & Research Clinical Anaesthesiology*, Vol. 20, pp. 81–99, 2006.

[59] S. Pilge, R. Zanner, G. Schneider, J. Blum, M. Kreuzer and E. F. Kochs; "Time delay of index calculation: analysis of cerebral state, bispectral, and narcotrend indices," *Anesthesiology*, Vol. 104, pp. 488–494, 2006.

[60] S. L. Shafer and K. M. Gregg; "Algorithms to rapidly achieve and maintain stable drug concentrations at the site of drug effect with a computer-controlled infusion pump," *Journal of Pharmacokinetics and Biopharmaceutics*, Vol. 20, pp. 147–169, 1992.

[61] H. Lange, H. Stephan, H. Rieke, M. Kellermann, H. Sonntag and J. Bircher; "Hepatic and extrahepatic disposition of propofol in patients undergoing coronary bypass surgery," *British Journal of Anaesthesia*, Vol. 64, pp. 563–570, 1990.

[62] T. J. Gan, P. S. Glass, A. Windsor, F. Payne, C. Rosow, P. Sebel and P. Manberg; "Bispectral Index monitoring allows faster emergence and improved recovery from propofol, alfentanil, and nitrous oxide anesthesia," *Anesthesiology*, Vol. 87, pp. 808–815, 1997.

[63] C. F. Minto, T. W. Schnider, K. M. Gregg, T. K. Henthorn and S. L. Shafer; "Using the time of maximum effect site concentration to combine pharmacokinetics and pharmacodynamics," *Anesthesiology*, Vol. 99, pp. 324–333, 2003.

[64] J. G. Wagner; "Kinetics of pharmacologic response I. Proposed relationships between response and drug concentration in the intact animal and man," *Journal of Theoretical Biology*, Vol. 20, pp. 173–201, 1968.

[65] A. Shafer, V. A. Doze, S. L. Shafer and P. F. White; "Pharmacokinetics and pharmacodynamics of propofol infusions during general anesthesia," *Anesthesiology*, Vol. 69, pp. 348–356, 1988.

[66] S. Tonegawa, E. Furutani and M. Araki; "Robust stability analysis of model predictive control systems for plants with a pure delay (in Japanese)," in Proceedings of the 42nd Annual Conference of the Institute of Systems, Control and Information Engineers, pp. 457–458, Kyoto, Japan, 1998.

[67] M. Jopling, R. C. Cork and S. Greenwald; "Changes in the Bispectral Index (BIS) in the presence of surgical stimulation reflect the level of analgesia," *Anesthesiology*, Vol. 84, p. A478, 1996.

[68] I. A. Iselin-Chaves, R. Flaishon, P. S. Sebel, S. Howell, T. J. Gan, J. Sigl, B. Ginsberg and P. S. Glass; "The effect of the interaction of propofol and alfentanil on recall, loss of consciousness, and the Bispectral Index," *Anesthesia and Analgesia*, Vol. 87, pp. 949–955, 1998.

[69] R. Sukhani, J. Vazquez, A. L. Pappas, K. Frey, M. Aasen and S. Slogoff; "Recovery after propofol with and without intraoperative fentanyl in patients undergoing ambulatory gynecologic laparoscopy," *Anesthesia and Analgesia*, Vol. 83, pp. 975–981, 1996.

[70] G. E. Morgan and M. S. Mikhail; Clinical Anesthesiology, Second Ed, Lange Medical Book/McGraw-Hill, 1992

[71] D. A. O'Hara, D. K. Bogen and A. Noordergraaf; "The use of computers for controlling the delivery of anesthesia," *Anesthesiology*, Vol. 77, pp. 563–581, 1992.

[72] M. M. R. F. Struys, E. P. Mortier and T. D. Smet; "Closed loops in anaesthesia," *Best Practice & Research Clinical Anaesthesiology*, Vol. 20, pp. 211–220, 2006.

[73] M. Mahfouf and D.A. Linkens; "Constrained multivariable generalized predictive control (GPC) for anaesthesia: the quadratic-programming approach (QP)," *International Journal of Control*, Vol. 67, pp. 507–527, 1997.

[74] C. S. Nunes, M. Mahfouf, D. A. Linkens and J. E. Peacock; "Modeling and multivariable control in anaesthesia using neural-fuzzy paradigms Part I. Classification of depth of anaesthesia and development of a patient model," *Artificial Intelligence in Medicine*, Vol. 35, pp. 195–206, 2005.

[75] M. Janda, J. Bajorat, B. Pohl, O. Simanski and R. Hofmockel; "Evaluation of a simultaneous closed-loop control system for depth of hypnosis and muscle relaxation," *Anesthesiology*, Vol. 105, p. A849, 2006.

[76] R. J. Fragen, L. H. D. J. Booij, F. van der Pol, E. N. Robertson and J. F. Crul; "Interactions of diisopropyl phenol (ICI 35 868) with suxamethonium, vecuronium and pancuronium in vitro," *British Journal of Anaesthesia*, Vol. 55, pp. 433–436, 1983.

[77] E. N. Rovertson, R. J. Fragen, L. H. D. J. Booij, J. van Egmond and J. F. Crul; "Some effects of diisopropyl phenol (ICI 35 868) on the pharmacodynamics of atracrium and vecuronium in anaesthetized man," *British Journal of Anaesthesia*, Vol. 55, pp. 723–728, 1983.

[78] K. Watanabe, Y. Ohmi, H. Adachi and T. Satoh; "Propofol potentiates the neuromuscular blocking effects of vecuronium in man (in Japanese)," *The Japanese Journal of Anesthesiology*, Vol. 49, pp. 2–6, 2000.

[79] P. M. R. M. De Grood, J. Van Egmond, M. Van De Wetering, H. B. Van Beem, L. H. D. J. Booij and J. F. Crul; "Lack of effects of emulsified propofol ('Diprivan') on vecuronium pharmacodynamics – preliminary results in man," *Postgraduate Medical Journal*, Vol. 61 Suppl. 3, pp. 28–30, 1985.

[80] P. Nightingale, N. V. Petts, T. E. J. Healy, B. Kay and K. McGuinness; "Induction of anaesthesia with propofol ('Diprivan') or thiopentone and interactions with suxamethonium, atracurium and vecuronium," *Postgraduate Medical Journal*, Vol. 61 Suppl. 3, pp. 31–34, 1985.

[81] G. J. McCarthy, R. K. Mirakhur and S. K. Pandit; "Lack of interaction between propofol and vecuronium," *Anesthesia and Analgesia*, Vol. 75, pp. 536–538, 1992.

[82] T. Suzuki, H. Nagai, N. Katsumata, S. Ogawa and H. Suzuki; "Neuromuscular inhibitory effects of propofol evaluated by cat's evoked EMG (in Japanese)," *The Japanese Journal of Anesthesiology*, Vol. 47, pp. 1433–1436, 1998.

[83] B. Vivien, S. D. Maria, A. Ouattara, O. Langeron, P. Coriat and B. Riou; "Overestimation of Bispectral Index in sedated intensive care unit patients revealed by administration of muscle relaxant," *Anesthesiology*, Vol. 99, pp. 9–17, 2003.

[84] S. Inoue, M. Kawaguchi, N. Sasaoka, K. Hirai and H. Furuya; "Effects of neuromuscular block on systemic and cerebral hemodynamics and Bispectral Index during moderate or deep sedation in critically ill patients," *Intensive Care Medicine*, Vol. 32, pp. 391–397, 2006.

[85] M. V. Kothare, P. J. Campo and M. Morari; "A unified framework for the study of anti-windup designs," *Automatica*, Vol. 30, pp. 1869–1883, 1994.

List of Publications by the Author

Journal Papers

1. Y. Sawaguchi, E. Furutani and M. Araki: State predictor for multivariable systems with multiple output delays , in Japanese); *Transactions of the Institute of Systems, Control and Information Engineers*, Vol. 19, No. 1, pp. 28–36, 2006.

2. Y. Sawaguchi, E. Furutani, G. Shirakami, M. Araki and K. Fukuda: Identification of time delay and pharmacokinetic-pharmacodynamic parameters of propofol using the Bispectral Index as the measure of effect (in Japanese); *The Journal of Japan Society for Clinical Anesthesia*, Vol. 27, No. 4, pp. 358–366, 2007.

3. Y. Sawaguchi, E. Furutani, G. Shirakami, M. Araki and K. Fukuda: A model-predictive hypnosis control system under total intravenous anesthesia; *IEEE Transactions on Biomedical Engineering*, Vol. 55, No. 3, pp. 874–887, 2008.

4. Y. Sawaguchi, E. Furutani and M. Araki: A state predictor for multivariable systems including multiple delays in each output path; *Submitted for publication in IEEE Transactions on Automatic Control*

5. Y. Sawaguchi, E. Furutani and M. Araki: Subspace identification of multivariable systems whose input and output paths have different time delays; *Submitted for publication in IEEE Transactions on Automatic Control*

Conference Papers (International)

1. Y. Sawaguchi, E. Furutani, G. Shirakami, M. Araki and K. Fukuda: A model predictive sedation control system under total intravenous anesthesia; the IEEE EMBS Asian-Pacific Conference on Biomedical Engineering 2003, Kyoto-Osaka-Nara, Japan, 2003.

2. G. Shirakami, Y. Sawaguchi, E. Furutani, M. Araki and K. Fukuda: Clinical application of a model predictive propofol anesthesia control system using Bispectral Index: comparison with manual control; the 13th World Congress of Anaesthesiologist, Paris, France, 2004.

3. Y. Sawaguchi, E. Furutani, G. Shirakami, M. Araki and K. Fukuda: Model predictive controller for closed-loop administration of propofol using Bispectral Index; the 7th EuroSIVA, Lisbon, Portugal, 2004.

4. Y. Sawaguchi, E. Furutani, G. Shirakami, M. Araki and K. Fukuda: Comparison of pharmacokinetic parameters of propofol for modeling Bispectral Index response: With or without consideration of dead-time; the 7th EuroSIVA, Lisbon, Portugal, 2004.

5. E. Furutani, Y. Sawaguchi, G. Shirakami, M. Araki and K. Fukuda: A hypnosis control system using a model predictive controller with online identification of individual parameters; the IEEE Conference on Control Applications, Toronto, Canada, pp. 154–159, 2005.

6. Y. Sawaguchi, E. Furutani and M. Araki: A state predictor for multivariable systems including multiple delays in each output path; the 44th IEEE Conference on Decision and Control, and the European Control Conference 2005, Seville, Spain, pp. 7204–7209, 2005.

7. E. Furutani, K. Asada, Y. Sawaguchi and H. Suga: A study of index for estimating effect of electrocovulsive therapy based on electroencephalogram; SICE Annual Conference 2007, Kagawa, Japan, pp. 2735–2738, 2007.

8. Y. Sawaguchi, E. Furutani, G. Shirakami, M. Araki and K. Fukuda: Identification of better pharmacokinetic parameters for propofol infusion to predict bispectral index response; the First World Congress of Total Intravenous Anaesthesia, Venice, Italy, p. 138, 2007.

Conference Papers (Domestic)

1. Y. Sawaguchi, E. Furutani, G. Shirakami, M. Araki and K. Fukuda: An intravenous anesthesia control system with pharmacodynamics identification function (in Japanese); the SICE Conference on Systems and Information 2001, pp. 319–324, 2001.

2. Y. Sawaguchi, E. Furutani, G. Shirakami, M. Araki and K. Fukuda: Clinical application of a model predictive intravenous anesthesia control system (in Japanese); the 46th Annual Conference of the Institute of Systems, Control and Information Engineers, pp. 141–142, 2002.

3. S. Watanabe, Y. Sawaguchi, E. Furutani, G. Shirakami, M. Araki and K. Fukuda: An intravenous anesthesia control system using a state predictive controller; the 46th Annual Conference of the Institute of Systems, Control and Information Engineers, pp. 139–140, 2002.

4. G. Shirakami, Y. Sawaguchi, E. Furutani, M. Araki and K. Fukuda: Clinical application of model predictive propofol infusion system using the Bispectral index: comparison with manual control (in Japanese); the 9th Annual Meeting of the Japanese Society of Intravenous Anesthesia, p. 37, 2002.

5. Y. Sawaguchi, E. Furutani, G. Shirakami, M. Araki and K. Fukuda: Improvement of a sedation control system under intravenous anesthesia (in Japanese); the 47th Annual Conference of the Institute of Systems, Control and Information Engineers, pp. 555–556, 2003.

6. Y. Sawaguchi, E. Furutani, G. Shirakami, M. Araki and K. Fukuda: A sedatikon control system under total intravenous anesthesia using model predictive controller (in Japanese); the 18th Symposium on Biological and Physiological Engineering, pp. 407–408, 2003.

7. Y. Sawaguchi, E. Furutani, G. Shirakami, M. Araki and K. Fukuda: Comparison of propofol pharmacokinetic model using the Bispcetral Index as a performance index (in Japanese); the 10th Annual Meeting of the Japanese Society of Intravenous Anesthesia, p. 27, 2003.

8. Y. Sawaguchi, E. Furutani, G. Shirakami, M. Araki and K. Fukuda: Robust stability analysis of a multivariable state predictive control system containing multiple output delays (in Japanese); the 48th Annual Conference of the Institute of Systems, Control and Information Engineers, pp. 93–94, 2004.

9. S. Watanabe, Y. Sawaguchi, E. Furutani, G. Shirakami, M. Araki and K. Fukuda: Sedation control in monitored anesthesia care using a state-predictive controller (in Japanese); the 48th Annual Conference of the Institute of Systems, Control and Information Engineers, pp. 373–374, 2004.

10. M. Taniguchi, Y. Sawaguchi, E. Furutani, G. Shirakami, M. Araki and K. Fukuda: Sedation and muscle relaxation control system in intravenous anesthesia using a state predictive controller (in Japanese); the 48th Annual Conference of the Institute of Systems, Control and Information Engineers, pp. 375–376, 2004.

11. E. Furutani, Y. Sawaguchi, S. Watanabe, G. Shirakami, M. Araki and K. Fukuda: Interaction of propofol and vecuronium on the Bispectral Index and Twitch –for more adequate automatic control of anesthesia– the 11th Annual Meeting of the Japanese Society of Intravenous Anesthesia, p. 53, 2004.

12. Y. Sawaguchi, E. Furutani, and M. Araki: State prediction for multivariable systems including multiple delays in each output (in Japanese); SICE Kansai 2005 Symposium, pp. 17–20, 2005.

13. Y. Sawaguchi, E. Furutani, and M. Araki: Inprovement of a state predictor for multivariable systems including multiple output delays (in Japanese); the 49th Annual Conference of the Institute of Systems, Control and Information Engineers, pp. 419–420, 2005.

14. K. Morishima, Y. Sawaguchi, E. Furutani, G. Shirakami, M. Araki and K. Fukuda: A control system of volatile anesthesia using a state-predictive controller (in Japanese); the 49th Annual Conference of the Institute of Systems, Control and Information Engineers, pp. 241–242, 2005.

15. Y. Sawaguchi, E. Furutani, and M. Araki: Stability analysis of state predictive control systems for multivariable systems including multiple output delays (in Japanese); the 48th Japan Joint Automatic Control Conference, pp. 103–106, 2005.

16. M. Taniguchi, Y. Sawaguchi, E. Furutani, G. Shirakami, M. Araki and K. Fukuda: Sedation control in monitored anesthesia care (in Japanese); SICE Kansai 2006 Symposium, pp. 39–40, 2006.

17. Y. Sawaguchi, E. Furutani, and M. Araki: Subspace identification of multivariable systems including multiple input/output delays (in Japanese); SICE Kansai 2006 Symposium, pp. 31–34, 2006.

18. Y. Sawaguchi, E. Furutani, and M. Araki: Subspace identification of multivariable systems including multiple input/output delays under the influence of colored noise (in Japanese); the 50th Annual Conference of the Institute of Systems, Control and Information Engineers, pp. 73–74, 2006.

19. T. Yokokawa, Y. Sawaguchi, E. Furutani, G. Shirakami, M. Araki and K. Fukuda: A study on a sedation index using wavelet transform (in Japanese); the 50th Annual Conference of the Institute of Systems, Control and Information Engineers, pp. 87–88, 2006.

20. Y. Sawaguchi, M. Taniguchi, E. Furutani, G. Shirakami, M. Araki and K. Fukuda: Improvement of sedation control system in monitored anesthesia care (in Japanese); the First Symposium on Complex Medical Engineering, pp. 100–101, 2006.

21. G. Shirakami, Y. Sawaguchi, E. Furutani and K. Fukuda: Influences of blink eye movement on values of bispecral index and electroencephalographic entropy monitors (in Japanese); the 53rd Annual Conference of the Japanese Society of Anesthesiologists, 2006.

22. Y. Sawaguchi, E. Furutani, G. Shirakami and K. Fukuda: Identification of propofol pharmacokinetic parameters using the Bispectral Index (in Japanese); the 13th Annual Meeting of the Japanese Society of Intravenous Anesthesia, p. 37, 2006.

23. G. Shirakami, Y. Sawaguchi, S. Matsuura and K. Fukuda: Comparison of total intravenous anesthesia and sevoflurane anesthesia for major breast cancer surgery: effects on intraoperative hemodynamics, heart rate variability, postoperative nausea and vomiting and postanesthesia recovery (in Japanese); the 13th Annual Meeting of the Japanese Society of Intravenous Anesthesia, p. 40, 2006.

24. H. Suga, Y. Sawaguchi and A. Kinoshita: Variations of Bispectral Index (BIS) by ECT in treatment-resistant depressed patients (in Japanese); the 28th Annual Conference of the Japanese Society of Biological Psychiatry, p. 438, 2006.

25. E. Furutani, Y. Sawaguchi, G. Shirakami, M. Araki and K. Fukuda: Anesthesia control using model predictive control (in Japanese); the 49th Japan Joint Automatic Control Conference, 2006.

26. Y. Sawaguchi, K. Kanamori, E. Furutani and M. Araki: An observer design method for compartment systems (in Japanese); the 49th Japan Joint Automatic Control Conference, 2006.

27. K. Morishima, Y. Sawaguchi, E. Furutani, G. Shirakami and K. Fukuda: A novel pharmacodynamic model considering drug interactions (in Japanese); SICE Kansai 2006 Symposium, pp. 17–18, 2007.

28. K. Asada, Y. Yokokawa, Y. Sawaguchi, E. Furutani and H. Suga: A study on index of effectiveness of modified electroconvulsive therapy (in Japanese); SICE Kansai 2006 Symposium, pp. 21–22, 2007.

29. G. Shirakami, S. Matsuura, Y. Sawaguchi, E. Furutani and K. Fukuda: Effects of Bispectral index-titrated "light" and "deep" sevoflurane anesthesia on heart rate variability in short-stay breast cancer surgery (in Japanese); the Eighth Annual Meeting of the Japanese Society of Perioperative Chronomedicine, p. 14, 2007.

30. Y. Sawaguchi, E. Furutani and M. Araki: Synthesis and robust stability analysis of state-predictive servo control system for multivariable systems including multiple output delays (in Japanese); SICE 7th Annual Conference on Control Systems, 2007.

31. S. Kusudo, Y. Sawaguchi, E. Furutani and M. Araki: Subspace identification method for Wiener systems with delays and its application to hypnosis and muscle relaxation process (in Japanese); the 51st Annual Conference of the Institute of Systems, Control and Information Engineers, pp. 221–222, 2007.

32. K. Morishima, Y. Sawaguchi, E. Furutani, G. Shirakami, M. Araki and K. Fukuda: A hypnosis control system using model predictive control with consideration of anesthetic drug interactions (in Japanese); the 51st Annual Conference of the Institute of Systems, Control and Information Engineers, pp. 411–412, 2007.

33. K. Asada, Y. Sawaguchi, E. Furutani and H. Suga: Study on indices for prediction of seizure duration in electroconvulsive therapy (in Japanese); the 51st Annual Conference of the Institute of Systems, Control and Information Engineers, pp. 537–538, 2007.

34. Y. Sawaguchi, Study on indices of sleep and awake electroencephalograms using a subspace identification method (in Japanese); the 13th Annual Conference of the Japan Association for College of Technology, pp. p-67–68, 2007.

35. Y. Sawaguchi, E. Furutani and M. Araki: Analysis of human sleep electroencephalogram using subspace identification method (in Japanese); the 50th Japan Joint Automatic Control Conference, pp. 324–325, 2007.